Methanobactin biosynthesis and redox activity

by

Philip Dershwitz

A dissertation submitted to the graduate faculty

in partial fulfillment of the requirements for the degree of

DOCTOR OF PHILOSOPHY

Major: Biophysics

Program of Study Committee:
Alan DiSpirito, Co-major Professor
Thomas Bobik, Co-major Professor
Richard Honzatko
Julian Roche
Gregory Phillips

The student author, whose presentation of the scholarship herein was approved by the program of study committee, is solely responsible for the content of this dissertation. The Graduate College will ensure this dissertation is globally accessible and will not permit alterations after a degree is conferred.

Iowa State University

Ames, Iowa

2022

DEDICATION

To my students, past and future. This work is an offering on the altar of academia, exchanged for the right to continue teaching you. I hope it, and I, are found worthy of the position.

TABLE OF CONTENTS

Page

ACKNOWLEDGMENTS

First I would like to thank Alan DiSpirito for taking a chance on a student who showed up out of the blue during his recruit visit and professed interest in, specifically, the weird and esoteric properties of Alan's pet microbe. Alan has been the ideal PI, trusting me to operate independently while simultaneously always being available when I sought his guidance. If I graduate as a competent scientist, it is a direct consequence of the quality of his mentorship.

I must also thank the rest of my committee for their invaluable support and guidance. Thomas Bobik, for providing me with a lab in which I could actually do genetics, and for his expertise in that field more broadly. Richard Honzatko, for recruiting me to Iowa State in the first place, for teaching me structural biology, and for guiding me as I navigated the black magic that is protein crystallography. Julian Roche, for teaching me how to do high-pressure NMR, without which my project would have been hopeless, and for trusting me with the hardware to do it. And Gregory Phillips, for serving as the non-departmental member of my committee and providing an outside perspective on my work.

Additionally, I would like to thank Bruce Fulton, for holding my hand as I learned to be an actual spectroscopist, Joel Nott, both for the enormous assistance of the protein facility and for all his help with troubleshooting and method development as I figured out how to isolate my proteins, and the entire Iowa State department of Biochemistry, Biophysics and Molecular Biology, for creating a community that I enjoyed working in throughout my PhD.

Finally, I owe an incredible debt to my family, for their unwavering support as I figured out what I wanted from life, and to my fiancée, Jennifer Schieltz, for supporting me mentally, emotionally, and materially. All of the stereotypical struggles of a PhD disappear when you are a kept man who returns every day to a loving home full of animals.

ABSTRACT

Methanobactins are low-molecular-mass (<1,300 Da), ribosomally synthesized and posttranslationally modified copper-binding peptides excreted by some methanotrophs as the extracellular component of a copper acquisition system. Structurally, methanobactins are characterized by the presence of a C-terminal oxazolone group with a C2-associated thioamide and by the presence of an N-terminal oxazolone, imidazolone or pyrazinedione group with an associated thioamide. Some methanobactins also contain a sulfate group in-place of the hydroxyl group on a Tyr adjacent to the C-terminal oxazolone group. The two nitrogens on the rings and the two thioamide sulfurs are the four atoms that coordinate with copper and are the source of methanobactins' copper-binding ability.

Methanobactins with two oxazolone groups are classified as Group I, while those with only one are classified as Group II. Group I methanobactins bind copper to form a stable tetrahedral structure, while Group II methanobactins form a more dynamic hairpin structure. These structural differences give rise to the two groups' physical and functional differences.

The first part of this dissertation focuses on a methanobactin-catalyzed redox reaction in which O_2 is generated from H_2O, the difference in activity between different methanobactins, and the functional and ecological implications of this reaction. Specifically, in methanotrophs that produce methanobactins, their ability to generate their own oxygen could allow them to perform aerobic methane oxidation in a range of environments in which that reaction would otherwise not be possible. The second part of this dissertation focuses on the biosynthesis of methanobactin from *Methylosinus trichosporium* OB3b. As ribosomally synthesized and posttranslationally modified peptides, methanobactins have an entire operon dedicated to the transport, chaperoning and modification of the proto-methanobactin gene product from the *mbnA*

gene. Several of the genes in this operon were and are unannotated, including *mbnC*. To that end a Δ*mbnC* knockout mutant was created and the structure of its resulting methanobactin was solved by metal-free NMR in order to determine that *mbnC* is not required for the formation of the N-terminal oxazolone the methanobactin from *M. trichosporium* OB3b. Finally, to elucidate the function of *mbnF* from *Methylocystis* strain SB2, the gene product was isolated, a crystal structure of the protein was solved, and preliminary enzymology was performed. From this work it was determined that *mbnF* encodes a NADPH-dependent flavin monooxygenase.

The results and methods in this research advance our understanding of the function and biosynthesis of methanobactin. In light of methanobactins' utility as a copper chelator for the treatment of Wilson's disease in a rat model, and methanotrophs' critical importance in the global carbon cycle, a better understanding of methanobactins' biosynthesis and catalytic activity could have far-reaching consequences for society.

CHAPTER 1. GENERAL INTRODUCTION

Methanotrophy

Aerobic methane oxidizing bacteria, or methanotrophs, are gram-negative bacteria that rely on methane to supply both their metabolic energy and their carbon for assimilation. Methanotrophs are ubiquitous throughout the environment and can be found anywhere methane is produced, including in oceans, sewage, marine sediments and in wetlands (Semrau *et al.*, 2010).

Methane is a major greenhouse gas and a major component of the global carbon cycle. It is twenty five times more effective at trapping heat than the most well-known greenhouse gas, CO_2, and human society is causing the concentration of atmospheric methane to rise precipitously (Semrau *et al.,* 2010). Given the increased methane production, and methanotrophs' critical role in the global carbon cycle, there is a pressing need for continued study of methanotrophy.

Methanotrophs were first described in 1906 by Söhngen, but the field did not fully develop until the work of the Whittenbury group in the 1970s. Whittenbury isolated over 100 different methanotrophs and classified them according to the arrangement of their membranes, their fatty acid chains, and their mechanism of carbon assimilation (Whittenbury *et al.*, 1970; Semrau *et al.*, 2010).

Methane Oxidation and Methanotroph Ecology

A schematic diagram of methane oxidation to CO_2 is shown in figure 1. The first step in the pathway is the oxidation of methane to methanol, which is catalyzed by the methane monooxygenase (MMO) (Hanson *et al.*, 1996; DiSpirito *et al.*, 2004; Semrau *et al.*, 2010). As the name implies, the monooxygenase' activity is oxygen dependent. This presents a problem,

however, because when investigating anaerobic methane oxidation, researchers persistently find monooxygenase-bearing methanotrophs, and until recently there was no explanation for their presence or how they could be able to perform methane oxidation (figure 2) (Bar-Or *et al.,* 2017; Liang *et al.,* 2019; Dershwitz *et al.,* 2021).

MMOs come in two forms, an iron-containing soluble MMO (sMMO) (Fox *et al.,* 1989; Lipscomb *et al.,* 1994) and an iron- and copper-containing membrane-associated, or particulate, MMO (pMMO) (Zahn *et al.,* 1994; Choi *et al.,* 2003; Chan *et al.,* 2004; Lieberman *et al.,* 2005; Martinho *et al.,* 2007, Ross *et al.,* 2019). Most methanotrophs express the pMMO, while *Methylocella* expresses the sMMO and a minority of methanotrophs express both (Stanley *et al.,* 1983; Semrau *et al.,* 2010; Chistoserdova *et al.,* 2013). sMMOs have higher activity than pMMOs, but lower affinity for copper. In organisms that express both forms, sMMO is expressed during times of copper scarcity, while pMMO is expressed when copper is plentiful. This regulation is known as the ”copper switch” (Stanley *et al.,* 1983; Lee *et al.,* 2006; Semrau *et al.,* 2010). Like the sMMO, there is a small copper-binding peptide called methanobactin (described below) that is inversely regulated by copper (Semrau *et al.,* 2013; Kenney *et al.,* 2016). Studies of knockout mutants lacking the methanobactin gene *mbnA* showed that while the copper switch functions in the absence of the gene, its presence significantly amplifies the expression of both MMOs (Semrau *et al.,* 2013).

Methanobactin

Methanobactins are low-molecular-mass (<1,300 Da), ribosomally synthesized and posttranslationally modified copper-binding peptides excreted by some methanotrophs as the extracellular component of a copper acquisition system. Structurally, methanobactins are characterized by the presence of a C-terminal oxazolone group with a C2-associated thioamide

and by the presence of an N-terminal oxazolone, imidazolone or pyrazinedione group with an associated thioamide. Some methanobactins also contain a sulfate group in-place of the hydroxyl group on a Tyr adjacent to the C-terminal oxazolone group. The two nitrogens on the rings and the two thioamide sulfurs are the four atoms that coordinate with copper and are the source of methanobactins' copper-binding ability (Kim *et al.,* 2004; Krentz *et al.,* 2010; El Ghazouani *et al.,* 2011; El Ghazouani *et al.,* 2012; DiSpirito *et al.,* 2016; Semrau *et al.,* 2018; Semrau *et al.,* 2020).

Methanobactins with two oxazolone groups are classified as Group I, while those with only one are classified as Group II (figure 3). Group I methanobactins bind copper to form a stable tetrahedral structure, while Group II methanobactins form a more dynamic hairpin structure.

Biosynthesis of Methanobactin

As ribosomally synthesized and posttranslationally modified peptides, methanobactins have an entire operon dedicated to the transport and modification of the proto-methanobactin gene product from the *mbnA* gene (Krentz *et al.,* 2010; Semrau *et al.,* 2020). Some of these modifications include (i) deamination of the N-terminal Leu, (ii) conversion of the N-terminal Leu-Cys dipeptide to 1-(N-(mercapto-(5-oxo-2-(3-methylbutanoyl)oxazol-(Z)-4-ylidene)methyl), (iii) conversion of the C-terminal Pro-Cys dipeptide into pyrrolidin-2-yl-(mercapto-(5-oxo-oxazol-(Z)-4-ylidene)methyl), and (iv) cleavage of the leader sequence (Kim *et al.,* 2004; Behling *et al.,* 2008; Krentz *et al.,* 2010; El Ghazouani *et al.,* 2011; Gu *et al.,* 2017; Kenney *et al.,* 2018; Semrau *et al.,* 2020).

mbnA is found in a gene cluster (figure 4) that contains both genes of known function, such as *mbnB* (Krentz *et al.,* 2010; Kenney *et al.,* 2018), *mbnN* (Gu *et al.,* 2017), and *mbnT* (Gu

et al., 2016), as well as unannotated genes, such as *mbnC* (Chou *et al.,* 2006; Krentz *et al.,* 2010; Kenney *et al.,* 2018; Semrau *et al.,* 2020; Dershwitz *et al.,* 2021).

Therapeutic Use of Methanobactin

Wilson disease is a genetic disorder of copper metabolism caused by mutations in the ATPase copper-transporting β (*ATP7B*) gene. Copper homeostasis is maintained by biliary excretion of excess copper by *ATP7B,* and in individuals with Wilson disease cannot excrete excess copper. This causes a buildup of copper in the mitochondria of the liver leading to defective mitochondria structure and function (figure 5) and eventually hepatitis (Summer *et al.,* 2011; Zischka *et al.,* 2011). Existing therapies for Wilson disease all have significant side effects and suboptimal efficacy, so there is a pressing need for better therapies for treating the disease (Lichtmannegger *et al.,* 2016). Our collaborators have developed a rat model of Wilson disease (Summer et al., 2011; Zischka et al., 2011;Lichtmannegger *et al.,* 2016) and have both *in vitro* and *in vivo* results showing that methanobactin can decrease the level of copper in hepatocytic mitochondria in Wilson disease rats, and can rescue them from liver failure (Choi *et al.,* 2008; Zischka *et al.,* 2011; Summer *et al.,* 2011; Lichtmannegger *et al.,* 2016; Zischka *et al.,* 2017; Müller *et al.,* 2018). Mechanistically, methanobactins are taken up dose-dependently by hepatocytes, and readily cross the mitochondrial membrane, where they bind to copper and then the entire complex is directed to the bile. This is the natural route of copper excretion, and methanobactin is unique decoppering primarily by this route, as all other therapeutic chelators primarily decopper by renal excretion (figure 6) (Lichtmannegger *et al.,* 2016; Kaler, 2016).

References

1. Abraham, M. J., Murtola, T., Schulz, R., Páll, S., Smith, J. C., Hess, B., & Lindahl, E. (2015). GROMACS: High performance molecular simulations through multi-level parallelism from laptops to supercomputers. *SoftwareX*, *1–2*, 19–25. https://doi.org/https://doi.org/10.1016/j.softx.2015.06.001

2. Vorobev, A., S. Jagadevan, B.S. Baral, A.A. DiSpirito, B.C. Freemeier, B.H. Bergman, N.L. Bandow and J.D. Semrau (2013). Detoxification of Mercury by Methanobactin from *Methylosinus trichosporium* OB3b. *Applied and Environmental Microbiology*, *79*(19), 5918–5926. https://doi.org/10.1128/AEM.01673-13

3. Amaral, J. A., & Knowles, R. (1995). Growth of methanotrophs in methane and oxygen counter gradients. *FEMS Microbiology Letters*, *126*(3), 215–220. https://doi.org/10.1111/j.1574-6968.1995.tb07421.x

4. Anthony, C. (1992). The structure of bacterial quinoprotein dehydrogenases. *International Journal of Biochemistry*, *24*(1), 29–39. https://doi.org/https://doi.org/10.1016/0020-711X(92)90226-Q

5. Anthony, C. (1982). *The biochemistry of methylotrophs*. Academic Press Ltd., London

6. Apel, K., & Hirt, H. (2004). REACTIVE OXYGEN SPECIES: Metabolism, Oxidative Stress, and Signal Transduction. *Annual Review of Plant Biology*, *55*(1), 373–399. https://doi.org/10.1146/annurev.arplant.55.031903.141701

7. Bab-Dinitz, E., Shmuely, H., Maupin-Furlow, J., Eichler, J., & Shaanan, B. (2006). Haloferax volcanii PitA: an example of functional interaction between the Pfam chlorite dismutase and antibiotic biosynthesis monooxygenase families? *Bioinformatics*, *22*(6), 671–675. https://doi.org/10.1093/bioinformatics/btk043

8. Bandow, N.L. W.H. Gallager, L. Behling, D.W. Choi, J.D. Semrau, S.C. Hartsel, V.S. Gilles, and A.A. DiSpirito. (2011). Isolation of Methanobactin from the spent media of methane-oxidizing bacteria. *Methods in Enzymology*, *495*, 259–269. https://doi.org/10.1016/B978-0-12-386905-0.00017-6

9. Bandow, N. L. (2014). *Isolation and binding properties of methanobactin from the facultative methanotroph Methylocystis strain SB2*. Iowa State University.

10. Bandow, N., Gilles, V. S., Freesmeier, B., Semrau, J. D., Krentz, B., Gallagher, W., McEllistrem, M. T., Hartsel, S. C., Choi, D. W., Hargrove, M. S., Heard, T. M., Chesner, L. N., Braunreiter, K. M., Cao, B. V., Gavitt, M. M., Hoopes, J. Z., Johnson, J. M., Polster, E. M., Schoenick, B. D., Umlauf, A. M., DiSpirito, A. A. (2012). Spectral and copper binding properties of methanobactin from the facultative methanotroph *Methylocystis* strain SB2. *Journal of Inorganic Biochemistry*, *110*, 72–82. https://doi.org/https://doi.org/10.1016/j.jinorgbio.2012.02.002

11. Baral, B. S., Bandow, N. L., Vorobev, A., Freemeier, B. C., Bergman, B. H., Herdendorf, T. J., Fuentes, N., Ellias, L., Turpin, E., Semrau, J. D., DiSpirito, A. A. (2014). Mercury binding by methanobactin from Methylocystis strain SB2. *Journal of Inorganic Biochemistry*, *141*, 161–169. https://doi.org/https://doi.org/10.1016/j.jinorgbio.2014.09.004

12. Baral, B. S. (2017). *Methanobactin: Metal binding proterties, physiological functions and biosynthesis*. Iowa State University.

13. Barlow, D. J., & Thornton, J. M. (1988). Helix geometry in proteins. *Journal of Molecular Biology*, *201*(3), 601–619. https://doi.org/https://doi.org/10.1016/0022-2836(88)90641-9

14. Bar-Or, I., Elvert, M., Eckert, W., Kushmaro, A., Vigderovich, H., Zhu, Q., Ben-Dov, E., Sivan, O. (2017). Iron-Coupled Anaerobic Oxidation of Methane Performed by a Mixed Bacterial-Archaeal Community Based on Poorly Reactive Minerals. *Environmental Science & Technology*, *51*(21), 12293–12301. https://doi.org/10.1021/acs.est.7b03126

15. Baslé, A., El Ghazouani, A., Lee, J., & Dennison, C. (2018). Insight into Metal Removal from Peptides that Sequester Copper for Methane Oxidation. *Chemistry - A European Journal*, *24*(18), 4515–4518. https://doi.org/10.1002/chem.201706035

16. Basu, P., Katterle, B., Andersson, K. K., & Dalton, H. (2003). The membrane-associated form of methane mono-oxygenase from *Methylococcus capsulatus* (Bath) is a copper/iron protein. *Biochemical Journal*, *369*(2), 417–427. https://doi.org/10.1042/bj20020823

17. Behling, L.E., S.C. Hartsel, D.E. Lewis, A.A. DiSpirito, L.R. Masterson, G. Veglia, W.H. Gallagher. (2008). NMR, Mass Spectrometry and Chemical Evidence Reveal a Different Chemical Structure for Methanobactin That Contains Oxazolone Rings. *Journal of the American Chemical Society*, *130*(38), 12604–12605. https://doi.org/10.1021/ja804747d

18. Berova, N., Bari, L. Di, & Pescitelli, G. (2007). Application of electronic circular dichroism in configurational and conformational analysis of organic compounds. *Chemical Society Reviews*, *36*(6), 914–931. https://doi.org/10.1039/B515476F

19. Berson, O., & Lidstrom, M. E. (1997). Cloning and characterization of corA, a gene encoding a copper-repressible polypeptide in the type I methanotroph, *Methylomicrobium albus* BG8. *FEMS Microbiology Letters*, *148*(2), 169–174. https://doi.org/10.1111/j.1574-6968.1997.tb10284.x

20. Gilbert, B., McDonald, I. R., Finch, R., Stafford, G. P., Nielsen, A. K., & Murrell, J. C. (2000). Molecular Analysis of the pmo (Particulate Methane Monooxygenase) Operons from Two Type II Methanotrophs. *Applied and Environmental Microbiology*, *66*(3), 966–975. https://doi.org/10.1128/AEM.66.3.966-975.2000

21. Kalidass, B, M.F. Ul-Haque, B.S. Baral, A.A. DiSpirito, and J.D. Semrau (2015). Competition between Metals for Binding to Methanobactin Enables Expression of Soluble Methane Monooxygenase in the Presence of Copper. *Applied and Environmental Microbiology*, *81*(3), 1024–1031. https://doi.org/10.1128/AEM.03151-14

22. Bowman, G. R. (2016). Accurately modeling nanosecond protein dynamics requires at least microseconds of simulation. *Journal of Computational Chemistry*, *37*(6), 558–566. https://doi.org/https://doi.org/10.1002/jcc.23973

23. Cao, L., Caldararu, O., Rosenzweig, A. C., & Ryde, U. (2018). Quantum Refinement Does Not Support Dinuclear Copper Sites in Crystal Structures of Particulate Methane Monooxygenase. *Angewandte Chemie - International Edition*, *57*(1), 162–166. https://doi.org/10.1002/anie.201708977

24. Carter, P. (1971). Spectrophotometric determination of serum iron at the submicrogram level with a new reagent (ferrozine). *Analytical Biochemistry*, *40*(2), 450–458. https://doi.org/https://doi.org/10.1016/0003-2697(71)90405-2

25. Chan, S. I., Chen, K. H., Yu, S. S., Chen, C. L., & Kuo, S. S. (2004). Toward Delineating the Structure and Function of the Particulate Methane Monooxygenase from Methanotrophic Bacteria. *Biochemistry*, *43*(15), 4421–4430. https://doi.org/10.1021/bi0497603

26. Chandlee, G. C. (1940). *Reference Book of Inorganic Chemistry. Revised edition (Latimer, WM*; *Hildebrand, JH)*. ACS Publications.

27. Chang, J., Gu, W., Park, D., Semrau, J. D., DiSpirito, A. A., & Yoon, S. (2018). Methanobactin from *Methylosinus trichosporium* OB3b inhibits N2O reduction in denitrifiers. *ISME Journal*, *12*(8), 2086–2089. https://doi.org/10.1038/s41396-017-0022-8

28. Chatwood, L. L., Müller, J., Gross, J. D., Wagner, G., & Lippard, S. J. (2004). NMR Structure of the Flavin Domain from Soluble Methane Monooxygenase Reductase from *Methylococcus capsulatus* (Bath),. *Biochemistry*, *43*(38), 11983–11991. https://doi.org/10.1021/bi049066n

29. Chen, Y., Patel, N. A., Crombie, A., Scrivens, J. H., & Murrell, J. C. (2011). Bacterial flavin-containing monooxygenase is trimethylamine monooxygenase. *Proceedings of the National Academy of Sciences*, *108*(43), 17791–17796. https://doi.org/10.1073/pnas.1112928108

30. Chi Fru, E., Gray, N. D., McCann, C., Baptista, J. D. C., Christgen, B., Talbot, H. M., El Ghazouani, A., Dennison, C., Graham, D. W. (2011). Effects of copper mineralogy and methanobactin on cell growth and sMMO activity in *Methylosinus trichosporium* OB3b. *Biogeosciences*, *8*(10), 2887–2894. https://doi.org/10.5194/bg-8-2887-2011

31. Choi, D. W., Kunz, R. C., Boyd, E. S., Semrau, J. D., Antholine, W. E., Han, J. I., Zahn, J. A., Boyd, J. M., de la Mora, A. M., & DiSpirito, A. A. (2003). The Membrane-Associated Methane Monooxygenase (pMMO) and pMMO-NADH:Quinone Oxidoreductase Complex from *Methylococcus capsulatus* Bath. *Journal of Bacteriology*, *185*(19), 5755–5764. https://doi.org/10.1128/JB.185.19.5755-5764.2003

32. Choi, D. W., Do, Y. S., Zea, C. J., McEllistrem, M. T., Lee, S. W., Semrau, J. D., Pohl, N. L., Kisting, C. J., Scardino, L. L., Hartsel, S. C., Boyd, E. S., Geesey, G. G., Riedel, T. P., Shafe, P. H., Kranski, K. A., Tritsch, J. R., Antholine, W. E., & DiSpirito, A. A. (2006). Spectral and thermodynamic properties of Ag(I), Au(III), Cd(II), Co(II), Fe(III), Hg(II), Mn(II), Ni(II), Pb(II), U(IV), and Zn(II) binding by methanobactin from *Methylosinus trichosporium* OB3b. *Journal of Inorganic Biochemistry*, *100*(12), 2150–2161. https://doi.org/10.1016/j.jinorgbio.2006.08.017

33. Choi, D. W., Zea, C. J., Do, Y. S., Semrau, J. D., Antholine, W. E., Hargrove, M. S., Pohl, N. L., Boyd, E. S., Geesey, G. G., Hartsel, S. C., Shafe, P. H., McEllistrem, M. T., Kisting, C. J., Campbell, D., Rao, V., de la Mora, A. M., & Dispirito, A. A. (2006). Spectral, kinetic, and thermodynamic properties of Cu(I) and Cu(II) binding by methanobactin from *Methylosinus trichosporium* OB3b. *Biochemistry*, *45*(5), 1442–1453. https://doi.org/10.1021/bi051815t

34. Choi, D. W., Semrau, J. D., Antholine, W. E., Hartsel, S. C., Anderson, R. C., Carey, J. N., Dreis, A. M., Kenseth, E. M., Renstrom, J. M., Scardino, L. L., Van Gorden, G. S., Volkert, A. A., Wingad, A. D., Yanzer, P. J., McEllistrem, M. T., de la Mora, A. M., & DiSpirito, A. A. (2008). Oxidase, superoxide dismutase, and hydrogen peroxide reductase activities of methanobactin from types I and II methanotrophs. *Journal of Inorganic Biochemistry*, *102*(8), 1571–1580. https://doi.org/https://doi.org/10.1016/j.jinorgbio.2008.02.003

35. Choi, D. W., Bandow, N. L., McEllistrem, M. T., Semrau, J. D., Antholine, W. E., Hartsel, S. C., Gallagher, W., Zea, C. J., Pohl, N. L., Zahn, J. A., & DiSpirito, A. A. (2010). Spectral and thermodynamic properties of methanobactin from γ-proteobacterial methane oxidizing bacteria: A case for copper competition on a molecular level. *Journal of Inorganic Biochemistry*, *104*(12), 1240–1247. https://doi.org/https://doi.org/10.1016/j.jinorgbio.2010.08.002

36. Chou, J. C.-C., Stafford, V. E., Kenney, G. E., & Dassama, L. M. K. (2021). The enzymology of oxazolone and thioamide synthesis in methanobactin. In E. J. B. T.-M. in E. Petersson (Ed.), *Synthetic and Enzymatic Modifications of the Peptide Backbone* (Vol. 656, pp. 341–373). https://doi.org/https://doi.org/10.1016/bs.mie.2021.04.008

37. Colby, J., & Dalton, H. (1978). Resolution of the methane mono-oxygenase of Methylococcus capsulatus (Bath) into three components. Purification and properties of component C, a flavoprotein. *Biochemical Journal*, *171*(2), 461–468. https://doi.org/10.1042/bj1710461

38. Cooper, S. R., McArdle, J. V, & Raymond, K. N. (1978). Siderophore electrochemistry: relation to intracellular iron release mechanism. *Proceedings of the National Academy of Sciences*, *75*(8), 3551–3554. https://doi.org/10.1073/pnas.75.8.3551

39. Cordes, F. S., Bright, J. N., & Sansom, M. S. P. (2002). Proline-induced Distortions of Transmembrane Helices. *Journal of Molecular Biology*, *323*(5), 951–960. https://doi.org/https://doi.org/10.1016/S0022-2836(02)01006-9

40. Crawford, R. L., & Hanson, R. S. (1984). *Microbial growth on C 1 compounds: proceedings* (No. CONF-8309357--). American Society for Microbiology.

41. Csáki, R., Bodrossy, L., Klem, J., Murrell, J. C., & Kovács, K. L. (2003). Genes involved in the copper-dependent regulation of soluble methane monooxygenase of *Methylococcus capsulatus* (Bath): cloning, sequencing and mutational analysis. *Microbiology (Reading, England)*, *149*(Pt 7), 1785–1795. https://doi.org/10.1099/mic.0.26061-0

42. Dershwitz, P., Gu, W., Roche, J., Kang-Yun, C. S., Semrau, J. D., Bobik, T. A., Fulton, B., Zischka, H., DiSpirito, A. A. (2022). *mbnC* Is Not Required for the Formation of the N-Terminal Oxazolone in the Methanobactin from *Methylosinus trichosporium* OB3b. *Applied and Environmental Microbiology*, *88*(2), e01841-21. https://doi.org/10.1128/AEM.01841-21

43. Dershwitz, P., Bandow, N. L., Yang, J., Semrau, J. D., McEllistrem, M. T., Heinze, R. A., Fonseca, M., Ledesma, J. C., Jennett, J. R., DiSpirito, A. M., Athwal, N. S., Hargrove, M. S., Bobik, T. A., Zischka, H., & DiSpirito, A. A. (2022). *mbnC* Is Not Required for the Formation of the N-Terminal Oxazolone in the Methanobactin from *Methylosinus trichosporium* OB3b. *Applied and Environmental Microbiology*, *88*(2), e01841-21. https://doi.org/10.1128/AEM.01841-21

44. Dennison, C. (2019). The Coordination Chemistry of Copper Uptake and Storage for Methane Oxidation. *Chemistry - A European Journal*, *25*(1), 74–86. https://doi.org/10.1002/chem.201803444

45. DiSpirito, A. A., Lipscomb, J. D., & Lidstrom, M. E. (1990). Soluble cytochromes from the marine methanotroph *Methylomonas* sp. strain A4. *Journal of Bacteriology*, *172*(9), 5360–5367. https://doi.org/10.1128/jb.172.9.5360-5367.1990

46. DiSpirito, A. A., Kunz, R. C., Choi, D.-W., & Zahn, J. A. (2004). *Respiration in Methanotrophs* (D. Zannoni, Ed.). https://doi.org/10.1007/978-1-4020-3163-2_7

47. DiSpirito, A. A., Semrau, J. D., Murrell, J. C., Gallagher, W. H., Dennison, C., & Vuilleumier, S. (2016). Methanobactin and the Link between Copper and Bacterial Methane Oxidation. *Microbiology and Molecular Biology Reviews : MMBR*, *80*(2), 387–409. https://doi.org/10.1128/MMBR.00058-15

48. Dou, C., Long, Z., Li, S., Zhou, D., Jin, Y., Zhang, L., Zhang, X., Zheng, Y., Li, L., Zhu, X., Liu, Z., He, S., Yan, W., Yang, L., Xiong, J., Fu, X., Qi, S., Ren, H., Chen, S., Dai, L., Cheng, W. (2022). Crystal structure and catalytic mechanism of the *mbnBC* holoenzyme required for methanobactin biosynthesis. *Cell Research*, (November 2021). https://doi.org/10.1038/s41422-022-00620-2

49. Eckert, P., Johs, A., Semrau, J. D., DiSpirito, A. A., Richardson, J., Sarangi, R., Herndon, E., Gu, B., & Pierce, E. M. (2021). Spectroscopic and computational investigations of organometallic complexation of group 12 transition metals by methanobactins from *Methylocystis* sp. SB2. *Journal of Inorganic Biochemistry*, *223*, 111496. https://doi.org/https://doi.org/10.1016/j.jinorgbio.2021.111496

50. Einer, C., Leitzinger, C., Lichtmannegger, J., Eberhagen, C., Rieder, T., Borchard, S., Wimmer, R., Denk, G., Popper, B., Neff, F., Polishchuk, E. V., Polishchuk, R. S., Hauck, S. M., von Toerne, C., Müller, J. C., Karst, U., Baral, B. S., DiSpirito, A. A., Kremer, A. E., Semrau, J., Weiss, K. H., Hohenester, S., Zischka, H. (2019). A High-Calorie Diet Aggravates Mitochondrial Dysfunction and Triggers Severe Liver Damage in Wilson Disease Rats. *Cellular and Molecular Gastroenterology and Hepatology*, *7*(3), 571–596. https://doi.org/https://doi.org/10.1016/j.jcmgh.2018.12.005

51. El Ghazouani, A., Baslé, A., Firbank, S. J., Knapp, C. W., Gray, J., Graham, D. W., & Dennison, C. (2011). Copper-binding properties and structures of methanobactins from *Methylosinus trichosporium* OB3b. *Inorganic Chemistry*, *50*(4), 1378–1391. https://doi.org/10.1021/ic101965j

52. El Ghazouani, A., Baslé, A., Gray, J., Graham, D. W., Firbank, S. J., & Dennison, C. (2012). Variations in methanobactin structure influences copper utilization by methane-oxidizing bacteria. *Proceedings of the National Academy of Sciences*, *109*(22), 8400–8404. https://doi.org/10.1073/pnas.1112921109

53. Elango, N. A., Radhakrishnan, R., Froland, W. A., Wallar, B. J., Earhart, C. A., Lipscomb, J. D., & Ohlendorf, D. H. (1997). Crystal structure of the hydroxylase component of methane monooxygenase from *Methylosinus trichosporium* OB3b. *Protein Science*, *6*(3), 556–568. https://doi.org/https://doi.org/10.1002/pro.5560060305

54. Ettwig, K. F., Butler, M. K., Le Paslier, D., Pelletier, E., Mangenot, S., Kuypers, M. M., Schreiber, F., Dutilh, B. E., Zedelius, J., de Beer, D., Gloerich, J., Wessels, H. J., van Alen, T., Luesken, F., Wu, M. L., van de Pas-Schoonen, K. T., Op den Camp, H. J., Janssen-Megens, E. M., Francoijs, K. J., Stunnenberg, H., Weissenbach, J., Jetten, M. S. M., Strous, M. (2010). Nitrite-driven anaerobic methane oxidation by oxygenic bacteria. *Nature*, *464*(7288), 543–548. https://doi.org/10.1038/nature08883

55. Fjellbirkeland, A., Kleivdal, H., Joergensen, C., Thestrup, H., & Jensen, H. B. (1997). Outer membrane proteins of *Methylococcus capsulatus* (Bath). *Archives of Microbiology*, *168*(2), 128–135. https://doi.org/10.1007/s002030050478

56. Fjellbirkeland, A., Kruger, P. G., Bemanian, V., Høgh, B. T., Murrell, C. J., & Jensen, H. B. (2001). The C-terminal part of the surface-associated protein MopE of the methanotroph *Methylococcus capsulatus* (Bath) is secreted into the growth medium. *Archives of Microbiology*, *176*(3), 197–203. https://doi.org/10.1007/s002030100307

57. Fox, B. G., Froland, W. A., Dege, J. E., & Lipscomb, J. D. (1989). Methane monooxygenase from Methylosinus trichosporium OB3b: Purification and properties of a three-component system with high specific activity from a type II methanotroph. *Journal of Biological Chemistry*, *264*(17), 10023–10033. https://doi.org/https://doi.org/10.1016/S0021-9258(18)81762-8

58. Fox, B. G., Hendrich, M. P., Surerus, K. K., Andersson, K. K., Froland, W. A., Lipscomb, J. D., & Munck, E. (1993). Moessbauer, EPR, and ENDOR studies of the hydroxylase and reductase components of methane monooxygenase from *Methylosinus trichosporium* OB3b. *Journal of the American Chemical Society*, *115*(9), 3688–3701. https://doi.org/10.1021/ja00062a039

59. Gilman, A., Fu, Y., Hendershott, M., Chu, F., Puri, A. W., Smith, A. L., Pesesky, M., Lieberman, R., Beck, D., & Lidstrom, M. E. (2017). Oxygen-limited metabolism in the methanotroph *Methylomicrobium buryatense* 5GB1C. *PeerJ*, *5*, e3945. https://doi.org/10.7717/peerj.3945

60. Griffiths, R. I., Whiteley, A. S., O'Donnell, A. G., & Bailey, M. J. (2000). Rapid Method for Coextraction of DNA and RNA from Natural Environments for Analysis of Ribosomal DNA- and rRNA-Based Microbial Community Composition. *Applied and Environmental Microbiology*, *66*(12), 5488–5491. https://doi.org/10.1128/AEM.66.12.5488-5491.2000

61. Gu, W., Farhan Ul Haque, M., DiSpirito, A. A., & Semrau, J. D. (2016). Uptake and effect of rare earth elements on gene expression in *Methylosinus trichosporium* OB3b. *FEMS Microbiology Letters*, *363*(13), fnw129. https://doi.org/10.1093/femsle/fnw129

62. Gu, W., Farhan Ul Haque, M., Baral, B. S., Turpin, E. A., Bandow, N. L., Kremmer, E., Flatley, A., Zischka, H., DiSpirito, A. A., & Semrau, J. D. (2016). A TonB-Dependent Transporter Is Responsible for Methanobactin Uptake by *Methylosinus trichosporium* OB3b. *Applied and Environmental Microbiology*, *82*(6), 1917–1923. https://doi.org/10.1128/AEM.03884-15

63. Gu, W., Baral, B. S., DiSpirito, A. A., & Semrau, J. D. (2016). An Aminotransferase Is Responsible for the Deamination of the N-Terminal Leucine and Required for Formation of Oxazolone Ring A in Methanobactin of *Methylosinus trichosporium* OB3b. *Applied and Environmental Microbiology*, *83*(1), e02619-16. https://doi.org/10.1128/AEM.02619-16

64. Hanson, R. S., & Hanson, T. E. (1996). Methanotrophic bacteria. *Microbiological Reviews*, *60*(2), 439–471. Retrieved from http://www.ncbi.nlm.nih.gov/pubmed/8801441%0Ahttp://www.pubmedcentral.nih.gov/articlerender.fcgi?artid=PMC239451

65. Harada, N., Nakanishi, K., & Berova, N. (2012). Electronic CD Exciton Chirality Method: Principles and Applications. In *Comprehensive Chiroptical Spectroscopy* (pp. 115–166). https://doi.org/https://doi.org/10.1002/9781118120392.ch4

66. Harris, D. C. (2010). *Quantitative chemical analysis*. Macmillan.

67. Hayyan, M., Hashim, M. A., & Al Nashef, I. M. (2016). Superoxide Ion: Generation and Chemical Implications. *Chemical Reviews*, *116*(5), 3029–3085. https://doi.org/10.1021/acs.chemrev.5b00407

68. Helland, R., Fjellbirkeland, A., Karlsen, O. A., Ve, T., Lillehaug, J. R., & Jensen, H. B. (2008). An Oxidized Tryptophan Facilitates Copper Binding in *Methylococcus capsulatus*-secreted Protein MopE*. *Journal of Biological Chemistry*, *283*(20), 13897–13904. https://doi.org/10.1074/jbc.M800340200

69. Henckel, T., Roslev, P., & Conrad, R. (2000). Effects of O2 and CH4 on presence and activity of the indigenous methanotrophic community in rice field soil. *Environmental Microbiology*, *2*(6), 666–679. https://doi.org/https://doi.org/10.1046/j.1462-2920.2000.00149.x

70. Holmes, A. J., Costello, A., Lidstrom, M. E., & Murrell, J. C. (1995). Evidence that participate methane monooxygenase and ammonia monooxygenase may be evolutionarily related. *FEMS Microbiology Letters*, *132*(3), 203–208. https://doi.org/10.1016/0378-1097(95)00311-R

71. Hornak, V., Abel, R., Okur, A., Strockbine, B., Roitberg, A., & Simmerling, C. (2006). Comparison of multiple Amber force fields and development of improved protein backbone parameters. *Proteins: Structure, Function, and Bioinformatics*, *65*(3), 712–725. https://doi.org/https://doi.org/10.1002/prot.21123

72. Jiang, H., Chen, Y., Jiang, P., Zhang, C., Smith, T. J., Murrell, J. C., & Xing, X.-H. (2010). Methanotrophs: Multifunctional bacteria with promising applications in environmental bioengineering. *Biochemical Engineering Journal*, *49*(3), 277–288. https://doi.org/https://doi.org/10.1016/j.bej.2010.01.003

73. Johnson, C. L. (2006). *Methanobactin: a potential novel biopreservative for use against the foodborne pathogen Listeria monocytogenes*. Iowa State University.

74. Johnson, K. A., Ve, T., Larsen, Ø., Pedersen, R. B., Lillehaug, J. R., Jensen, H. B., … Karlsen, O. A. (2014). CorA Is a Copper Repressible Surface-Associated Copper(I)-Binding Protein Produced in *Methylomicrobium album* BG8. *PLOS ONE*, *9*(2), e87750. Retrieved from https://doi.org/10.1371/journal.pone.0087750

75. Jollie, D. R., & Lipscomb, J. D. (1991). Formate dehydrogenase from *Methylosinus trichosporium* OB3b: Purification and spectroscopic characterization of the cofactors. *Journal of Biological Chemistry*, *266*(32), 21853–21863. https://doi.org/10.1016/s0021-9258(18)54716-5

76. Jollie, D. R., & Lipscomb, J. D. B. T.-M. in E. (1990). Formate dehydrogenase from *Methylosinus trichosporium* OB3b. In *Hydrocarbons and Methylotrophy* (Vol. 188, pp. 331–334). https://doi.org/https://doi.org/10.1016/0076-6879(90)88051-B

77. Jumper, J., Evans, R., Pritzel, A., Green, T., Figurnov, M., Ronneberger, O., Tunyasuvunakool, K., Bates, R., Žídek, A., Potapenko, A., Bridgland, A., Meyer, C., Kohl, S., Ballard, A. J., Cowie, A., Romera-Paredes, B., Nikolov, S., Jain, R., Adler, J., Back, T., … Hassabis, D. (2021). Highly accurate protein structure prediction with AlphaFold. *Nature*, *596*(7873), 583–589. https://doi.org/10.1038/s41586-021-03819-2

78. Kaler, S. G. (2016). Microbial peptide de-coppers mitochondria: implications for Wilson disease. *The Journal of Clinical Investigation*, *126*(7), 2412–2414. https://doi.org/10.1172/JCI88617

79. Kalyuzhnaya, M. G., Puri, A. W., & Lidstrom, M. E. (2015). Metabolic engineering in methanotrophic bacteria. *Metabolic Engineering*, *29*, 142–152. https://doi.org/10.1016/j.ymben.2015.03.010

80. Kang, C. S., Dunfield, P. F., & Semrau, J. D. (2019). The origin of aerobic methanotrophy within the Proteobacteria. *FEMS Microbiology Letters*, *366*(9), 1–11. https://doi.org/10.1093/femsle/fnz096

81. Kang-Yun, C. S., Liang, X., Dershwitz, P., Gu, W., Schepers, A., Flatley, A., Lichtmannegger, J., Zischka, H., Zhang, L., Lu, X., Gu, B., Ledesma, J. C., Pelger, D. J., DiSpirito, A. A. & Semrau, J. D. (2022). Evidence for methanobactin “Theft” and novel chalkophore production in methanotrophs: impact on methanotrophic-mediated methylmercury degradation. *The ISME Journal*, *16*(1), 211–220. https://doi.org/10.1038/s41396-021-01062-1

82. Kenney, G. E., Dassama, L. M. K., Manesis, A. C., Ross, M. O., Chen, S., Hoffman, B. M., & Rosenzweig, A. C. (2019). mbnH is a diheme MauG-like protein associated with microbial copper homeostasis. *Journal of Biological Chemistry*. https://doi.org/10.1074/jbc.RA119.010202

83. Kenney, G. E., Dassama, L., Pandelia, M. E., Gizzi, A. S., Martinie, R. J., Gao, P., DeHart, C. J., Schachner, L. F., Skinner, O. S., Ro, S. Y., Zhu, X., Sadek, M., Thomas, P. M., Almo, S. C., Bollinger, J. M., Jr, Krebs, C., Kelleher, N. L., & Rosenzweig, A. C. (2018). The biosynthesis of methanobactin. *Science*, *359*(6382), 1411–1416. https://doi.org/10.1126/science.aap9437

84. Kenney, G. E., Goering, A. W., Ross, M. O., DeHart, C. J., Thomas, P. M., Hoffman, B. M., Kelleher, N. L., & Rosenzweig, A. C. (2016). Characterization of Methanobactin from *Methylosinus* sp. LW4. *Journal of the American Chemical Society*, *138*(35), 11124–11127. https://doi.org/10.1021/jacs.6b06821

85. Kenney, G. E., & Rosenzweig, A. C. (2012). Chemistry and Biology of the Copper Chelator Methanobactin. *ACS Chemical Biology*, *7*(2), 260–268. https://doi.org/10.1021/cb2003913

86. Kenney, G. E., & Rosenzweig, A. C. (2013). Genome mining for methanobactins. *BMC Biology*, *11*(1), 17. https://doi.org/10.1186/1741-7007-11-17

87. Kenney, G. E., Sadek, M., & Rosenzweig, A. C. (2016). Copper-responsive gene expression in the methanotroph *Methylosinus trichosporium* OB3b. *Metallomics*, *8*(9), 931–940. https://doi.org/10.1039/c5mt00289c

88. Kim, H. J., Graham, D. W., DiSpirito, A. A., Alterman, M. A., Galeva, N., Larive, C. K., Asunskis, D., & Sherwood, P. M. (2004). Methanobactin a Copper-Acquisition Compound from Methane-Oxidizing Bacteria. *Science*, *305*(274), 935–939. https://doi.org/10.1086/275028

89. Kits, K. D., Klotz, M. G., & Stein, L. Y. (2015). Methane oxidation coupled to nitrate reduction under hypoxia by the Gammaproteobacterium Methylomonas denitrificans, sp. nov. type strain FJG1. *Environmental Microbiology*, *17*(9), 3219–3232. https://doi.org/https://doi.org/10.1111/1462-2920.12772

90. Koo, C. W., Tucci, F. J., He, Y., & Rosenzweig, A. C. (2022). Recovery of particulate methane monooxygenase structure and activity in a lipid bilayer. *Science*, *375*(6586), 1287–1291. https://doi.org/10.1126/science.abm3282

91. Krentz, B. D., Mulheron, H. J., Semrau, J. D., Dispirito, A. A., Bandow, N. L., Haft, D. H., Vuilleumier, S., Murrell, J. C., McEllistrem, M. T., Hartsel, S. C., & Gallagher, W. H. (2010). A Comparison of Methanobactins from *Methylosinus trichosporium* OB3b and *Methylocystis* Strain SB2 Predicts Methanobactins Are Synthesized from Diverse Peptide Precursors Modified To Create a Common Core for Binding and Reducing Copper Ions. *Biochemistry*, *49*(47), 10117–10130. https://doi.org/10.1021/bi1014375

92. Le, V. H., Buscaglia, R., Chaires, J. B., & Lewis, E. A. (2013). Modeling complex equilibria in isothermal titration calorimetry experiments: Thermodynamic parameters estimation for a three-binding-site model. *Analytical Biochemistry*, *434*(2), 233–241. https://doi.org/https://doi.org/10.1016/j.ab.2012.11.030

93. Lee, H. J., Jeong, S. E., Kim, P. J., Madsen, E., & Jeon, C. O. (2015). High resolution depth distribution of Bacteria, Archaea, methanotrophs, and methanogens in the bulk and rhizosphere soils of a flooded rice paddy . *Frontiers in Microbiology* , Vol. 6. Retrieved from https://www.frontiersin.org/articles/10.3389/fmicb.2015.00639

94. Lee, S. J., McCormick, M. S., Lippard, S. J., & Cho, U.-S. (2013). Control of substrate access to the active site in methane monooxygenase. *Nature*, *494*(7437), 380–384. https://doi.org/10.1038/nature11880

95. Li, Y.-M., Milne, J. C., Madison, L. L., Kolter, R., & Walsh, C. T. (1996). From Peptide Precursors to Oxazole and Thiazole-Containing Peptide Antibiotics: Microcin B17 Synthase. *Science*, *274*(5290), 1188–1193. https://doi.org/10.1126/science.274.5290.1188

96. Liang, L., Wang, Y., Sivan, O., & Wang, F. (2019). Metal-dependent anaerobic methane oxidation in marine sediment: Insights from marine settings and other systems. *Science China Life Sciences*, *62*(10), 1287–1295. https://doi.org/10.1007/s11427-018-9554-5

97. Lichtmannegger, J., Leitzinger, C., Wimmer, R., Schmitt, S., Schulz, S., Kabiri, Y., Eberhagen, C., Rieder, T., Janik, D., Neff, F., Straub, B. K., Schirmacher, P., DiSpirito, A. A., Bandow, N., Baral, B. S., Flatley, A., Kremmer, E., Denk, G., Reiter, F. P., Hohenester, S., Eckardt-Schupp, F., Dencher, N. A., Adamski, J., Sauer, V., Niemietz, C., Schmidt, H. H. J., Merle, U., Gotthardt, D. N., Kroemer, G., Weiss, K. H., Zischka, H. (2016). Methanobactin reverses acute liver failure in a rat model of Wilson disease. *The Journal of Clinical Investigation*, *126*(7), 2721–2735. https://doi.org/10.1172/JCI85226

98. Lieberman, R. L., & Rosenzweig, A. C. (2005). Crystal structure of a membrane-bound metalloenzyme that catalyses the biological oxidation of methane. *Nature*, *434*(7030), 177–182. https://doi.org/10.1038/nature03311

99. Liew, E. F., Tong, D., Coleman, N. V, & Holmes, A. J. (2014). Mutagenesis of the hydrocarbon monooxygenase indicates a metal centre in subunit-C, and not subunit-B, is essential for copper-containing membrane monooxygenase activity. *Microbiology (Reading, England)*, *160*(Pt 6), 1267–1277. https://doi.org/10.1099/mic.0.078584-0

100. Lindqvist, Y., Koskiniemi, H., Jansson, A., Sandalova, T., Schnell, R., Liu, Z., Mäntsälä, P., Niemi, J., & Schneider, G. (2009). Structural Basis for Substrate Recognition and Specificity in Aklavinone-11-Hydroxylase from Rhodomycin Biosynthesis. *Journal of Molecular Biology*, *393*(4), 966–977. https://doi.org/https://doi.org/10.1016/j.jmb.2009.09.003

101. Lipscomb, J. D. (1994). Biochemistry of the Soluble Methane Monooxygenase. *Annual Review of Microbiology*, *48*(1), 371–399. https://doi.org/10.1146/annurev.mi.48.100194.002103

102. Liu, J., Wu, P., Yan, S., Li, Y., Cao, Z., & Wang, B. (2021). Spin-Regulated Inner-Sphere Electron Transfer Enables Efficient O—O Bond Activation in Nonheme Diiron Monooxygenase MIOX. *ACS Catalysis*, 6141–6152. https://doi.org/10.1021/acscatal.1c00898

103. Lu, X., Gu, W., Zhao, L., Farhan Ul Haque, M., DiSpirito, A. A., Semrau, J. D., & Gu, B. (2017). Methylmercury uptake and degradation by methanotrophs. *Science Advances*, *3*(5), e1700041. https://doi.org/10.1126/sciadv.1700041

104. Mandal, M., Kawashima, K., Saito, K., & Ishikita, H. (2020). Redox Potential of the Oxygen-Evolving Complex in the Electron Transfer Cascade of Photosystem II. *The Journal of Physical Chemistry Letters*, *11*(1), 249–255. https://doi.org/10.1021/acs.jpclett.9b02831

105. Martin, H., & Murrell, J. C. (1995). Methane monooxygenase mutants of *Methylosinus trichosporium* constructed by marker-exchange mutagenesis. *FEMS Microbiology Letters*, *127*(3), 243–248. https://doi.org/10.1111/j.1574-6968.1995.tb07480.x

106. Martinho, M., Choi, D. W., DiSpirito, A. A., Antholine, W. E., Semrau, J. D., & Münck, E. (2007). Mössbauer Studies of the Membrane-Associated Methane Monooxygenase from *Methylococcus capsulatus* Bath: Evidence for a Diiron Center. *Journal of the American Chemical Society*, *129*(51), 15783–15785. https://doi.org/10.1021/ja077682b

107. McCoy, A. J. (2007). Solving structures of protein complexes by molecular replacement with {\it Phaser}. *Acta Crystallographica Section D*, *63*(1), 32–41. https://doi.org/10.1107/S0907444906045975

108. Meruvu, H., Wu, H., Jiao, Z., Wang, L., & Fei, Q. (2020). From nature to nurture: Essence and methods to isolate robust methanotrophic bacteria. *Synthetic and Systems Biotechnology*, *5*(3), 173–178. https://doi.org/https://doi.org/10.1016/j.synbio.2020.06.007

109. Milucka, J., Kirf, M., Lu, L., Krupke, A., Lam, P., Littmann, S., Kuypers, M. M., & Schubert, C. J. (2015). Methane oxidation coupled to oxygenic photosynthesis in anoxic waters. *The ISME Journal*, *9*(9), 1991–2002. https://doi.org/10.1038/ismej.2015.12

110. Moody, M. D., & Dailey, H. A. (1983). Aerobic ferrisiderophore reductase assay and activity stain for native polyacrylamide gels. *Analytical Biochemistry*, *134*(1), 235–239. https://doi.org/https://doi.org/10.1016/0003-2697(83)90290-7

111. Müller, J. C., Lichtmannegger, J., Zischka, H., Sperling, M., & Karst, U. (2018). High spatial resolution LA-ICP-MS demonstrates massive liver copper depletion in Wilson disease rats upon Methanobactin treatment. *Journal of Trace Elements in Medicine and Biology*, *49*(May), 119–127. https://doi.org/10.1016/j.jtemb.2018.05.009

112. Murrell, J. C., McDonald, I. R., & Gilbert, B. (2000). Regulation of expression of methane monooxygenases by copper ions. *Trends in Microbiology*, *8*(5), 221–225. https://doi.org/10.1016/S0966-842X(00)01739-X

113. Neilands, J. B. (1995). Siderophores: Structure and Function of Microbial Iron Transport Compounds. *Journal of Biological Chemistry*, *270*(45), 26723–26726. https://doi.org/10.1074/jbc.270.45.26723

114. Nicholls, P., Fita, I., & Loewen, P. C. (2000). Enzymology and structure of catalases. *Advances in Inorganic Chemistry*, *51*, 51-106. https://doi.org/10.1016/S0898-8838(00)51001-0

115. Nielsen, A. K., Gerdes, K., & Murrell, J. C. (1997). Copper-dependent reciprocal transcriptional regulation of methane monooxygenase genes in Methylococcus capsulatus and Methylosinus trichosporium. *Molecular Microbiology*, *25*(2), 399–409. https://doi.org/https://doi.org/10.1046/j.1365-2958.1997.4801846.x

116. Ogra, Y., Aoyama, M., & Suzuki, K. T. (2006). Protective role of metallothionein against copper depletion. *Archives of Biochemistry and Biophysics*, *451*(2), 112–118. https://doi.org/https://doi.org/10.1016/j.abb.2006.04.017

117. Oswald, K., Jegge, C., Tischer, J., Berg, J., Brand, A., Miracle, M. R., Soria, X., Vicente, E., Lehmann, M. F., Zopfi, J., & Schubert, C. J. (2016). Methanotrophy under Versatile Conditions in the Water Column of the Ferruginous Meromictic Lake La Cruz (Spain) . *Frontiers in Microbiology* , Vol. 7. Retrieved from https://www.frontiersin.org/articles/10.3389/fmicb.2016.01762

118. Oswald, K., Milucka, J., Brand, A., Littmann, S., Wehrli, B., Kuypers, M. M. M., & Schubert, C. J. (2015). Light-Dependent Aerobic Methane Oxidation Reduces Methane Emissions from Seasonally Stratified Lakes. *PLOS ONE*, *10*(7), e0132574. Retrieved from https://doi.org/10.1371/journal.pone.0132574

119. Park, Y. J., Jodts, R. J., Slater, J. W., Reyes, R. M., Winton, V. J., Montaser, R. A., Thomas, P. M., Dowdle, W. B., Ruiz, A., Kelleher, N. L., Bollinger Jr., J. M., Krebs, C., Hoffman, B. M., Thomas, P. M., Rosenzweig, A. C. (2022). A mixed-valent Fe(II)Fe(III) species converts cysteine to an oxazolone/thioamide pair in methanobactin biosynthesis. *Proceedings of the National Academy of Sciences of the United States of America*, *119*(13), e2123566119. https://doi.org/10.1073/pnas.2123566119

120. Peng, P., Gu, W., DiSpirito, A. A., & Semrau, J. D. (2022). Multiple Mechanisms for Copper Uptake by Methylosinus trichosporium OB3b in the Presence of Heterologous Methanobactin. *MBio*. https://doi.org/10.1128/mbio.02239-22

121. Peng, P., Kang-Yun, C. S., Chang, J., Gu, W., DiSpirito, A. A., & Semrau, J. D. (2022). Two TonB-Dependent Transporters in Methylosinus trichosporium OB3b Are Responsible for Uptake of Different Forms of Methanobactin and Are Involved in the Canonical “Copper Switch.” *Applied and Environmental Microbiology*, *88*(1), e01793-21. https://doi.org/10.1128/AEM.01793-21

122. Pesch, M. L., Hoffmann, M., Christl, I., Kraemer, S. M., & Kretzschmar, R. (2013). Competitive ligand exchange between Cu–humic acid complexes and methanobactin. *Geobiology*, *11*(1), 44–54. https://doi.org/https://doi.org/10.1111/gbi.12010

123. Picone, N., & Op den Camp, H. J. M. (2019). Role of rare earth elements in methanol oxidation. *Current Opinion in Chemical Biology*, *49*, 39–44. https://doi.org/https://doi.org/10.1016/j.cbpa.2018.09.019

124. Read, J., Gill, R., Dales, S. L., Cooper, J. B., Wood, S. P., & Anthony, C. (1999). The molecular structure of an unusual cytochrome c2 determined at 2.0 å; the cytochrome ch from M*ethylobacterium extorquens*. *Protein Science*, *8*(6), 1232–1240. https://doi.org/https://doi.org/10.1110/ps.8.6.1232

125. Rhee, S.-K., Awala, S. I., & Nguyen, N.-L. (2019). Enrichment and Isolation of Aerobic and Anaerobic Methanotrophs. In E. Y. Lee (Ed.), *Methanotrophs: Microbiology Fundamentals and Biotechnological Applications* (pp. 39–69). https://doi.org/10.1007/978-3-030-23261-0_2

126. Ro, S. Y., & Rosenzweig, A. C. (2018). Recent Advances in the Genetic Manipulation of *Methylosinus trichosporium* OB3b. In *Methods in Enzymology* (1st ed., Vol. 605). https://doi.org/10.1016/bs.mie.2018.02.011

127. Robinson, N. J. (2008). A bacterial copper metallothionein. *Nature Chemical Biology*, *4*(10), 582–583. https://doi.org/10.1038/nchembio1008-582

128. Ross, M. O., MacMillan, F., Wang, J., Nisthal, A., Lawton, T. J., Olafson, B. D., Mayo, S. L., Rosenzweig, A. C., & Hoffman, B. M. (2019). Particulate methane monooxygenase contains only mononuclear copper centers. *Science*, *364*(6440), 566–570. https://doi.org/10.1126/science.aav2572

129. Ryan, K. S., Chakraborty, S., Howard-Jones, A. R., Walsh, C. T., Ballou, D. P., & Drennan, C. L. (2008). The FAD Cofactor of RebC Shifts to an IN Conformation upon Flavin Reduction,. *Biochemistry*, *47*(51), 13506–13513. https://doi.org/10.1021/bi801229w

130. Scanlan, J., Dumont, M. G., & Murrell, J. C. (2009). Involvement of MmoR and MmoG in the transcriptional activation of soluble methane monooxygenase genes in Methylosinus trichosporium OB3b. *FEMS Microbiology Letters*, *301*(2), 181–187. https://doi.org/10.1111/j.1574-6968.2009.01816.x

131. Schalk, I. J. (2008). Metal trafficking via siderophores in Gram-negative bacteria: Specificities and characteristics of the pyoverdine pathway. *Journal of Inorganic Biochemistry*, *102*(5), 1159–1169. https://doi.org/https://doi.org/10.1016/j.jinorgbio.2007.11.017

132. Semrau, J. D., DiSpirito, A. A., Gu, W., & Yoon, S. (2018). Metals and Methanotrophy. *Applied and Environmental Microbiology*, *84*(6), e02289--17. https://doi.org/10.1128/AEM.02289-17

133. Semrau, J. D., & DiSpirito, A. A. (2019). *Methanobactin: A Novel Copper-Binding Compound Produced by Methanotrophs BT - Methanotrophs: Microbiology Fundamentals and Biotechnological Applications* (E. Y. Lee, Ed.). https://doi.org/10.1007/978-3-030-23261-0_7

134. Semrau, J. D., Dispirito, A. A., Gu, W., Yoon, S. (2019). *Methanotrophs: Microbiology Fundamentals and Biotechnological Applications* (Vol. 84).

135. Semrau, J. D., Dispirito, A. A., Obulisamy, P. K., & Kang-Yun, C. S. (2020). Methanobactin from methanotrophs: Genetics, structure, function and potential applications. *FEMS Microbiology Letters*. https://doi.org/10.1093/femsle/fnaa045

136. Semrau, J. D., DiSpirito, A. A., & Yoon, S. (2010). Methanotrophs and copper. *FEMS Microbiology Reviews*, *34*(4), 496–531. https://doi.org/10.1111/j.1574-6976.2010.00212.x

137. Semrau, J. D., Jagadevan, S., DiSpirito, A. A., Khalifa, A., Scanlan, J., Bergman, B. H., Freemeier, B. C., Baral, B. S., Bandow, N. L., Vorobev, A., Haft, D. H., Vuilleumier, S., & Murrell, J. C. (2013). Methanobactin and MmoD work in concert to act as the 'copper-switch' in methanotrophs. *Environmental Microbiology*, *15*(11), 3077–3086. https://doi.org/https://doi.org/10.1111/1462-2920.12150

138. Simon, R. (1984). High frequency mobilization of gram-negative bacterial replicons by the in vitro constructed Tn5-Mob transposon. *Molecular and General Genetics MGG*, *196*(3), 413–420. https://doi.org/10.1007/BF00436188

139. Singh, B. K., Bardgett, R. D., Smith, P., & Reay, D. S. (2010). Microorganisms and climate change: terrestrial feedbacks and mitigation options. *Nature Reviews Microbiology*, *8*(11), 779–790. https://doi.org/10.1038/nrmicro2439

140. Smith, T. J., Slade, S. E., Burton, N. P., Murrell, J. C., & Dalton, H. (2002). Improved System for Protein Engineering of the Hydroxylase Component of Soluble Methane Monooxygenase. *Applied and Environmental Microbiology*, *68*(11), 5265–5273. https://doi.org/10.1128/AEM.68.11.5265-5273.2002

141. Söhngen, N. L. (1906). Über bakterien, welche methan als kohlenstoffnahrung und energiequelle gebrauchen. *Zentrabl Bakteriol Parasitenk Infektionskr*, *15*, 513–517.

142. Stafford, G. P., Scanlan, J., McDonald, I. R., & Murrell, J. C. (2003). rpoN, mmoR and mmoG, genes involved in regulating the expression of soluble methane monooxygenase in *Methylosinus trichosporium* OB3b. *Microbiology (Reading, England)*, *149*(Pt 7), 1771–1784. https://doi.org/10.1099/mic.0.26060-0

143. Stanley, S. H., Prior, S. D., Leak, D. J., & Dalton, H. (1983). Copper stress underlies the fundamental change in intracellular location of methane mono-oxygenase in methane-oxidizing organisms: Studies in batch and continuous cultures. *Biotechnology Letters*, *5*(7), 487–492. https://doi.org/10.1007/BF00132233

144. Storhoff, J. J., Lazarides, A. A., Mucic, R. C., Mirkin, C. A., Letsinger, R. L., & Schatz, G. C. (2000). What Controls the Optical Properties of DNA-Linked Gold Nanoparticle Assemblies? *Journal of the American Chemical Society*, *122*(19), 4640–4650. https://doi.org/10.1021/ja993825l

145. Summer, K. H., Lichtmannegger, J., Bandow, N., Choi, D. W., DiSpirito, A. A., & Michalke, B. (2011). The biogenic methanobactin is an effective chelator for copper in a rat model for Wilson disease. *Journal of Trace Elements in Medicine and Biology*, *25*(1), 36–41. https://doi.org/https://doi.org/10.1016/j.jtemb.2010.12.002

146. Sung-Woo, L., R., K. D., Dong-Hee, L., A., D. A., & D., S. J. (2006). Mixed Pollutant Degradation by *Methylosinus trichosporium* OB3b Expressing either Soluble or Particulate Methane Monooxygenase: Can the Tortoise Beat the Hare? *Applied and Environmental Microbiology*, *72*(12), 7503–7509. https://doi.org/10.1128/AEM.01604-06

147. Suzuki, K. T., Someya, A., Komada, Y., & Ogra, Y. (2002). Roles of metallothionein in copper homeostasis: responses to Cu-deficient diets in mice. *Journal of Inorganic Biochemistry*, *88*(2), 173–182. https://doi.org/https://doi.org/10.1016/S0162-0134(01)00376-2

148. Thi, D., Nguyen, N., Lee, O. K., Nguyen, T. T., & Lee, E. Y. (2021). Type II methanotrophs : A promising microbial cell-factory platform for bioconversion of methane to chemicals. *Biotechnology Advances*, *47*(February), 107700. https://doi.org/10.1016/j.biotechadv.2021.107700

149. Tinberg, C. E., & Lippard, S. J. (2011). Dioxygen Activation in Soluble Methane Monooxygenase. *Accounts of Chemical Research*, *44*(4), 280–288. https://doi.org/10.1021/ar1001473

150. van Grinsven, S., Sinninghe Damsté, J. S., Harrison, J., & Villanueva, L. (2020). Impact of Electron Acceptor Availability on Methane-Influenced Microorganisms in an Enrichment Culture Obtained From a Stratified Lake . *Frontiers in Microbiology* , Vol. 11. Retrieved from https://www.frontiersin.org/articles/10.3389/fmicb.2020.00715

151. Varadi, M., Anyango, S., Deshpande, M., Nair, S., Natassia, C., Yordanova, G., Yuan, D., Stroe, O., Wood, G., Laydon, A., Žídek, A., Green, T., Tunyasuvunakool, K., Petersen, S., Jumper, J., Clancy, E., Green, R., Vora, A., Lutfi, M., Figurnov, M., Cowie, A., Hobbs, N., Kohli, P., Kleywegt, G., Birney, E., Hassabis, D., Velankar, S. (2022). AlphaFold Protein Structure Database: massively expanding the structural coverage of protein-sequence space with high-accuracy models. *Nucleic Acids Research*, *50*(D1), D439–D444. https://doi.org/10.1093/nar/gkab1061

152. Vass, I., & Styring, S. (1991). pH-Dependent charge equilibria between tyrosine-D and the S states in photosystem II. Estimation of relative midpoint redox potentials. *Biochemistry*, *30*(3), 830–839. https://doi.org/10.1021/bi00217a037

153. Ve, T., Mathisen, K., Helland, R., Karlsen, O. A., Fjellbirkeland, A., Røhr, Å. K., Andersson, K. K., Pedersen, R. B., Lillehaug, J. R., & Jensen, H. B. (2012). The Methylococcus capsulatus (Bath) Secreted Protein, MopE*, Binds Both Reduced and Oxidized Copper. *PLOS ONE*, *7*(8), e43146. Retrieved from https://doi.org/10.1371/journal.pone.0043146

154. Vita, N., Landolfi, G., Baslé, A., Platsaki, S., Lee, J., Waldron, K. J., & Dennison, C. (2016). Bacterial cytosolic proteins with a high capacity for Cu(I) that protect against copper toxicity. *Scientific Reports*, *6*(1), 39065. https://doi.org/10.1038/srep39065

155. Vita, N., Platsaki, S., Baslé, A., Allen, S. J., Paterson, N. G., Crombie, A. T., Murrell, J. C., Waldron, K. J., & Dennison, C. (2015). A four-helix bundle stores copper for methane oxidation. *Nature*, *525*(7567), 140–143. https://doi.org/10.1038/nature14854

156. Vorholt, J. A. (2002). Cofactor-dependent pathways of formaldehyde oxidation in methylotrophic bacteria. *Archives of Microbiology*, *178*(4), 239–249. https://doi.org/10.1007/s00203-002-0450-2

157. Vorholt, J. A., Chistoserdova, L., Lidstrom, M. E., & Thauer, R. K. (1998). The NADP-Dependent Methylene Tetrahydromethanopterin Dehydrogenase in *Methylobacterium extorquens* AM1. *Journal of Bacteriology*, *180*(20), 5351–5356. https://doi.org/10.1128/JB.180.20.5351-5356.1998

158. Vorholt, J. A., Chistoserdova, L., Stolyar, S. M., Thauer, R. K., & Lidstrom, M. E. (1999). Distribution of Tetrahydromethanopterin-Dependent Enzymes in Methylotrophic Bacteria and Phylogeny of Methenyl Tetrahydromethanopterin Cyclohydrolases. *Journal of Bacteriology*, *181*(18), 5750–5757. https://doi.org/10.1128/JB.181.18.5750-5757.1999

159. Ward, N., Larsen, Ø., Sakwa, J., Bruseth, L., Khouri, H., Durkin, A. S., Dimitrov, G., Jiang, L., Scanlan, D., Kang, K. H., Lewis, M., Nelson, K. E., Methé, B., Wu, M., Heidelberg, J. F., Paulsen, I. T., Fouts, D., Ravel, J., Tettelin, H., Ren, Q., Read, T., DeBoy, R. T., Seshadri, R., Salzberg, S. L., Jensen, H. B., Birkeland, N. K., Nelson, W. C., Dodson, R. J., Grindhaug, S. H., Holt, I., Eidhammer, I., Jonasen, I., Vanaken, S., Utterback, T., Feldblyum, T. V., Fraser, C. M., Lillehaug, J. R., Eisen, J. A. (2004). Genomic Insights into Methanotrophy: The Complete Genome Sequence of Methylococcus capsulatus (Bath). *PLOS Biology*, *2*(10), null. https://doi.org/10.1371/journal.pbio.0020303

160. Whittenbury, R., Phillips, K. C., & Wilkinson, J. F. (1970). Enrichment, Isolation and Some Properties of Methane-utilizing Bacteria. *Journal of General Microbiology*, *61*(2), 205–218. https://doi.org/10.1099/00221287-61-2-205

161. Williams, P. A., Coates, L., Mohammed, F., Gill, R., Erskine, P. T., Coker, A., Wood, S. P., Anthony, C., & Cooper, J. B. (2005). The atomic resolution structure of methanol dehydrogenase from *Methylobacterium extorquens*. *Acta Crystallographica Section D*, *61*(1), 75–79. Retrieved from https://doi.org/10.1107/S0907444904026964

162. Yoch, D. C., Chen, Y. P., & Hardin, M. G. (1990). Formate dehydrogenase from the methane oxidizer *Methylosinus trichosporium* OB3b. *Journal of Bacteriology*, *172*(8), 4456–4463. https://doi.org/10.1128/jb.172.8.4456-4463.1990

163. Youngblut, M. D., Tsai, C. L., Clark, I. C., Carlson, H. K., Maglaqui, A. P., Gau-Pan, P. S., Redford, S. A., Wong, A., Tainer, J. A., & Coates, J. D. (2016). Perchlorate Reductase Is Distinguished by Active Site Aromatic Gate Residues. *Journal of Biological Chemistry*, *291*(17), 9190–9202. https://doi.org/10.1074/jbc.M116.714618

164. Zahn, J. A., & DiSpirito, A. A. (1996). Membrane-associated methane monooxygenase from *Methylococcus capsulatus* (Bath). *Journal of Bacteriology*, *178*(4), 1018–1029. https://doi.org/10.1128/jb.178.4.1018-1029.1996

165. Zahn, J. A., Bergmann, D. J., Boyd, J. M., Kunz, R. C., & DiSpirito, A. A. (2001). Membrane-Associated Quinoprotein Formaldehyde Dehydrogenase from *Methylococcus capsulatus* Bath. *Journal of Bacteriology*, *183*(23), 6832–6840. https://doi.org/10.1128/JB.183.23.6832-6840.2001

166. Zannoni, D. (2004). *Respiration in archaea and bacteria*. Springer.

167. Zhao, P., Li, N., & Astruc, D. (2013). State of the art in gold nanoparticle synthesis. *Coordination Chemistry Reviews*, *257*(3), 638–665. https://doi.org/https://doi.org/10.1016/j.ccr.2012.09.002

168. Zheng, Y., Wang, H., Liu, Y., Zhu, B., Li, J., Yang, Y., Qin, W., Chen, L., Wu, X., Chistoserdova, L., Zhao, F. (2020). Methane-Dependent Mineral Reduction by Aerobic Methanotrophs under Hypoxia. *Environmental Science & Technology Letters*, *7*(8), 606–612. https://doi.org/10.1021/acs.estlett.0c00436

169. Zischka, H., Lichtmannegger, J., DiSpirito, A. A., & Semrau, J. D. (2021, December 2). *Means and methods for treating copper-related diseases*. International Patent application WO 2017/103094 A2 (**2020**); US Patent **11,000,568 B2** (**2021**).
170. Zischka, H., Lichtmannegger, J., Schmitt, S., Jägemann, N., Schulz, S., Wartini, D., Jennen, L., Rust, C., Larochette, N., Galluzzi, L., Chajes, V., Bandow, N., Gilles, V. S., DiSpirito, A. A., Esposito, I., Goettlicher, M., Summer, K. H., & Kroemer, G. (2011). Liver mitochondrial membrane crosslinking and destruction in a rat model of Wilson disease. *The Journal of Clinical Investigation*, *121*(4), 1508–1518. https://doi.org/10.1172/JCI45401

Figures

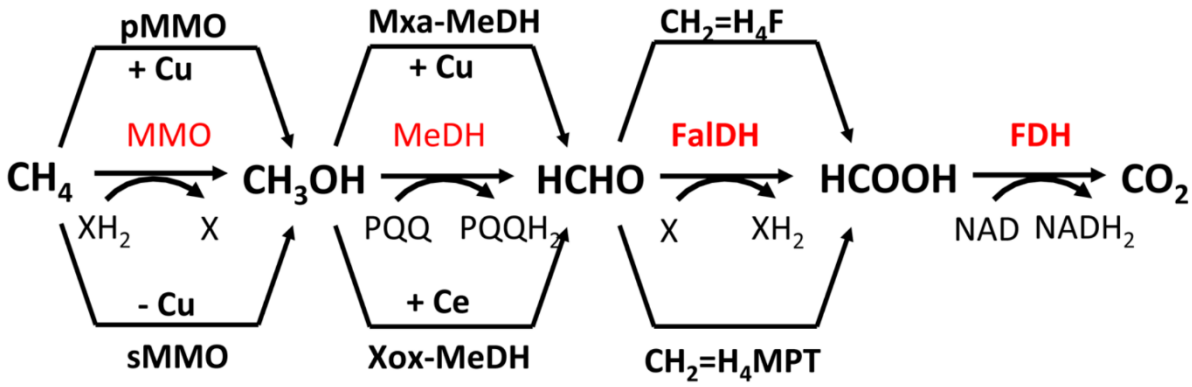

Figure 1. Schematic diagram of methane oxidation to carbon dioxide in a methanotroph Methylococcus capsulatus Bath. Abbreviations: sMMO, soluble MMO; pMMO, membrane associated MMO; Mxa-MeDH, Ca-dependent MeDH; XoX-MeDH, rare earth dependent MeDH; CH3=H4F, methylene tetrahydrofolate; CH3H4MPT, methylene tetrahydromethopterin. Figure provided by J.D. Semrau, University of Michigan.

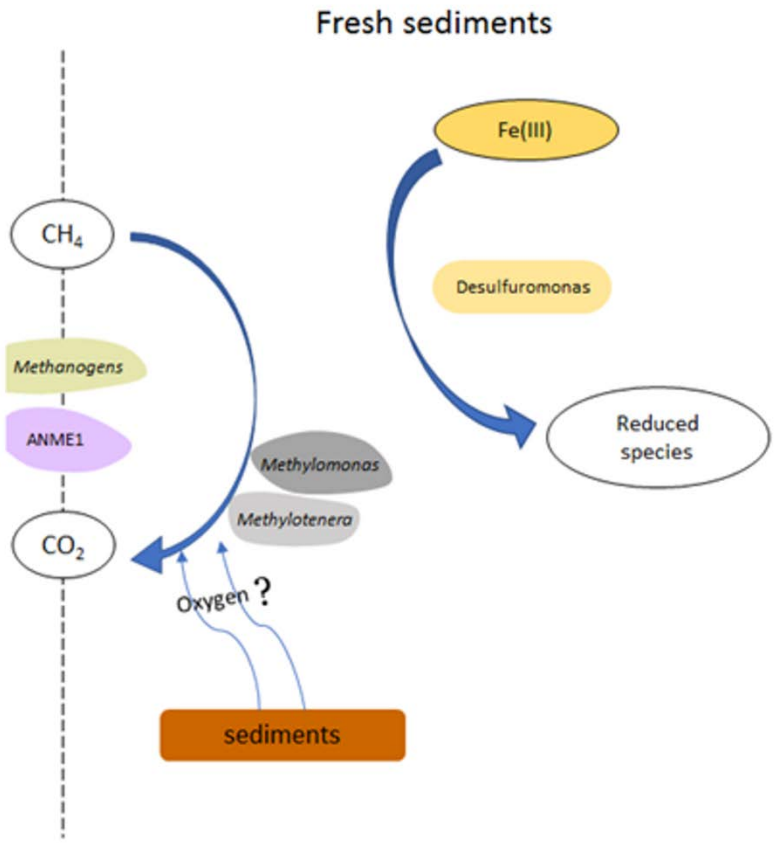

Figure 2. Diagram of carbon cycling in anaerobic methane oxidation. Figure provided by Orit Sivan, Ben Gurion University.

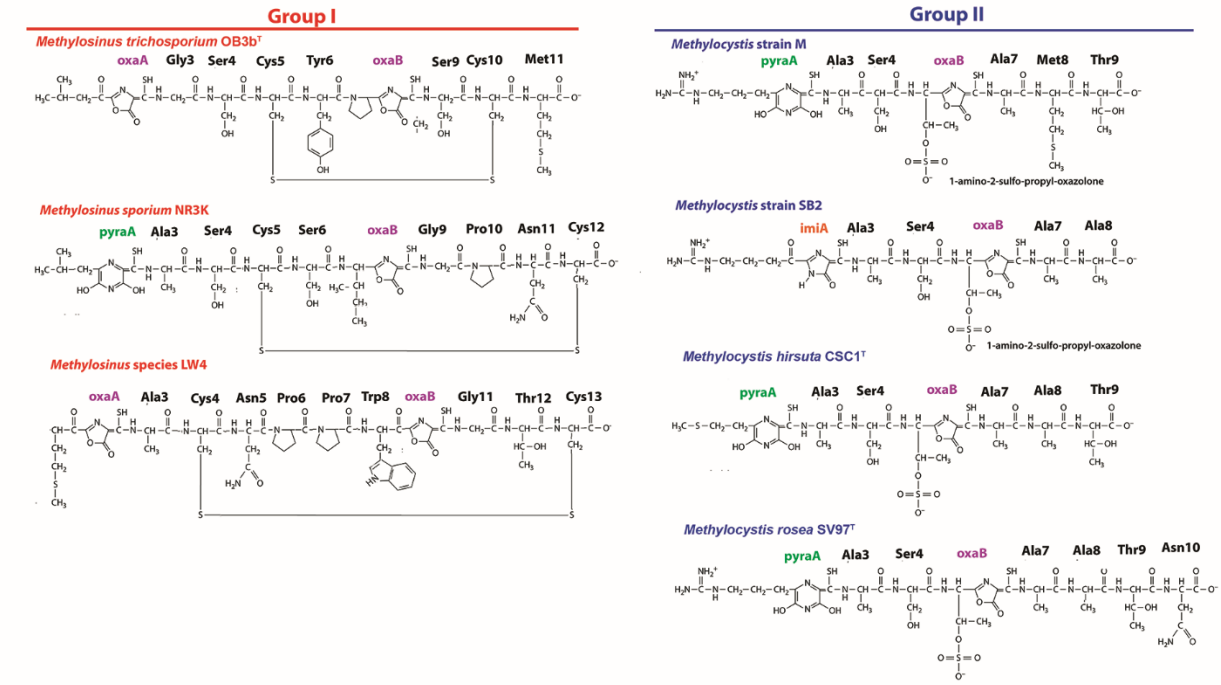

Figure 3. Structures of structurally characterized methanobactins, divided by group. From Semrau *et al.*, 2010.

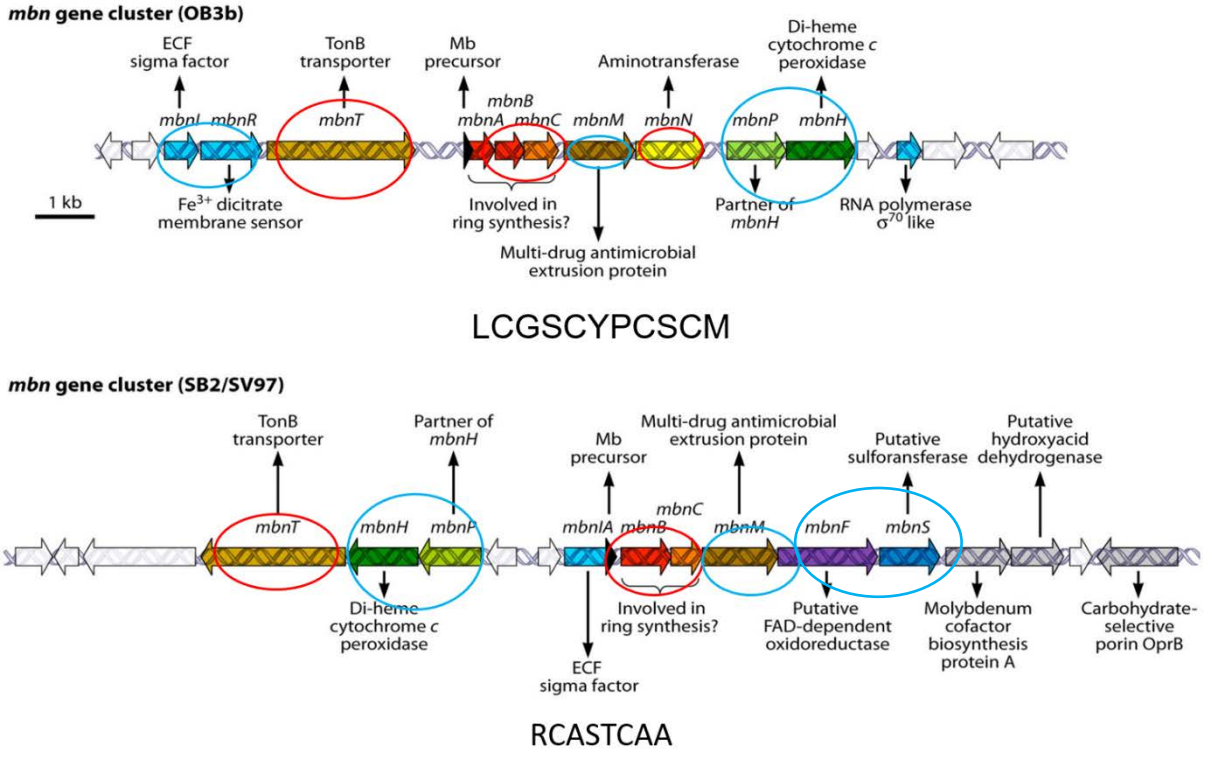

Figure 4. Methanobactin operons from Group I (top) and Group II (bottom) methanobactins, showing the myriad genes involved in the methanotroph's copper acquisition system. Some genes have been structurally characterized (red) while others have been inferred bioinformatically (blue). Adapted from DiSpirito *et al.*, 2010.

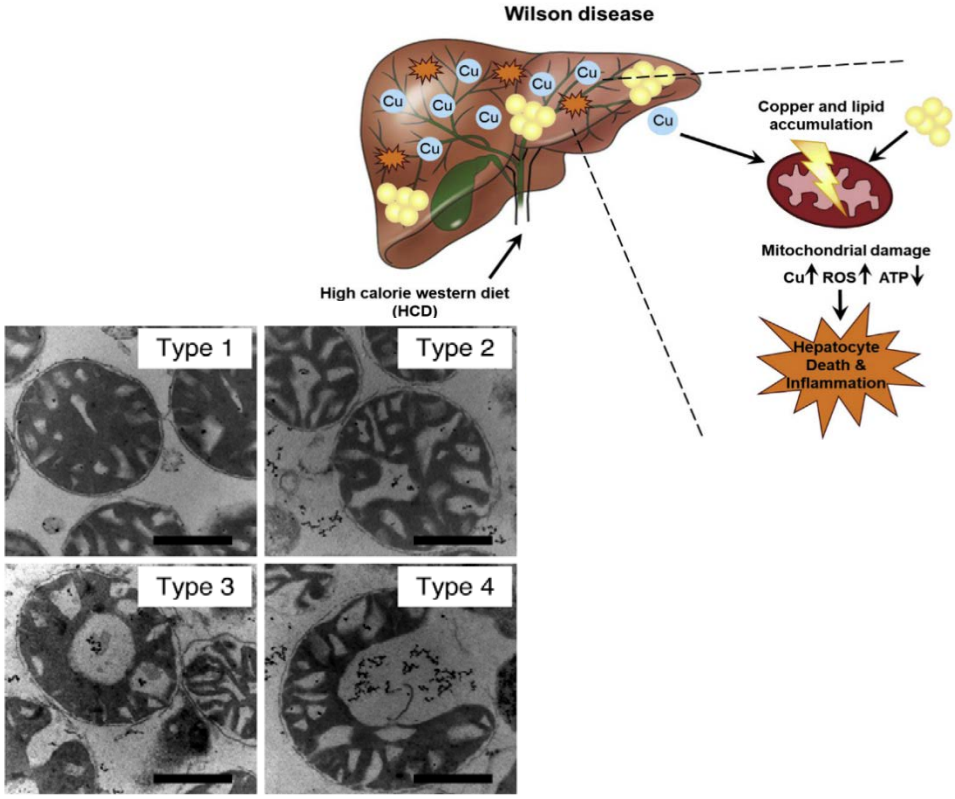

Figure 5. Images of mitochondria disruption due to Wilson's disease. Also shown is a cartoon of the mechanism of copper toxicity from copper accumulation. From Leitzinger *et al.*, 2019.

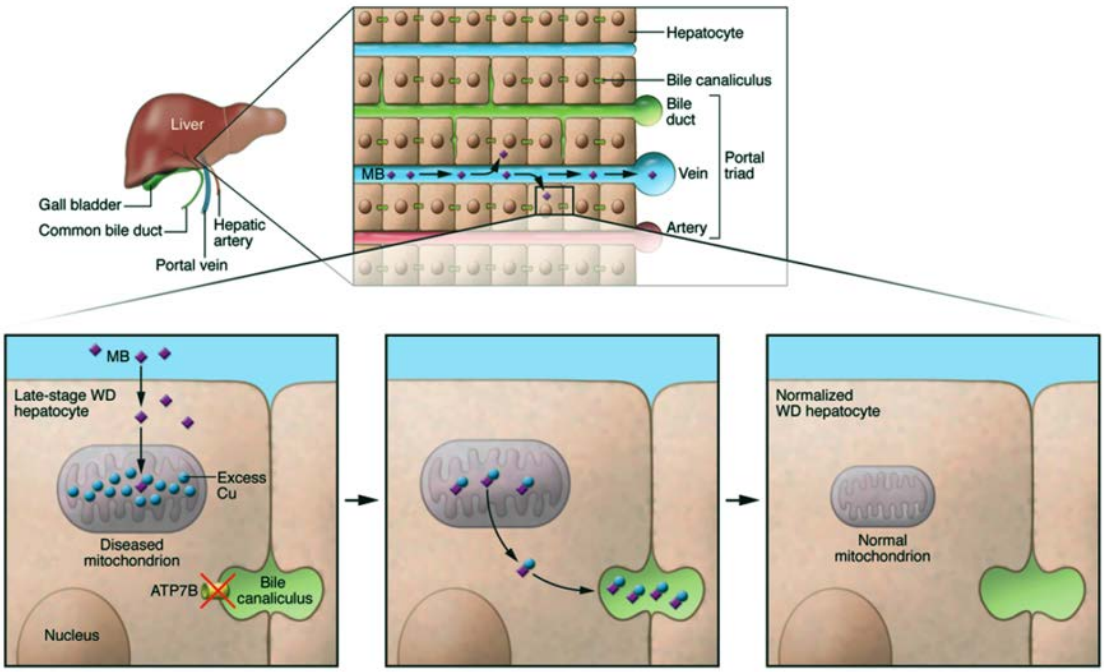

Figure 6. A diagram showing the arrangement of cells in the liver (top), the route by which methanobactin accesses copper deposits (top and left panel), the point of failure in patients with Wilson disease (left panel), and the route of copper excretion after it is bound by methanobactin (center panel). From Kaler, 2016.

CHAPTER 2. OXYGEN GENERATION VIA WATER SPLITTING BY A NOVEL BIOGENIC METAL BINDING COMPOUND

Philip Dershwitz[1], Nathan L. Bandow[1Ψ], Jeremy D. Semrau[2], Marcus T. McEllistrem[3], Rafael A. Heinze[3], Matheus Fonseca[3], Joshua C. Ledesma[1], Jacob R. Jennett[1], Ana M. DiSpirito[1], Navjot S. Athwal[1ϒ], Mark S. Hargrove[1], Thomas A. Bobik[1], Hans Zischka[4], and Alan A. DiSpirito[1]*

[1]Roy J. Carver Department of Biochemistry, Biophysics and Molecular Biology. Iowa State University, Ames, IA 50011-3260, USA

[2]Department of Civil and Environmental Engineering, University of Michigan, Ann Arbor, MI, 48109-2125, USA

[3]Department of Chemistry, University of Wisconsin-Eau Claire, WI, 54602, USA

[4]Institute of Molecular Toxicology and Pharmacology, Helmholtz Center Munich, German Research Center and Environmental Health, Ingolsteadter Landstrasse, Germany

[Ψ]Current address: Allogene Therapeutics, Inc., South San Francisco, CA 94080, USA

[ϒ]Current address: Stemcell Technologies, Vancouver, BC Canada

Modified from the paper published in *Applied and Environmental Microbiology*

Abstract

Methanobactins (MBs) are small (<1,300 Da) post-translationally modified copper-binding peptides and represent the extracellular component of a copper acquisition system in some methanotrophs. Interestingly, MBs can bind a range of metals, with some reduced after

binding, e.g., Cu^{2+} reduced to Cu^{+} and Au^{3+} to Au^{0}. Other metals, however, are bound but not reduced, e.g., K^{+}. The source of electrons for selective metal reduction has been speculated to be water but never experimentally shown. Here, using $H_2{}^{18}O$, we show that when MB from *Methylocystis sp*. strain SB2 (MB-SB2) and *Methylosinus trichosporium* OB3b (MB-OB3) were incubated in the presence of either Au^{3+}, Cu^{2}, and Ag^{+}, $^{18,18}O_2$ and free protons were released. No $^{18,18}O_2$ production was observed either in presence of MB-SB2 or MB-OB3b alone, gold alone, copper alone, silver alone or when K^{+} or Mo^{2+} was incubated with MB-SB2. In contrast to MB-OB3b, MB-SB2 binds Fe^{3+} with an N_2S_2 coordination and will also reduce Fe^{3+} to Fe^{2+}. Iron reduction was also found to be coupled to oxidation of $2H_2O$ and generation of O_2. MB-SB2 will also couple Hg^{2+}, Ni^{2+} and Co^{2+} reduction to the oxidation of $2H_2O$ and generation of O_2, but MB-OB3b will not, ostensibly as MB-OB3b binds but does not reduce these metals.

Introduction

Aerobic methane oxidizing bacteria (methanotrophs) oxidize methane to carbon dioxide via a series of two electron steps with methanol, formaldehyde, and formate as intermediates (Semrau *et al.,* 2010). The initial oxidation of methane to methanol is an oxygen and energy dependent reaction and is catalyzed by either a soluble cytoplasmic methane monooxygenase (sMMO) or a particulate or membrane-associated methane monooxygenase (pMMO) (Semrau *et al.,* 2010; Basu *et al.,* 2003; Choi *et al.,* 2003; Elango *et al.,* 1997; Fox *et al.,* 1993; Lipscomb *et al.,* 1994; Colby *et al.,* 1978; Lieberman *et al.,* 2005). The reductant for the initial oxidation of methane is supplied by NADH for the sMMO and by quinols for the pMMO (2, 3, 9-11). Methanol is oxidized to formaldehyde by a calcium- or rare-earth-dependent methanol dehydrogenase using a *c*-type cytochrome as an electron acceptor (Picone *et al.,* 2019; Anthony

et al., 1982; Anthony *et al.,* 1992; Williams *et al.,* 2005; Read *et al.,* 1999; DiSpirito *et al.,* 1999) Formaldehyde is either assimilated or oxidized using either NAD^+ or quinone as the electron acceptor (Zahn *et al.,* 2001; Vorholt *et al.,* 2002; Vorholt *et al.,* 1998; Vorholt *et al.,* 1999). The final two-electron oxidation of formate to carbon dioxide is catalyzed by the NAD^+-linked formate dehydrogenase (Jollie *et al.,* 1990; Jollie *et al.,* 1991; Yoch *et al.,* 1990). Electrons from NADH, quinol or cytochrome *c* are either utilized in biosynthetic reactions or oxidized for energy using either dioxygen (DiSpirito *et al.,* 2004), nitrate (Kits *et al.,* 2015) or ferric iron (Sheng *et al.,* 2020) as the terminal electron acceptor.

In methanotrophs capable of expressing both forms of the MMO, expression is regulated by copper (Semrau *et al.,* 2010; Dalton *et al.,* 1984; Csaki *et al.,* 2003; Murrell *et al.,* 2000; Prior *et al.,* 1985). In addition to the MMOs, a number of genes are regulated by copper (Semrau *et al.,* 2010) and some methanotrophs of the *Alphaproteobacteria* have a novel copper acquisition systems based on the extracellular copper-binding peptide methanobactin (DiSpirito *et al.,* 2016; El Ghazouani *et al.,* 2012; Semrau *et al.,* 2020). Methanobactins (MBs) are low molecular mass (<1,300Da), high potential (E_m 483 – 745 mV) ribosomally synthesized post-translationally modified peptides (RiPPs) and were the first examples of a chalkophore, i.e., a compound excreted by bacteria for the purpose of scavenging copper from the surrounding environment (El Ghazouani *et al.,* 2012; Kim *et al.,* 2004). Structurally MBs are divided into two groups. Both Group I and II MBs are characterized by an internal oxazolone group with an associated thioamide and a second N-terminal 5 or 6 membered ring which in Group I MBs is either an oxazolone or pyrazinedione group with an associated thioamide while Group II MBs has either an imidazoline or pyrazinedione group with an associated thioamide (El Ghazouani *et al.,* 2012; Kim *et al.,* 2004; Behling *et al.,* 2008; El Ghazouani *et al.,* 2011; Kenney *et al.,* 2016; Krentz *et*

al., 2010). The ring and associated thioamide are derived from an X-Cys dipeptide via a series of partially characterized post-translational modifications (DiSpirito *et al.,* 2016; Semrau *et al.,* 2020; Gu *et al.,* 2017). Group I MBs are characterized by an internal disulfide bridge and the copper bound form a dicyclic structure (Behling *et al.,* 2008; El Ghazouani *et al.,* 2011; Choi *et al.,* 2006). Group II MBs lack this disulfide bridge and the copper-bound form has a hairpin-like structure and is characterized by a central sulfonated threonine (El Ghazouani *et al.,* 2012; Krentz *et al.,* 2010).

In addition to copper, MBs will bind many metals (Choi *et al.,* 2006; Baral *et al.,* 2014; Bandow 2014, Lu *et al.,* 2017) and reduce some, but not all metals that are bound (Choi *et al.,* 2006; Bandow *et al.,* 2012). In MB from *Methylosinus trichosporium* OB3b (MB-OB3b) metals such as copper, silver and gold are coordinated via an N_2S_2 ligand set utilizing a N from each ring and the two thioamides and these metals are reduced after binding (El Ghazouani *et al.,* 2012; El Ghazouani *et al.,* 2011; Choi *et al.,* 2006; Choi *et al.,* 2006). Other metals such as iron, nickel and cobalt are coordinated via an N_1S_1 ligand set using one ring and its associated thioamide and are not reduced (Choi *et al.,* 2006). Based on coordination, metals were classified as either Group A metals coordinated by a N_2S_2 ligand set, or Group B metals coordinated by a N_1S_1 ligand set. In contrast, all of the metals bound by MB from *Methylocystis* strain SB2 (MB-SB2) are coordinated by a N_2S_2 ligand set ((Baral *et al.,* 2014; Bandow 2014, Bandow *et al.,* 2012; Baral 2017) and this report)

Since metal reduction assays are often carried out in unbuffered reaction mixtures in the absence of an external reductant, water has been proposed, but not shown to be the electron donor (Krentz *et al.,* 2010). Here, we examine the binding and reduction of oxidized forms of gold (as $HAuCl_4$), copper (as $CuCl_2$), silver (as AgF), iron (as $FeCl_3$), nickel (as $NiCl_2$), mercury

($HgCl_2$), cobalt (as $CoCl_2$) and potassium (as KCl) in the presence and absence of $H_2{}^{18}O$ by MB-SB2 as well as the binding and reduction of gold, copper and silver in the presence of $H_2{}^{18}O$ by MB-OB3b.

Materials and Methods

Materials

Anhydrous $CuCl_2$ (Acros Organics, Geel, Belgium), $HAuCl_4$ (Acros Organics), $HgCl_2$ (Acros Organics, Geel, Belgium), AgF (Acros Organics, Geel, Belgium), $FeCl_3$ (Acros Organics, Geel, Belgium), $NiCl_2$ (Acros Organics, Geel, Belgium), $CoCl_2$ (Acros Organics, Geel, Belgium), $NaMoO_4$ (Sigma-Aldrich) and KCl (Sigma-Aldrich) were stored in a desiccator under Ar_2. $H_2{}^{18}O$ was obtained from Cambridge Isotope Laboratories, Inc. (Andover, MA, USA) and $^{18,18}O_2$ from Sigma Aldrich. Ar_2, $^{16,16}O_2$ and CP grade CH_4 were obtained from Airgas USA LLC. HPLC grade acetonitrile, methanol and other reagents/chemicals were purchased from Fisher Scientific and used without additional purification. Dianion HP-20 was purchased from Sigma-Aldrich C. LLC.

Organism, Culture Conditions, and Isolation of Methanobactin

Methylocystis strain SB2 and *M. trichosporium* OB3b were cultured in nitrate mineral salts media (Whittenbury *et al.*, 1970) amended with either 0.2 or 1.0 µM $CuSO_4$ to optimize production of its methanobactin (MB-SB2). MB-SB2 was purified from the spent media as previously described with the following exception (Bandow *et al.*, 2011). The freeze-dried sample from the Dianion HP20 column was resuspended in deionized H_2O and loaded onto a 250mm x 20mmTarga C18 column (Higgins Analytical Inc., Mountain View, Ca, USA) on an Azurk HPLC system (Knauer, Berlin, Germany). MB-SB2 eluted in the 12-25% methanol

fraction in a methanol:H_2O gradient. The purified methanobactin was then freeze-dried as described above.

X-Ray Photoelectric Spectroscopy (XPS)

XPS was performed as previously described (Choi *et al.*, 2006; Choi *et al.*, 2006) with the following modifications. $HAuCl_4$ and $HAuCl_4$ plus MB-SB2 samples were dried onto highly oriented pyrolytic graphite by freeze-drying. The 1 cm square graphite substrates were immersed in either $HAuCl_4$ or $HAuCl_4$ plus MB-SB2 solutions, frozen in liquid nitrogen and lyophilized overnight. The graphite was then mounted onto an XPS puck and analyzed. Other drying methods were employed such as drying in air under a stream of He gas with a drying time of 30 min or filtered through a porous alumina filter followed by a 2 min drying time. However, samples produced by these methods showed additional reduction.

As previously observed (Choi *et al.*, 2006), XPS analysis of Au was complicated by X-ray induced reduction during the measurement process. Au 4f peak areas were therefore measured as a function of X-ray exposure, the peak areas for a given X-ray dose determined using the CASA XPS fitting program, and the areas plotted as a function of time. An exponential fit to the data using Igor Pro fitting program allowed a determination of the unirradiated sample's Au^{3+} and Au^0 peak areas. XPS measurements were carried out on a custom-designed system that incorporated a SPECS hemispherical analyzer (SPECS Scientific Instruments, Sarasota, FL, USA), Al X-ray source, and load-lock to allow for rapid sample exchanges.

Kinetics of Au^{3+} Binding

The rates of Au^{3+} binding to mb-SB2 were determined by measuring absorption changes at 338 nm and 387 nm using a four-syringe Biologic SFM/4000/S stopped flow reactor coupled to a MOS-500 spectrophotometer (Bio-Logic Science Instrument SA, Claix, France) at 4°C as

previous described. In contrast to the absorbance maxima using Cary 50 spectrometer, the absorbance maximum for the oxazolone was 338 nm and for the imidazolone ring 387 nm on with this system. Stock solutions of $HAuCl_4$ were prepared in >18MΩ • cm H_2O. The stock solutions for MB-SB2 were prepared by dissolving freeze-dried MB-SB2 in > 18MΩ • cm H_2O. Final concentration of the stock solutions of MB-SB2 were determined after filtration by UV-visible absorption spectroscopy as previously described (Baral *et al.*, 2014). Path length for the cuvette used in the Biologic SFM/4000/S stopped flow reactor was 1.5 mm and dead time of the system was 1.4 ms. The system was cooled and maintained at $4^{\circ C}$. Reaction Mixtures contained 400 µM of MB-SB2 and either 40, 100, 200, 240, 280, 320, 360, 400, 600, 700, or 800 µM of $HAuCl_4$. Rates obtained for each concentration were an average of either 5 or 7 traces. The rates were determined by fitting the traces to the exponential function in Biokine operational software (Bio-Logic Science Instrument SA). Binding rates were calculated in mol Au bound per sec per mol MB-SB2 and reported as the binding number (s^{-1}).

Fluorescence changes overtime were monitored at 429 nm on a Cary Eclipse (Agilent Technologies Inc. Santa Clara, CA, USA following excitation at 341nm.

Water Oxidation

Saturated solutions of anhydrous $CuCl_2$, $HAuCl_4$, $HgCl_2$, AgF, $FeCl_3$, $NiCl_2$, $CoCl_2$, $NaMoO_4$ and KCl were prepared in a Coy anaerobic chamber (atmosphere 95% Ar 5% H_2)(Coy Laboratory Products, Ann Arbor, MI, USA). An amount sufficient to create a 0.5 to 10-fold excess of metal was added to 100µl of between 1mM and 10mM of MB-SB2 or MB-OB3b and head space gas samples were collected from the vial. All solutions were made with 97% $H_2{}^{18}O$ (Sigma Aldrich, St. Louis, Mo, USA) in 0.8 ml brown airtight vials (DWK Life Sciences, Millville, NJ, USA).

Oxidation of $2H_2O$ to $O_2 + 4H^+$ in reaction mixtures containing a metal and MB-SB2 was determined by monitoring production of $^{18,18}O_2$ and H^+ and in the case of $HAuCl_4$, production of Cl^-. In oxygen evolution experiments, freeze-dried MB-SB2, MB-OB3b, catalase, as well as anhydrous metal stock solution were prepared in 97% $H_2{}^{18}O$. Reaction mixtures contained 2mM MB-SB2 or MB-OB3b and 0.5 – 20mM metal in a final volume of 100µl $H_2{}^{18}O$. Reaction mixtures were prepared in 2 ml brown serum vials, sealed with Teflon lined silicon septa. Initial experiments were determined with aluminum foil wrapped vials, but that practice was discontinued once it was clear that identical results were produced regardless if vials were wrapped or not. Generation of $^{18,18}O_2$ from $H_2{}^{18}O$ was monitored by direct injection (1µl or 2µl) of head space.

Gas samples were manually injected into an Agilent 7890B GC system (Santa Clara, CA, USA with a 7250 Accurate-Mass Q-TOF GC/MS and a DB5-ms column. Except for the $^{18,18}O_2$ injections for standard curves, all injections were 1µl using gas tight Hamilton syringes. Standard curves were generated with 1µl, 1.5µl and 2 µl injections of 97% $^{18,18}O_2$ (Sigma Aldrich, St. Louis, Mo, USA). The head space in the vials was sampled before and after the addition of the metals, as was the outside air in the mass spectroscopy as controls. After the standards and controls were injected, the samples were mixed and head space samples were immediately collected, with subsequent samples taken every 30-60 seconds. After several minutes, collection slowed to 1 sample every 2-3 minutes. The quantization of generated $^{18,18}O_2$ came from an extracted-ion chromatogram set to 35.9978 Da. A small shift in the MS location of the $^{18,18}O_2$ was observed on some dates. If a drift in the MS of $^{18,18}O_2$ was observed, identify of the peak was verified with 97% $^{18,18}O_2$ standard.

Oxidase, Superoxide Dismutase, Hydrogen Peroxide Reductase and Iron reductase Activity and pH Measurements

Oxidase, superoxide dismutase and hydrogen peroxide reductase activity were determined as previously described by Choi *et al.,* (Choi *et al.,* 2008). Ferrozine assay was used to determine iron reductase activity (Carter 1971, Moody *et al.,* 1983).

pH changes during metal titrations were monitored on either a Radiometer PHM 220 meter with a pH2005-7 combined pH electrode (Radiometer Analytical, Villeurbanne Cerdex, France) or on an Oakion Ion 700 pH meter (Cole-Parmer, Vermon Hills, IL, USA).

Free chloride produced from the binding and deduction of $HAuCl_4$ to Au^0 was measured via argentometric titration (Harris 2007). $HAuCl_4$:MB-SB2 solutions were prepared at a molar ratio of 9:1 and incubated for at least 72 h. Following the incubation period, the solution was titrated with a standardized $AgNO_3$ solution, delivered with a Ramé-hart 2.0 ml microsyringe. The titration processes were monitored with a custom-made Ag wire working electrode and Ag/AgCl reference electrode

Results

Spectral and Thermodynamic Properties of $AuCl_4^-$ binding by MB-SB2

UV-visible absorption, fluorescence, and circular dichroism spectra (Figs. S1-S3) and thermodynamic measurements (Fig. S4; Table S1) demonstrate changes following the addition of $HAuCl_4$ to MB-SB2 were complex with transitions apparent at 0.25, 0.5, 0.75, 1.0 and 2.0 Au per MB-SB2. As MB-SB2 has only one identified metal binding motif (i.e. an N_2S_2 ligand set), we therefore interpret these data to indicate changes in Au coordination, when MB-SB2 transitions from an oligomeric state(s) to a monomer.

The increased fluorescence emission intensity following $HAuCl_4$ addition may be due to disruption of internal quenching between the imidazolone and oxazolone groups and is consistent with the intramolecular exciton transfer previously demonstrated following hydrolysis of the oxazolone group (Bandow *et al.*, 2012)(Fig. S2). The decreased fluorescence at $HAuCl_4$ to MB-SB2 ratios greater than 1.0 suggests direct metal quenching or intra-/ inter-exciton transfer between the oxazolone and imidazolone groups, or may be associated with nanoparticle formation which occurs at Au to MB-SB2 ratios greater than 1:1.

As Au nanoparticle formation requires Au^{3+} reduction (Zhao *et al.*, 2013), nanoparticle formation (Fig. S5; Table 2S) by MB-SB2 indicated that MB-SB2 binds and reduces multiple Au^{3+} to Au^0. Such findings accentuated the need to determine the electron source for metal reduction by MBs. To extend these preliminary studies, we examined reduction of $HAuCl_4$ via MB-SB2 when dissolved in either $H_2{}^{16}O$ or $H_2{}^{18}O$.

X-Ray Photoelectric Spectroscopy (XPS), Kinetics and Chloride Determination

In reaction mixtures containing $HAuCl_4$ and MB-SB2 dissolved in $H_2{}^{16}O$, MB-SB2 was observed to reduce $AuCl_4^-$ to $Au^0 + 4Cl^-$, as determined by XPS and argentometric titrations, respectively (Fig. 1; Table 1). MB-SB2 reduced up to 19 Au^{3+} to $19Au^0$ with a time-dependent average Au^{3+} to Au^0 reduction rate of 0.3 ± 0.06 min^{-1} for those assays where rates could be determined. This time-dependent reduction was the reason samples were frozen in liquid nitrogen and lyophilized overnight to stop the reaction and dry the samples for analysis. As observed with MB-OB3b (39), Au^{3+} and Au^0 were the only oxidation states detected, indicating a direct three-electron reduction of $HAuCl_4$ (Fig. 1).

Kinetics of $AuCl_4^-$ Binding and Reduction

The time course for the binding of Au^{3+} to the oxazolone and imidazolone rings in MB-SB2 was measured as the decrease in absorbance at 341 and 389 nm, respectively, following stopped- flow mixing of MB-SB2 with Au^{3+} at 4°C (Fig. 2A). Unfortunately, even at 4°C, initial binding rates could only be determined for the oxazolone ring, since the binding to the imidazolone ring was complete before mixing of the sample was complete (1.4 msec). In contrast, the binding rates to the oxazolone ring were low, 12 - 57 s^{-1}, at Au^{3+} to MB-SB2 ratios below 0.3, increased at Au^{3+} to MB--SB2 ratios between 0.3 and 1.5 Au^{3+} per MB-SB2 up to a maximum rate of ~1600 s^{-1}, followed by a decline in rate at molar ratios >1.5 Au^{3+} per MB-SB2 (Fig. 2A).

Au^{3+} reduction rates (0.3 ± 0.06 min^{-1}; Table 1) were much slower to the initial binding rates (greater than 2,000 s^{-1}; Fig. 2A). The difference may be due to the different binding rates between the imidazolone and oxazolone groups. Monitoring the florescent changes over time at $HAuCl_4$ to MB-SB2 below 1:1, suggest final Au coordination required several minutes to complete (Fig. 2B). At gold to MB-SB2 concentrations greater than 1.0 an initial disruption of exciton coupling resulting in increased florescent intensity followed by quenching (Fig. 2B). What is pertinent to this discussion is that Au initially binds primarily if not exclusively to the imidazolone group followed by binding to the oxazolone group and a final reorientation. The time scale for these changes is in keeping with gold reduction rates.

Oxidation of H_2O coupled to Au^{3+} reduction by MB-SB2

As four Cl^- were generated in reaction mixtures for every $HAuCl_4$ reduced to Au^0, chlorine was ruled out as a potential electron donor. To determine if H_2O was the electron donor, H^+ concentrations were monitored during $HAuCl_4$ titrations of MB-SB2. Unfortunately, pH

changes associated with the addition of $HAuCl_4$ to unbuffered reaction mixtures made pH changes associated with binding of $AuCl_4^-$ difficult to determine (Fig. 3A). To examine if H_2O could serve as an electron source for Au^{3+} reduction, $^{18,18}O_2$ production was monitored in reaction mixtures containing 97% $H_2{}^{18}O$. No $^{18,18}O_2$ production was observed in reaction mixtures containing either MB-SB2 alone (Fig. 4A) or $HAuCl_4$ alone (result not shown). However, following $HAuCl_4$ addition to MB-SB2, $^{18,18}O_2$ was observed demonstrating the coupling of water oxidation with metal reduction (Figs. 4B and 5).

It should be noted that there is seemingly an electron imbalance, with three electrons required for Au^{3+} to Au^0 while four electrons are released for every two molecules of water oxidized. There are two possibilities to resolve this issue (Chatwood *et al.*, 2004): (i) the reduction of four atoms of Au^{3+} are coupled to the oxidation of six molecules of water and (ii) the reduction of one atom of Au^{3+} is coupled to the oxidation of two molecules of water with the fourth electron used to reduce dioxygen to superoxide. Assays show that reduced MB-SB2 will reduce dioxygen to superoxide (Table S3). Under the low pH conditions following $HAuCl_4$ addition to MB-SB2 (Fig. 3) superoxide would be expected to undergo dismutation reactions generating H_2O_2 (Hayyan *et al.*, 2016). In addition, as observed in MB-OB3b (Choi *et al.*, 2008), Au-MB-SB2 complexes show superoxide dismutase activity (Table S3). Thus, H_2O_2 should appear in reaction mixtures if the fourth electron was used to reduce dioxygen. The rate of $^{18,18}O_2$ production increased by approximately 18% following the addition of catalase, suggesting the production of H_2O_2 (Fig. 5).

Oxidation of H_2O coupled to Cu^{2+} reduction by MB-SB2

Although the oxidation of water to dioxygen coupled to Au^{3+} reduction is chemically interesting it is not likely biologically relevant. To determine if the oxidation of H_2O was specific

to Au^{3+} reduction or a more general property of metal reduction by MB-SB2, similar experiments in $H_2{}^{18}O$ were carried out with $CuCl_2$ as it is believed the primary purpose of MB is the collection of copper critical for methanotrophic activity. Previous spectral and thermodynamic studies have shown MB-SB2 will reduce multiple Cu^{2+} to Cu^{+} in the absence of an external reductant, suggesting that water served as the reductant (Bandow *et al.*, 2012). $^{18,18}O_2$ evolution was observed following the addition of $CuCl_2$ to a $H_2{}^{18}O$ solution of MB-SB2 (Fig 4C). Further, such evolution followed a similar trend to that for $HAuCl_4$ and a substantial pH drop was observed (Fig. 3B - 5). Perhaps of greater environmental relevance is the finding of substantial (> 100 µM) evolution of dioxygen from water oxidation when MB-SB2 bound and reduced copper (Fig. 5).

The ratio of $AuCl_4^-$ and Cu^{2+} to MB-SB2 in the experiments described above showing $O_2{}^{18,18}$ production was 10:1. To determine the number of electrons needed to be extracted from MB-SB2 before water oxidation occurs, reaction mixtures containing 0.5, 1, 2, 3, 4, and 5 Cu^{2+} per MB-SB2 in 97% H_2O^{18} were examined. No $O_2{}^{18,18}$ was observed in samples containing 0.5, 1, 2, 3, or 4 Cu^{2+} per MB-SB2 (results not shown). $O_2{}^{18,18}$ was observed in samples containing 5 Cu^{2+} per MB-SB2 indicating for the initial water oxidation to occur five electrons must be extracted from MS-SB2 (Fig.4D).

KCl was also examined as a metal bound by MB-SB2 (Fig. S6A), but not reduced, as no evidence of the formation of metallic K^0 was observed (Latimer *et al.*, 1940). No $^{18,18}O_2$ was observed following the addition of KCl (Fig.4E) and comparatively minor changes in pH (Fig. 3C) were observed demonstrating water oxidation by MB-SB2 after binding a metal is contingent upon that metal being reduced. MB-SB2 does not bind Mo^{2+} (Fig. S6B) and was used as a negative control. As expected, no $^{18,18}O_2$ was observed in reaction mixtures containing $NaMoO_4$ and MB-SB2 (results not shown).

Oxidation of H_2O coupled to Ag^+, Hg^{2+} Fe^{3+}, Ni^{2+} and Co^{2+} reduction by MB-SB2

As described above Group A metals bound by MB-OB3b are reduced following binding. Ag^+ and Hg^{2+} are Group A metals, MB-SB2 bound both metals via an N_2S_2 coordination (Figs. S6C and S6D) and $^{18,18}O_2$ was observed in reaction mixtures containing MB-SB2 and AgF (Fig. 4F) or $HgCl_2$ (Fig. 4G) at levels similar to that observed with gold and copper.

In contrast to MB-OB3b (Choi *et al.*, 2006), MB-SB2 binds all metals tested via an N_2S_2 coordination (Baral *et al.*, 2014; Bandow 2014, Bandow *et al.*, 2012) (Fig. S6). Also in contrast to MB-OB3b, MB-SB2 will reduce Fe^{3+} to Fe^{2+} at a rate of 1.02 ± 0.09 min^{-1} as measured via the ferrozine assay (Carter 1970, Moody *et al.*, 1983) (Fig. 6A). In fact, MB-SB2 will dissolve insoluble Fe^{3+} hydroxides in the light (Fig. S6E insert) or dark (Fig. 6C). On an electron basis, the ferric iron reduction rate was almost identical to the gold reduction rate described above. In reaction mixtures containing MB-SB2 and $FeCl_3$ (Fig. 4H) $^{18,18}O_2$ was observed at concentrations similar to that observed for Au^{3+} and Cu^{2+}. Similar results were observed in reaction mixtures containing $NiCl_2$ (Figs. 4I and S6F) or $CoCl_2$ (Figs. 4H and S6G) and MB-SB2, although the concentration of $^{18,18}O_2$ was consistently low with $CoCl_2$.

Oxidation of H_2O coupled to Au^{3+}, Cu^{2+}, and Ag^+ reduction by MB-OB3b

To determine if water oxidation coupled to metal reduction was specific to MB-SB2, a Group II MB, or a more general property of MBs, water oxidation was examined in the Group I MB from *M. trichosporium* OB3b, MB-OB3b (Semrau *et al.*, 2020). Previous studies have shown MB-OB3b binds and reduces Au^{3+}, Cu^{2+} and Ag^+ to Au^0, Cu^+ and Ag^0, respectively, and bound but did not reduce Fe^{3+} (Fig. 6B; (Choi *et al.*, 2006; Choi *et al.*, 2006)). Thus, $^{18,18}O_2$ production was monitored in reaction mixtures containing $HAuCl_4$, $CuCl_2$, AgF and $FeCl_3$ with or without MB-OB3b prepared in 97% $H_2{}^{18}O$. Again, no $^{18,18}O_2$ production was observed in

reaction mixtures containing either MB-OB3b alone (Fig. 7A) or with $HAuCl_4$, $CuCl_2$ or AgF alone (result not shown). However, following $HAuCl_4$ (Fig. 7B), $CuCl_2$(Fig. 7C) or AgF (Fig. 7D) addition to reaction mixtures containing MB-OB3b, $^{18,18}O_2$ was observed although the concentrations of $^{18,18}O_2$ were less than 25% of the $^{18,18}O_2$ produced in similar reactions with MB-SB2. No $^{18,18}O_2$ was observed following $FeCl_3$ addition to a reaction mixture containing MB-OB3b.

Methane oxidation coupled to O2 generated from Cu2+ reduction by MB-OB3b

To determine if dioxygen generated during metal ion reduction could support methane oxidation by *M. trichosporium* OB3b, incubations with $^{13}CH_4$ in the presence and absence of MB-OB3b and Cu^{2+} were performed under anoxic conditions in an anaerobic glove box. In cell suspensions with no additional amendments of either copper or MB-OB3b, 0.72 ± 0.17 μmol $^{13}CO_2$ was observed after 3 days (assumed to be driven by the presence of residual dioxygen in the reaction mixtures [Fig. 8]). In cell suspensions amended with 25 μM Cu^{2+}, 0.97 ± 0.03 μmol $^{13}CO_2$ was observed (a 34% increase, not significantly different from the amount of $^{13}CO_2$ measured with no amendment [P = 0.06]). If 5μM MB-OB3b was added instead, 1.47 ± 0.08 μmol $^{13}CO_2$ was measured (an increase of ~104%, significantly higher than with no amendment [$P = 2.2 \times 10^{-3}$], presumably due to MB-OB3b binding and reducing metals that are part of the growth medium). If both 25μM Cu and 5μM MB-OB3b were added, 2.5 ± 0.37 μmol $^{13}CO_2$ was observed, an increase of ~250% from that with no amendment (again, significantly different [$P = 1.5 \times 10^{-3}$]), indicating that metal ion reduction by MB can support methane oxidation under anoxic conditions (Fig. 8).

Discussion

Metal binding by MBs has focused on MB-OB3b, a Group I MB (34, 39, 44). MB-OB3b bound Group A metals such as Cu^{2+}, Au^{3+}, Ag^{+}, Hg^{2+} via an N_2S_2 ligand set. Other metals such as Fe^{3+}, Co^{2+}, Cd^{2+} Mn^{2+}, Ni^{2+} and Zn^{2+} showed an N_1S_1 coordination and were placed in Group B. Of the metals examined Group A metals were reduced following binding whereas Group B metals were not. In this and previous reports (Baral *et al.,* 2014; Bandow 2014, Bandow *et al.,* 2012; Baral 2017), MB-SB2, a Group II MB, coordinates all metals bound via N_2S_2 coordination and reduced metals previously place Group A and B. With the exception of KCl, metals bound via an N_2S_2 coordination are reduced and here we show that H_2O can serve as an electron donor driving metal reduction.

The finding that MB, after binding specific metals can split water to form dioxygen suggests that this may be another strategy whereby aerobic methanotrophy can occur in an anoxic environment. That is, it has been shown that methane oxidation via aerobic methanotrophy occurs in anoxic zones of shallow lakes (i.e., at a depth of ~10 m), with such activity driven by oxygenic photosynthesis as sunlight could penetrate to this depth (Milucka *et al.*, 2015; Oswald *et al.,* 2015). In these studies, it was found that methane oxidation rates increased in the light vs. dark, and such activity was abolished when a selective inhibitor of photosynthesis was added. Thus, it appears that methanotrophs can form highly effective relationships with oxygenic photosynthetic microbes to scavenge trace amounts of dioxygen, and by so doing, enhance methane removal from these environments.

More germane to the findings here, however, is the discovery that aerobic methanotrophs were also active in deep lake water (~160 m) where oxygenic photosynthesis is highly unlikely as sunlight cannot penetrate to this depth (Oswald *et al.,* 2016). Such activity, however, could be

stimulated by the addition of dioxygen and oxidized metals. Here it was concluded that methanotrophs may survive anoxic environments by utilizing alternative electron acceptors. Others have shown that aerobic methanotrophs of the *Methylobacter* genus can be stimulated in anoxic lake waters through the addition of either nitrate or sulfate (van Grinsven *et al.,* 2020). Indeed, it has been shown that some aerobic methanotrophs can respire nitrate (Kits *et al.,* 2015) or ferric iron (Sheng *et al.,* 2020). Such a strategy could conserve trace amounts of dioxygen to enable methane oxidation by the MMOs. Alternatively, it has been shown that some methanotrophs will couple methane oxidation to fermentation to putatively conserve dioxygen (Gilman *et al.,* 2017), and such a strategy has been speculated to be responsible for methanotrophic activity in dioxygen-limited lakes (van Grinsven *et al.,* 2020). Finally, it has been speculated that alternatively or in conjunction, methanotrophs may form syntrophic partnerships with other microbes to facilitate methane oxidation (van Grinsven *et al.,* 2020) when dioxygen is limiting.

It should be noted, however, that in studies of methane oxidation in anoxic lake water samples, great care was taken to exclude any oxygen intrusion and any trace amounts of oxygen present were quite small and could not explain the extent of methane oxidation observed. How these microbes then are able to oxidize methane in the absence of dioxygen is still unclear. That is, for the identified methanotrophs to oxidize methane, dioxygen is required for either form of MMO regardless if alternative terminal electron acceptors can be used or if effective microbial partnership(s) can be formed. Thus, either unknown sources of dioxygen exist in these environments and/or these microbes possess some novel, as yet undescribed mechanism of anaerobic methane oxidation, i.e., novel forms of MMO that can utilize oxidized sulfur and nitrogen species in place of dioxygen.

Here we present an alternative explanation for the presence and activity of aerobic methanotrophs in anoxic environments, particularly alphaproteobacterial methanotrophs. That is, genes for MB biosynthesis have only been found in the genomes of various *Methylosinus* and *Methylocystis* species of the *Alphaproteobacteria* (Semrau *et al.*, 2020). It has been repeatedly shown that these genera prefer high methane/low oxygen conditions found at the oxic-anoxic interface *in situ* (Amaral *et al.*, 1995; Henckel *et al.*, 2000). Further, they are the predominant methanotrophic genera present in completely anoxic zones of rice paddy soils (Lee *et al.*, 2015). Thus, it is tempting to speculate that the ability to produce MB enables methanotrophs to colonize methane-rich environments by self-producing dioxygen to ensure that methane oxidation can continue even when ambient concentrations of dioxygen are quite low. Such a strategy is particularly important for methanotrophs that colonize the oxic-anoxic interface in soils, for not only are these locations dark (thus excluding the possibility of methanotrophy/phototrophy synergy), this interface shifts quickly in response to episodic precipitation and drying periods. As such, methanotrophs that colonize this interface must be prepared to tolerate periodic and possibly quite extended anoxic conditions. The ability to produce dioxygen from water would thus enable these microbes to continue to oxidize methane under anoxia, thereby generating ATP, as well as providing intermediates required for carbon assimilation (i.e., formaldehyde). Doing so would enable them to survive extended periods in the absence of oxygen, if not allow for some continued growth in anoxic conditions.

It should be noted, however, is that in aforementioned lake studies concluding aerobic methanotrophy occurs in anoxic environments, gammaproteobacterial methanotrophs appeared to be predominantly responsible for methane oxidation and to date, no representatives of this group have been shown to have the genes required for MB biosynthesis, although it is clear that

at least some can and do secrete a copper-binding compound (Choi *et al.,* 2010). It may be that these methanotrophs utilize dioxygen created by others via MB production (i.e., some sort of collaboration between gamma- and alpha-proteobacteria as concluded between methanotrophs and oxygenic photosynthetic microbes) and/or also can generate dioxygen via some unknown mechanism.

Finally, prior to discovery of dioxygen production via splitting of water by metal-MB complexes reported here, dioxygen production by biological systems has been observed in only four known pathways: oxygenic photosynthesis (Mandal *et al.,* 2020; Vass *et al.,* 1991), detoxification of oxygen radicals (Nicholls *et al.,* 2000; Apel *et al.,* 2004), (per)chlorate respiration (Youngblut *et al.,* 2016) and nitric oxide dismutation by *Candidatus* Methylomirabilis oxyferans of the NC10 phylum (Ettwig *et al.,* 2010). The latter two mechanisms may provide some explanation as to the significance of MB-mediated water oxidation. That is, it has been shown that dioxygen evolution from (per)chlorate respiration occurs when the intermediate chlorite is dismutated to chloride and dioxygen, and it is speculated that the dioxygen is then used for an antibiotic-producing monooxygenase in *Haloferax volcanii* (Bab-Dinitz *et al.,* 2006). Further, *Ca*. M. oxyferans is a methanotroph, but respires nitrite rather than dioxygen. Interestingly, dioxygen is critical for its growth as this microbe utilizes the membrane-associated methane monooxygenase for methane oxidation to methanol (Ettwig *et al.,* 2010). Stable isotope studies showed that *Ca*. M. oxyferans dismutates nitric oxide to dinitrogen and dioxygen, the latter which is used for methane oxidation (the mechanism(s) by which this occurs, however, is still unknown). It may be that MB-expressing aerobic methanotrophs perform a similar feat to ensure that there is adequate dioxygen for continued MMO activity in hypoxic/anoxic conditions.

In conclusion, the discovery of water oxidation by specific metal-methanobactin complexes is not only unusual, it also implies a strategy whereby aerobic methanotrophs can survive, if not thrive in anoxic conditions. As such, MB-driven dioxygen generation may be an important but hitherto unrecognized process whereby methane emissions are regulated.

Acknowledgements

Funding

This research was supported by the Office of Science (BER), U.S. Department of Energy (JDS and ADS), the Materials Science and Engineering Center at UW-Eau Claire (MTM), and the ISU Bailey Research and Career Development (TAB). Use of ITC and Biologic SFM/4000 stopped flow reactor coupled to a MOS-500 spectrophotometer was made possible through a generous gift from the Roy J. Carver Charitable Trust (Muscatine, Iowa).

Competing interests

Authors declare they have no competing interests.

References

1. Semrau JD, DiSpirito AA, Yoon S. 2010. Methanotrophs and copper. FEMS Microbiol Rev 34:496–531. https://doi.org/10.1111/j.1574-6976.2010.00212.x.

2. Basu P, Katterle B, Andersson KK, Dalton H. 2003. The membrane-associated form of methane mono-oxygenase from *Methylococcus capsulatus* (Bath) is a copper/iron protein. Biochem J 369:417–427. https://doi.org/10 .1042/bj20020823.

3. Choi DW, Kunz RC, Boyd ES, Semrau JD, Antholine WE, Han JI, Zahn JA, Boyd JM, de la Mora AM, DiSpirito AA. 2003. The membrane-associated methane monooxygenase (pMMO) and pMMO-NADH:quinone oxidoreductase complex from *Methylococcus capsulatus* Bath. J Bacteriol 185:5755–5764. https://doi.org/10.1128/JB.185.19.5755-5764.2003.

4. Elango N, Radhakrishnan R, Froland WA, Wallar BJ, Earhart CA, Lipscomb JD, Ohlendorf DH. 1997. Crystal structure of the hydroxylase component of methane monooxygenase from *Methylosinus trichosporium* OB3b. Protein Sci 6:556–568. https://doi.org/10.1002/pro.5560060305.

5. Fox BG, Hendrich MP, Surerus KK, Andersson KK, Froland WA, Lipscomb JD, Münck E. 1993. Mössbauer, EPR, and ENDOR studies of the hydroxylase and reductase components of methane monooxygenase from *Methylosinus trichosporium* Ob3b. J Am Chem Soc 115:3688–3701. https://doi.org/10.1021/ja00062a039.

6. Lipscomb JD. 1994. Biochemistry of the soluble methane monooxygenase. Annu Rev Microbiol 48:371–399. https://doi.org/10.1146/annurev.mi .48.100194.002103.

7. Colby J, Dalton H. 1978. Resolution of the methane monooxygenase of *Methylococcus capsulatus* (Bath) into three components. Purification and properties of component C, a flavoprotein. Biochem J 171:461–468. https://doi.org/10.1042/bj1710461.

8. Lieberman RL, Rosenzweig AC. 2005. Crystal structure of a membrane-bound metalloenzyme that catalyses the biological oxidation of methane. Nature 434:177–182. https://doi.org/10.1038/nature03311.

9. Dalton H, Prior SD, Leak DJ, Stanley SH. 1984. Regulation and control of methane monooxygenase, p 75–82. In Crawford RL, Hanson RS (ed), Microbial growth in C1 compounds. Proceedings of the 4th International Symposium. American Society for Microbiology, Washington, DC.

10. Zahn JA, Bergmann DJ, Boyd JM, Kunz RC, DiSpirito AA. 2001. Membrane-associated quinoprotein formaldehyde dehydrogenase from *Methylococcus capsulatus* Bath. J Bacteriol 183:6832–6840. https://doi.org/10.1128/JB.183 .23.6832-6840.2001.

11. DiSpirito AA, Kunz RC, Choi DW, Zahn JA. 2004. Electron flow during methane oxidation in methanotrophs, p 141–169. *In* Zannoni D (ed), Respiration in archaea and bacteria. Kluwer Scientific, Dordrecht, The Netherlands.

12. Picone N, Op den Camp HJM. 2019. Role of rare earth elements in methanol oxidation. Curr Opin Chem Biol 49:39–44. https://doi.org/10.1016/j .cbpa.2018.09.019.

13. Anthony C. 1982. The biochemistry of methylotrophs. Academic Press, London, United Kingdom.

14. Anthony C. 1992. The structure of bacterial quinoprotein dehydrogenases. Int J Biochem 24:29–30. https://doi.org/10.1016/0020-711X(92)90226-Q.

15. Williams PA, Coates L, Mohammed F, Gill R, Erskine PT, Coker A, Wood SP, Anthony C, Cooper JB. 2005. The atomic structure of methanol dehydrogenase from *Methylobacterium extorquens*. Acta Crystallogr D Biol Crystal-logr 61:75–79. https://doi.org/10.1107/S0907444904026964.

16. Read J, Gill R, Dales SL, Cooper JB, Wood SP, Anthony C. 1999. The molecular structure of an unusual cytochrome c_2 determined at 2.0 Å; the cytochrome *cH* from *Methylobacterium extorquens*. Protein Sci 8:1232–1240. https://doi.org/10.1110/ps.8.6.1232.

17. DiSpirito AA, Lipscomb JD, Lidstrom ME. 1990. Soluble cytochromes from the marine methanotroph *Methylomonas* sp. strain A4. J Bacteriol 172:5360–5367. https://doi.org/10.1128/JB.172.9.5360-5367.1990.

18. Vorholt JA. 2002. Cofactor-dependent pathways of formaldehyde oxidation in methylotrophic bacteria. Arch Microbiol 178:239–249. https://doi .org/10.1007/s00203-002-0450-2.

19. Vorholt JA, Chistoserdova L, Lidstrom ME, Thauer RK. 1998. The NADP-dependent methylene tetrahydromethanopterin dehydrogenase in *Methylobacterium extorquens* AM1. J Bacteriol 180:5351–5356. https://doi.org/10 .1128/JB.180.20.5351-5356.1998.

20. Vorholt JA, Chistoserdova L, Stolyar SM, Thauer RK, Lidstrom ME. 1999. Distribution of tetrahydromethanopterin-dependent enzymes in methylotrophic bacteria and phylogeny of methenyl tetrahydromethanopterin cyclohydrolases. J Bacteriol 181:5750–5757. https://doi.org/10.1128/JB .181.18.5750-5757.1999.

21. Jollie DR, Lipscomb JD. 1990. Formate dehydrogenase from *Methylosinus trichosporium* OB3b. Methods Enzymol 188:331–334. https://doi.org/10 .1016/0076-6879(90)88051-b.

22. Jollie DR, Lipscomb JD. 1991. Formate dehydrogenase from *Methylosinus trichosporium* OB3b. J Biol Chem 266:21853–21863. https://doi.org/10 .1016/S0021-9258(18)54716-5.

23. Yoch DC, Chen Y-P, Hardin MG. 1990. Formate dehydrogenase from the methane oxidizer *Methylosinus trichosporium* OB3b. J Bacteriol 172:4456–4463. https://doi.org/10.1128/JB.172.8.4456-4463.1990.

24. Kits KD, Klotz MG, Stein LY. 2015. Methane oxidation coupled to nitrate reduction under hypoxia by gammaproteobacterium *Methylomonas denitrificans*, sp. nov. type strain FJG1. Environ Microbiol 17:3219–3232. https://doi.org/10.1111/1462-2920.12772.

25. Sheng Y, Wang H, Liu Y, Zhu B, Li J, Yang Y, Qin W, Chen L, Wu X, Chistoserdova L, Zhao F. 2020. Methane-dependent mineral reduction by aerobic methanotrophs under hypoxia. Environ Sci Technol Lett 7:606–612. https://doi.org/10.1021/acs.estlett.0c00436.

26. Csaki R, Bodrossy L, Klem J, Murrell JC, Kovacs KL. 2003. Genes involved in the copper-dependent regulation of soluble methane monooxygenase of *Methylococcus capsulatus* (Bath): cloning, sequencing and mutational analysis. Microbiology 149:1785–1795. https://doi.org/10.1099/mic.0.26061-0.

27. Murrell JC, McDonald IR, Gilbert B. 2000. Regulation of expression of methane monooxygenases by copper ions. Trends Microbiol 8:221–225. https://doi.org/10.1016/S0966-842X(00)01739-X.

28. Prior SD, Dalton H. 1985. Copper stress underlines the fundamental change in intracellular location of the membrane monooxygenase in methane oxidizing organisms: studies in batch and continuous culture. J Gen Microbiol 131:155–163.

29. DiSpirito AA, Semrau JD, Murrell JC, Gallagher WH, Dennison C, Vuilleumier S. 2016. Methanobactin and the link between copper and bacterial methane oxidation. Microbiol Mol Biol Rev 80:387–409. https://doi.org/10.1128/MMBR.00058-15.

30. El Ghazouani A, Basle A, Gray J, Graham DW, Firbank SJ, Dennison C. 2012. Variations in methanobactin structure influences copper utilization by methane-oxidizing bacteria. Proc Natl Acad Sci U S A 109:8400–8404. https://doi.org/10.1073/pnas.1112921109.

31. Semrau JD, DiSpirito AA, Obulisamy PK, Kang-Yun CS. 2020. Methanobactin from methanotrophs: genetics, structure, function and potential applications. FEMS Microbiol Lett 367:fnaa045. https://doi.org/10.1093/femsle/fnaa045.

32. Kim HJ, Graham DW, DiSpirito AA, Alterman MA, Galeva N, Larive CK, Asunskis D, Sherwood PMA. 2004. Methanobactin, a copper-acquisition compound from methane-oxidizing bacteria. Science 305:1612–1615. https://doi.org/10.1126/science.1098322.

33. Behling LA, Hartsel SC, Lewis DE, DiSpirito AA, Choi DW, Masterson LR, Veglia G, Gallagher WH. 2008. NMR, mass spectrometry and chemical evidence reveal a different chemical structure for methanobactin that contains oxazolone rings. J Am Chem Soc 130:12604–12605. https://doi.org/ 10.1021/ja804747d.

34. El Ghazouani A, Basle A, Firbank SJ, Knapp CW, Gray J, Graham DW, Dennison C. 2011. Copper-binding properties and structures of methanobactins from *Methylosinus trichosporium* OB3b. Inorg Chem 50:1378–1391. https://doi.org/10.1021/ic101965j.

35. Kenney GE, Goering AW, Ross MO, DeHart CJ, Thomas PM, Hoffman BM, Kelleher NL, Rosenzweig AC. 2016. Characterization of methanobactin from *Methylosinus* sp. SW4. J Am Chem Soc 138:11124–11127. https://doi .org/10.1021/jacs.6b06821.

36. Krentz BD, Mulheron HJ, Semrau JD, DiSpirito AA, Bandow NL, Haft DH, Vuilleumier S, Murrell JC, McEllistrem MT, Hartsel SC, Gallagher WH. 2010. A comparison of methanobactins from *Methylosinus trichosporium* OB3b and *Methylocystis* strain SB2 predicts methanobactins are synthesized from diverse peptide precursors modified to create a common core for binding and reducing copper ions. Biochemistry 49:10117–10130. https://doi.org/ 10.1021/bi1014375.

37. Gu W, Baral BS, DiSpirito AA, Semrau JD. 2017. An aminotransferase is responsible for the deamination of the N-terminal leucine and required for formation of oxazolone ring A in methanobactin of Methylosinus trichosporium OB3b. Appl Environ Microbiol 83:e02619-16. https://doi.org/10 .1128/AEM.02619-16.

38. Choi DW, Do YS, Zea CJ, McEllistrem MT, Lee SW, Semrau JD, Pohl NL, Kisting CJ, Scardino LL, Hartsel SC, Boyd ES, Geesey GG, Riedel TP, Shafe PH, Kranski KA, Tritsch JR, Antholine WE, DiSpirito AA. 2006. Spectral and thermodynamic properties of Ag(I), Au(III), Cd(II), Co(II), Fe(III), Hg(II), Mn (II), Ni(II), Pb(II), U(IV), and Zn(II) binding by methanobactin from *Methylosinus trichosporium* OB3b. J Inorg Biochem 100:2150–2161. https://doi .org/10.1016/j.jinorgbio.2006.08.017.

39. Baral BS, Bandow NL, Vorobev A, Freemeier BC, Bergman BH, Herdendorf T, Fuentes N, Ellias L, Turpin E, Semrau JD, DiSpirito AA. 2014. Mercury binding by methanobactin from *Methylocystis* strain SB2. J Inorg Biochem 141:161–169. https://doi.org/10.1016/j.jinorgbio.2014.09.004.

40. Bandow NL. 2014. Isolation and binding properties of methanobactin from the facultative methanotroph *Methylocystis* strain SB2. PhD thesis. Iowa State University, Ames, IA.

41. Lu X, Gu W, Zhao L, Farhan Ul Haque M, DiSpirito AA, Semrau JD, Gu B. 2017. Methylmercury uptake and degradation by methanotrophs. Sci Adv 3:e1700041. https://doi.org/10.1126/sciadv.1700041.

42. Bandow N, Gilles VS, Freesmeier B, Semrau JD, Krentz B, Gallagher W, McEllistrem MT, Hartse SC, Cho DW, Hargrove MS, Heard TM, Chesner LM, Braunreiter KM, Cao BV, Gavitt MM, Hoopes JZ, Johnson JM, Polster EM, Schoenick BD, Umlauf AM, DiSpirito AA. 2012. Spectral and copper binding properties of methanobactin from the facultative methanotroph *Methylocystis* strain SB2. J Inorg Biochem 110:72–82. https://doi.org/10 .1016/j.jinorgbio.2012.02.002.

43. Choi DW, Zea CJ, Do YS, Semrau JD, Antholine WE, Hargrove MS, Pohl NL, Boyd ES, Geesey GG, Hartsel SC, Shafe PH, McEllistrem MT, Kisting CJ, Campbell D, Rao V, de la Mora AM, DiSpirito AA. 2006. Spectral, kinetic, and thermodynamic properties of Cu(I) and Cu(II) binding by methanobactin from *Methylosinus trichosporium* OB3b. Biochemistry 45:1442–1453. https://doi.org/10.1021/bi051815t.

44. Baral BS. 2017. Methanobactin: metal binding properties, physiological function and biosynthesis. PhD thesis. Iowa State University, Ames, IA.

45. Zhao P, Li N, Astruc D. 2013. State of the art in gold nanoparticle synthesis. Coord Chem Rev 257:638–665. https://doi.org/10.1016/j.ccr.2012.09 .002.

46. Chatwood LL, Müller J, Gross JD, Wagner G, Lippard SJ. 2004. NMR structure of the flavin domain from soluble methane monooxygenase reductase from *Methylococcus capsulatus* (Bath). Biochemistry 43:11983–11991. https://doi.org/10.1021/bi049066n.

47. Hayyan M, Hashim MA, Al Nashef IM. 2016. Superoxide ion: generation and chemical implications. Chem Rev 116:3029–3065. https://doi.org/10 .1021/acs.chemrev.5b00407.

48. Choi DW, Semrau JD, Antholine WE, Hartsel SC, Anderson RC, Carey JN, Dreis AM, Kenseth EM, Renstrom JM, Scardino LL, Van Gorden GS, Volkert AA, Wingad AD, Yanzer PJ, McEllistrem MT, de la Mora AM, DiSpirito AA. 2008. Oxidase, superoxide dismutase, and hydrogen peroxide reductase activities of methanobactin from types I and II methanotrophs. J Inorg Biochem 102:1571–1580. https://doi.org/10.1016/j.jinorgbio.2008.02.003.

49. Latimer WM, Hildebrand JH. 1940. Reference book of inorganic chemistry. The Macmillan Co, New York, NY.

50. Carter P. 1971. Spectrometric determination of serum iron at the submicrogram level with a new reagent (ferrozine). Anal Biochem 40:450–458. https://doi.org/10.1016/0003-2697(71)90405-2.

51. Moody MD, Dailey HA. 1983. Aerobic ferrisiderophore reductase assay and activity stain for native polyacrylamide gels. Anal Biochem 134:235–239. https://doi.org/10.1016/0003-2697(83)90290-7.

52. Milucka J, Kirf M, Lu L, Krupke A, Lam P, Littmann S, Kuypers MMM, Schubert CJ. 2015. Methane oxidation coupled to oxygenic photosynthesis in anoxic waters. ISME J 9:1991–2002. https://doi.org/10.1038/ismej .2015.12.

53. Oswald K, Milucka J, Brand A, Littmann S, Wehrli B, Kuypers MMM, Schubert CJ. 2015. Light-dependent aerobic methane oxidation reduces methane emissions from seasonally stratified lakes. PLoS One 10: e0132574. https://doi.org/10.1371/journal.pone.0132574.

54. Oswald K, Jegge C, Tischer J, Berg J, Brand A, Miracle MR, Soria X, Vicente E, Lehmann M, Zopfi J, Schubert CJ. 2016. Methanotrophy under versatile conditions in water column of the ferruginous meromictic lake La Crus (Spain). Front Microbiol 7:1762. https://doi.org/10.3389/fmicb.2016.01762.

55. van Grinsven S, Sinninghe Damste JS, Harrison J, Villanueva L. 2020. Impact of electron acceptor availability on methane-influenced microorganisms in an enrichment culture obtained from a stratified lake. Front Microbiol 11:715. https://doi.org/10.3389/fmicb.2020.00715.

56. Gilman A, Fu Y, Hendershott M, Chu F, Puri AW, Smith AL, Pesesky M, Lieberman R, Beck DAC, Lidstrom ME. 2017. Oxygen-limited metabolism in the methanotroph *Methylomicrobium buryatense* 5GB1C. PeerJ 5: e3945. https://doi.org/10.7717/peerj.3945.

57. Amaral JA, Knowles R. 1995. Growth of methanotrophs in methane and oxygen counter gradients. FEMS Microbiol Lett 126:215–220. https://doi .org/10.1111/j.1574-6968.1995.tb07421.x.

58. Henckel T, Roslev P, Conrad R. 2000. Effects of O2 and CH4 on presence and activity of the indigenous methanotrophic community in rice field soil. Environ Microbiol 2:666–679. https://doi.org/10.1046/j.1462-2920 .2000.00149.x.

59. Lee HJ, Jeong SE, Kim PJ, Madsen EL, Jeon CO. 2015. High resolution depth distribution of bacteria, archaea, methanotrophs, and methanogens in the bulk and rhizosphere soils of a flooded rice paddy. Front Microbiol 6:639. https://doi.org/10.3389/fmicb.2015.00639.

60. Choi DW, Bandow NL, McEllistrem MT, Semrau JD, Antholine WE, Hartsel SC, Gallagher W, Zea CJ, Pohl NL, Zahn JA, DiSpirito AA. 2010. Spectral and thermodynamic properties of methanobactin from gamma-proteo-bacterial methane oxidizing bacteria: a case for copper competition on a molecular level. J Inorg Biochem 104:1240–1247. https://doi.org/10.1016/j.jinorgbio.2010.08.002.

61. Mandal M, Kawashima K, Saito K, Ishikita H. 2020. Redox potential of the oxygen-evolving complex in electron transfer cascade of photosystem II. J Phys Chem Lett 11:249–255. https://doi.org/10.1021/acs.jpclett.9b02831.

62. Vass I, Styring S. 1991. pH-dependent charge equilibria between tyrosine-D and the S states in photosystem II. Estimation of relative midpoint redox potentials. Biochemistry 30:830–839. https://doi.org/10.1021/bi00217a037.

63. Nicholls P, Fita I, Loewen PC. 2000. Enzymology and structure of catalases. Adv Inorg Chem 51:51–106. https://doi.org/10.1016/S0898-8838(00)51001-0.

64. Apel K, Hirt H. 2004. Reactive oxygen species: metabolism, oxidative stress, and signal transduction. Annu Rev Plant Biol 55:373–399. https://doi.org/10.1146/annurev.arplant.55.031903.141701.

65. Youngblut MD, Tsai C-L, Clark IC, Carlson HK, Maglaqui AP, Gau-Pan PS, Redford SA, Wong A, Tainer JA, Coates JD. 2016. Perchlorate reductase is distinguished by active site aromatic gate residues. J Biol Chem 291:9190–9202. https://doi.org/10.1074/jbc.M116.714618.

66. Ettwig KF, Butler MK, Le Paslier D, Pelletier E, Mangenot S, Kuypers MMM, Schreiber F, Dutilh BE, Zedelius J, de Beer D, Gloerich J, Wessels HJCT, van Alen T, Luesken F, Wu ML, van de Pas-Schoonen KT, Op den Camp HJM, Janssen-Megens EM, Francoijs K-J, Stunnenberg H, Weissenbach J, Jetten MSM, Strous M. 2010. Nitrite-driven anaerobic methane oxidation by oxy-genic bacteria. Nature 464:543–548. https://doi.org/10.1038/nature08883.

67. Bab-Dinitz E, Shmuely H, Maupin-Furlow J, Eichler J, Shaanan B. 2006. *Haloferax volcanii* PitA: an example of functional interaction between Pfam chlorite dismutase and antibiotic biosynthesis monooxygenase families. Bioinformatics 22:671–675. https://doi.org/10.1093/bioinformatics/btk043.

68. Whittenbury R, Phillips KC, Wilkinson JF. 1970. Enrichment, isolation and some properties of methane-utilizing bacteria. J Gen Microbiol 61:205–218. https://doi.org/10.1099/00221287-61-2-205.

69. Bandow NL, Gallagher WH, Behling L, Choi DW, Semrau JD, Hartsel SC, Gilles VS, DiSpirito AA. 2011. Isolation of methanobactin from the spent media of methane-oxidizing bacteria. Methods Enzymol 495:259–269. https://doi.org/10.1016/B978-0-12-386905-0.00017-6.

70. Harris DC. 2007. Quantitative chemical analysis, 7th ed. WH Freeman and Company, New York, NY.

71. Le VH, Buscaglia R, Chaires JB, Lewis EA. 2013. Modeling complex equilibria in isothermal titration calorimetry experiments: Thermodynamic parameters estimation for a three-binding-site model. Anal Biochem 434:233 - 241.

72. Berova N, Di Bari L, Pescitelli G. 2007. Application of electronic circular dichroism in configurational and conformational analysis of organic compounds. Chem Soc Rev 36:914 - 931.

73. Berova N, Nakagawa KH. 2000. Exciton chirality method: principles and applications, p 337 - 382. *In* Berova N, Nakagawa KH, Woody RW (ed), Circular Dichroism Principles and Applications, Second ed. Wiley_VCH, Inc, New York, NY USA.

74. Bandow N, Gilles VS, Freesmeier B, Semrau JD, Krentz B, Gallaghe W, McEllistrem MT, Hartse SC, Cho DW, Hargrove MS, Heard TM, Chesner LM, Braunreiter KM, Cao BV, Gavitt MM, Hoopes JZ, Johnson JM, Polster EM, Schoenick BD, A.M. U, DiSpirito AA. 2012. Spectral and copper binding properties of methanobactin from the facultative methanotroph *Methylocystis* strain SB2. J Inorgan Biochem 110:72 - 82.

75. Storhoff JJ, Lazarides AA, Mucic R, C.A. M, Letsinger RL, Schatz GC. 2000. What controls the optical properties of DNA-linked gold nanoparticle assemblies. J Am Chem Soc 122:4640-4650.

Tables

Table 1. Distribution of Au as Au^{3+} and Au^{0} following incubation of MB-SB2 and HAuCl4. Reduction rate was determined from samples where less than 100 percent reduction was observed.

$HAuCl_4$:MB-SB2 ratio	Time (min)	% Au^{3+}	% Au^{0}	Reduction Rate (Au^{3+} min^{-1})
0.9	30	0	100	-
2.25	30	0	100	-
9	30	8	92	0.27
14	30	11	89	0.41
19	30	59	41	0.26
9	60	0	100	-
14	60	0	100	-
19	60	10	90	0.28
19	360	0	100	-

Figures

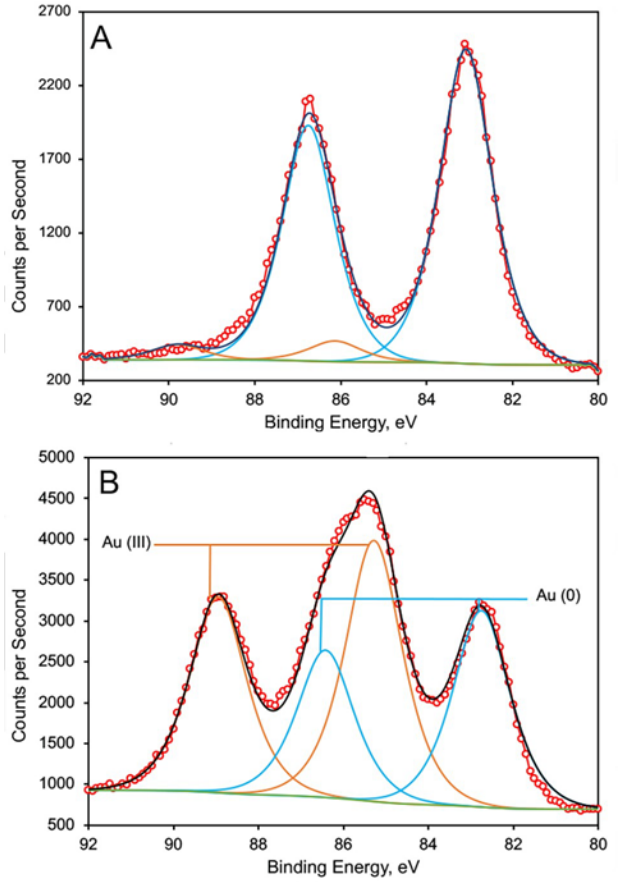

Figure 1. Gold X-ray photoelectric spectra of MS-SB2 (**A**) at gold to MB-SB2 molar ratio of 14 to 1 after 30 min incubation (○) and (**B**) at gold to MB-SB2 molar ratio of 19 to 1 after 30 min incubation. Experimental results (circles) fit with CASA XPS software to four 696 Gaussian/Lorentzian curves, using two peaks for Au^{3+} (orange curves) and two peaks for Au^{0} (blue curves). Gold 4f core electrons are spin-orbit split as $4f_{7/2}$ and $4f_{5/2}$, with a splitting of 3.7 eV and area ratio of 4:3, so that only two peaks are independently fit: the $4f_{7/2}$ peaks for Au^{3+} and Au^{0}. The $4f_{5/2}$ peaks' position and area are determined by the spin-orbit splitting; those parameters and the peak widths are fixed in the fitting program. Background used was a Shirley type.

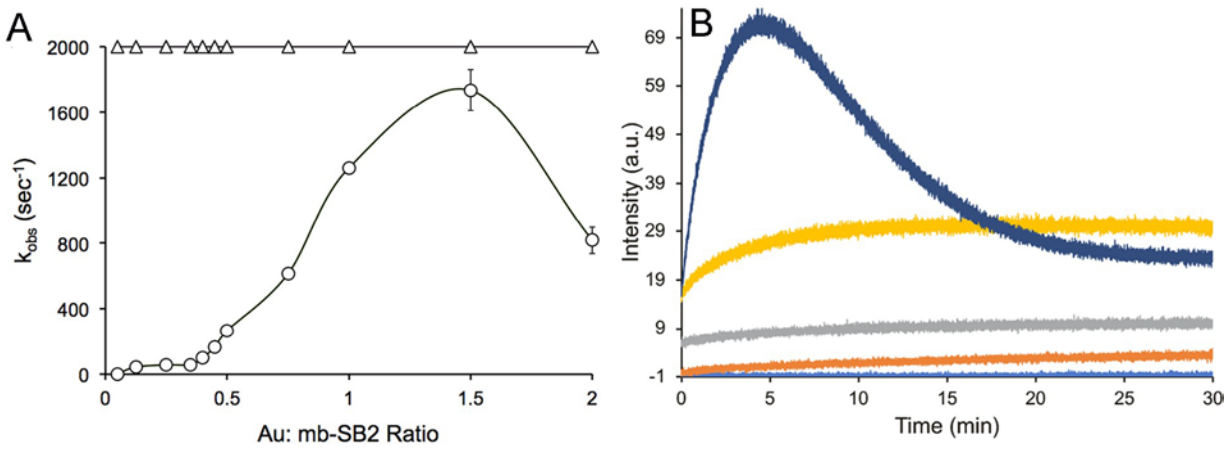

Figure 2. Kinetics of Au binding by MB-SB2 at 4°C. (A) Rate of $HAuCl_4$ binding to the imidazolone (△) and oxazolone (○) rings of mb-SB2 at 4°C as measured from the absorbance change at 386 nm and 341 nm, respectively. The rates for Au binding >2000 sec^{-1}, and were set at 2000 sec^{-1} in the figure. B. Emission at 429nm from SB2-MB following excitation at 341nm after the addition of 0 (**light blue**), 0.25 (**orange**), 0.5 709 (**grey**), 0.75 (**yellow**), or 2.25 (**dark blue**) $HAuCl_4$ per MB-SB2.

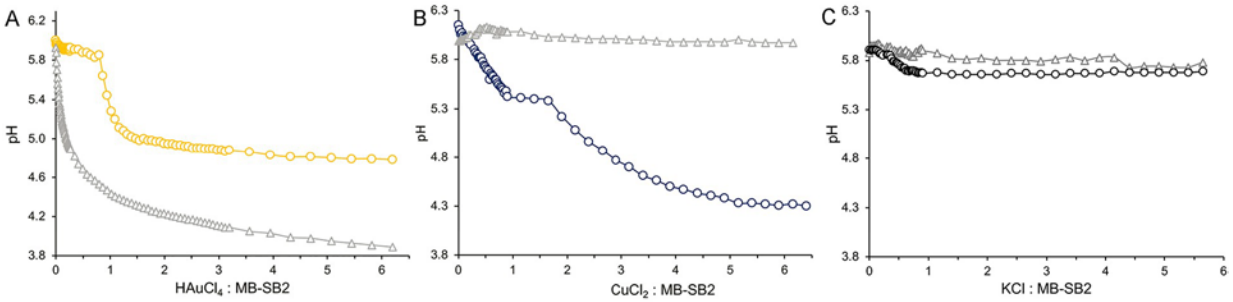

Figure 3. **A.** pH changes following the addition of $HAuCl_4$, to aqueous solutions (△)or aqueous solution of 40 µM MB-SB2 (○). **B.** pH changes following the addition of $CuCl_2$ to aqueous solutions (△) or aqueous solution of 40 µM MB-SB2 (○). **C.** pH changes following the addition of KCl to aqueous solutions (△) or aqueous solution of 40 µM MB-SB2 (○).

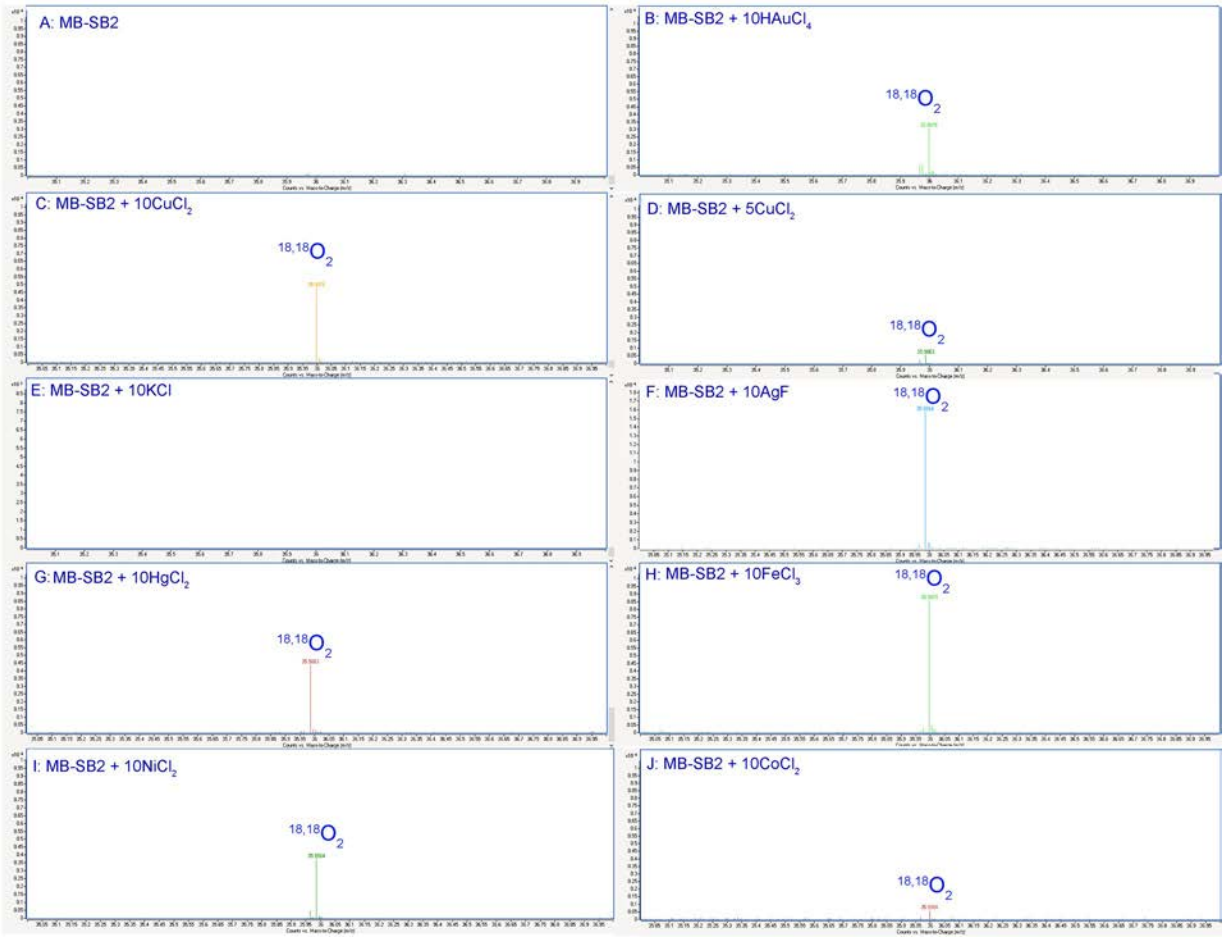

Figure 4. Mass spectra of head space gas of a reaction mixture containing 2mM MB-SB2 in 97% $H_2{}^{18}O$ (A) and following the addition of 20mM $HAuCl_4$ (B), 20mM $CuCl_2$ (C), 10mM $CuCl_2$ (D), 20mM KCl (E), 20mM AgF (F), 20mM $HgCl_2$ (G), 20mM $FeCl_3$ (H), 20mM $NiCl_2$ (I), or 20mM $CoCl_2$ (J).

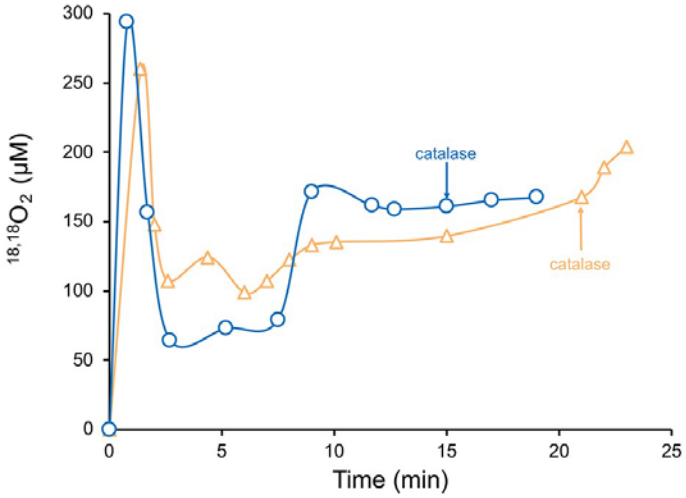

Figure 5. $^{18,18}O_2$ concentration in the head space of a reaction mixture containing 2 mM MB-SB2 plus 20mM $HAuCl_4$ (△) or 20mM $CuCl_2$ (○) in 97% $H_2{}^{18}O$ and following the addition of 7.3 mM of catalase.

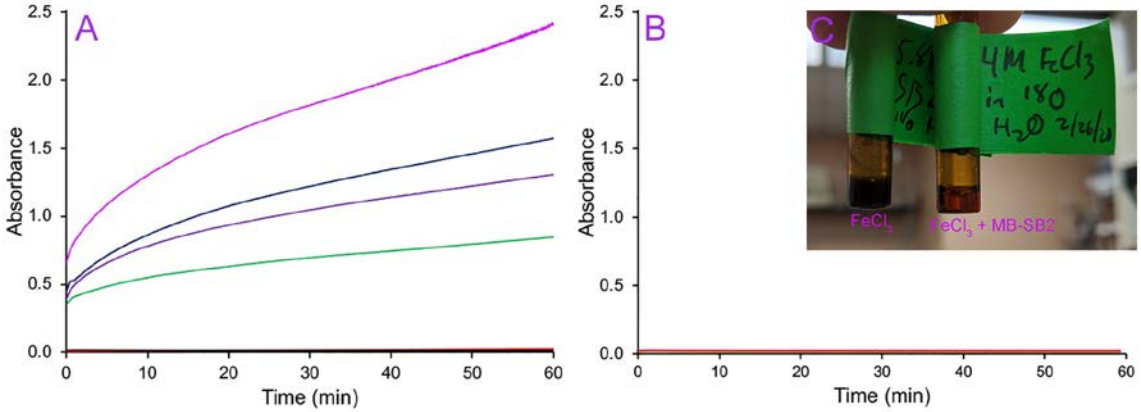

Figure 6. Iron reductase activity of MB-SB2 (A) and MB-OB3b (B). Absorption change at 562 nm of reaction mixtures containing 1mM ferrozine plus 10mM $FeCl_3$ (**black**),1mM ferrozine plus 23.4μM MB-SB (**red**), 1mM ferrozine plus 10mM $FeCl_3$ and either 5.8 (**green**), 11.6 (**dark purple**), 17.4 (**blue**) or 23.4 (**purple**) μM MB-SB2 (A) or MB-OB3b (B). C. Aqueous 4M $FeCl_3$ solution (a) and a 4M $FeCl_3$ solution plus 20 mM MB-SB2 4 hours after the addition of MB-SB2.

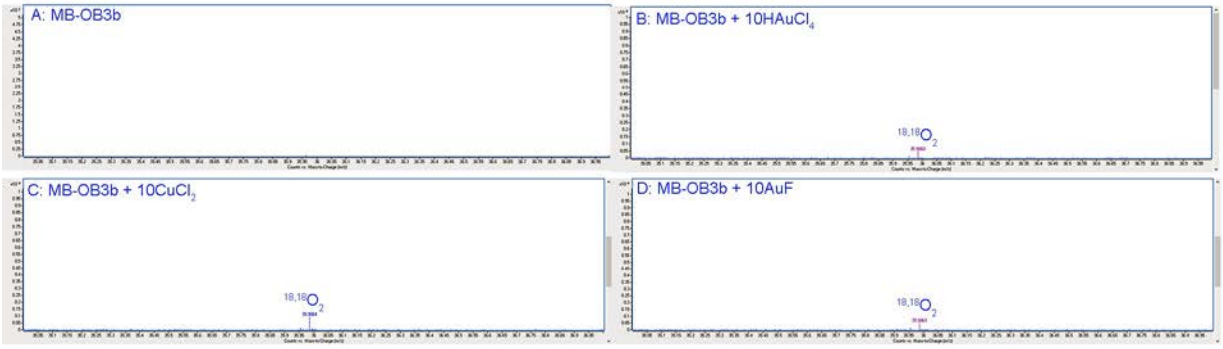

Figure 7. Mass spectra of head space gas of a reaction mixture containing 2mM MB-OB3b in 97% 742 $H_2{}^{18}O$ (A) and following the addition of 20mM $HAuCl_4$ (B), 20mM $CuCl_2$ (C), and 20mM AgF (D).

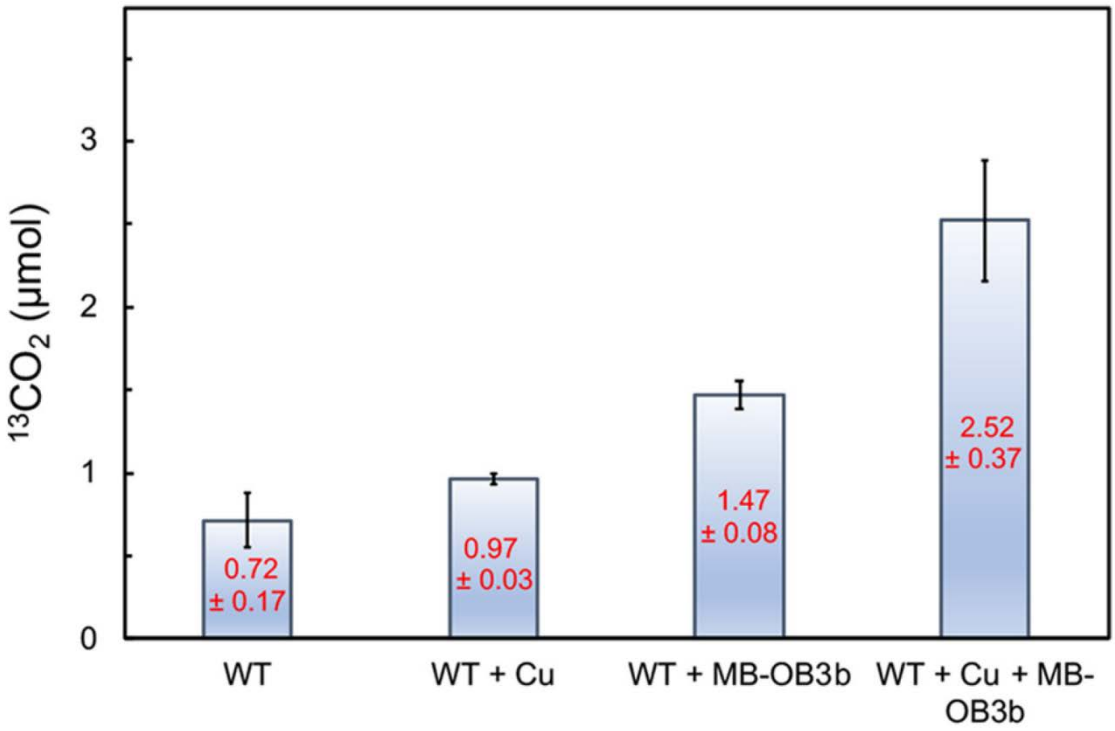

Figure 8. $^{13}CO_2$ production by the *M. trichosporium* OB3b wild type (WT), the WT plus 25µM $CuCl_2$, the WT plus 5µM MB-OB3b, and the WT plus 25µM $CuCl_2$ and 5µM MB-OB3b incubated in an anaerobic glove box for 3 days.

Supplemental Information

Table S1. Thermodynamic parameters as calculated by Origin and by CHASM for $HAuCl_4$ binding to MB-SB2

Parameter	Tetramer	Dimer	Monomer	Nanoparticle Formation
$HauCl_3$ Origin				
T_K	298.15	298.15	298.15	298.15
N (Au:mb-SB2^{-1})	0.207	0.447	1.10	0.380
K (M^{-1})	**$1.97 \times 10^{34} \pm 1.73 \times 10^{13}$**	**3.65×10^{8}**	**7.87×10^{11}**	**3.09×10^{10}**
ΔH (cal•mol^{-1})	-71,560*	-93,900	-68,190	-5,689
ΔS (cal^{-1} • mol^{-1} •deg^{-1})	96.7	-276	-174	28.9
ΔG (cal•mol^{-1})	-100,391	-11,611	-16,312	-14,306
χ^2	2.40×10^{9}	7.25×10^{6}	5.97×10^{5}	5.97×10^{5}
$HauCl_3$ CHASM				
N (Au:mb-SB2^{-1})	0.21 ± 5.83	0.67 ± 2.18	0.36 ± 4.33	0.24 ± 2.20
K (M^{-1})	**$4.97 \times 10^{35} \pm 6.63 \times 10^{24}$**	**$3.54 \times 10^{8} \pm 4.8 \times 10^{8}$**	**$1.60 \times 10^{7} \pm 2.23 \times 10^{7}$**	**$2.35 \times 10^{10} \pm 3.55 \times 10^{10}$**
ΔH (cal•mol^{-1})	-78,140 ± 5,800	-62,050 ± 2,200	-9,841 ± 4,300	-91,490 ± 2,200
ΔS (cal^{-1} • mol^{-1} •deg^{-1})	-29.47	-50.4	0.02	77.35
ΔG (cal•mol^{-1})	-48,700	-11,700	-9,820	-14,100

Table S2. Nanoparticle size distribution in reaction mixtures containing 2.25 $HAuCl_4$ per MB-SB2.

		Average	**Percent**			
MB-SB2 µM	**Time (h)**	**Diameter (nm)**	**X ≤ 3 (nm)**	**3 > X ≤ 10 (nm)**	**10 > X ≤ 15 (nm)**	**n**
25	6	1.9 ± 0.5	99.1	0.8	0.1	2565
25	24	2.0 ± 0.3	99.0	0.9	0.1	258
50	6	1.8 ± 0.4	99.3	0.7	0	715
50	24	2.0 ± 0.4	98.2	1.8	0	1099
100	6	2.0 ± 0.5	99.1	0.9	0	683
250	6	2.0 ± 0.4	97.1	0.9	0	280

Table S3. Superoxide dismutase (SOD), oxidase and hydrogen peroxide reductase (HPR) activities of MB-SB2, copper containing MB-SB2 (Cu-MB-SB2) and gold containing MB-SB2 (Au-MB-SB2). NADH (0.5 mM) was used as the reductant for oxidase and HPR activities.

MB	**SOD** ($O_2^{\bullet-}$ **min^{-1} mb^{-1}**)	**Oxidase** (O_2^- **min^{-1} mb^{-1}**)	**HPR** ($H_2O_2^-$ **min^{-1} mb^{-1}**)
MB-SB2	0	0.5±0.01	0
Cu-MB-SB2	2350±420	0.9±0.05	18±0.02
Au-MB-SB2	1980±37	0.7±0.01	11±0.03

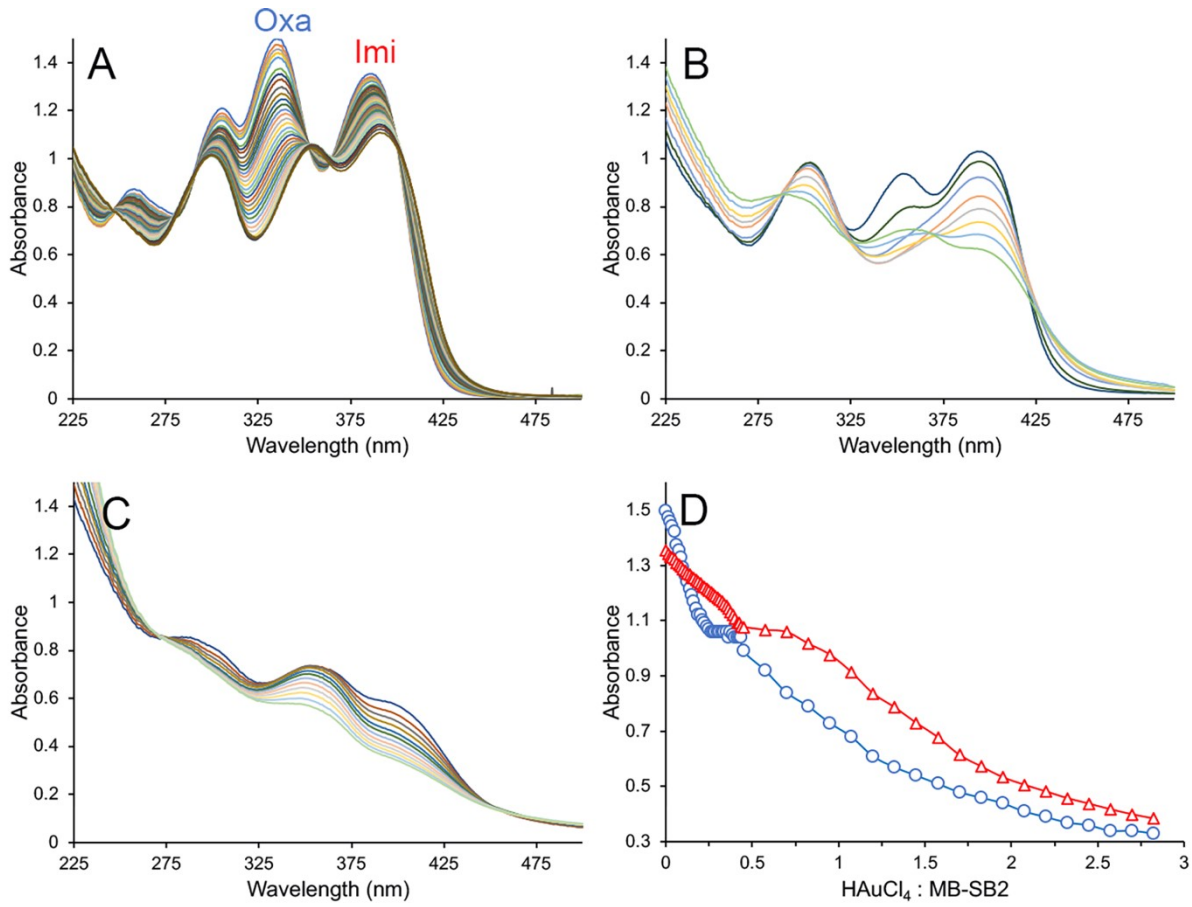

Figure S1. UV-visible absorption spectra of 40µM SB2-MB as isolated and following thirty-three 0.0125 molar additions of $HAuCl_4$ (**A**), followed by eight 0.125 molar additions of $HAuCl_4$ (**B**) and followed by another eleven 0.125 molar additions of $HAuCl_4$ (**C**)**. D.** Absorbance of the oxazolone (○) and imidazolone (△) groups at 336 and 387 nm, respectively as a function of $HAuCl_4$ to MB-SB2 molar ratios. Initial MB-SB2 and $HAuCl_4$ solutions were identical to the solutions used in the pH titration in Figure 1.

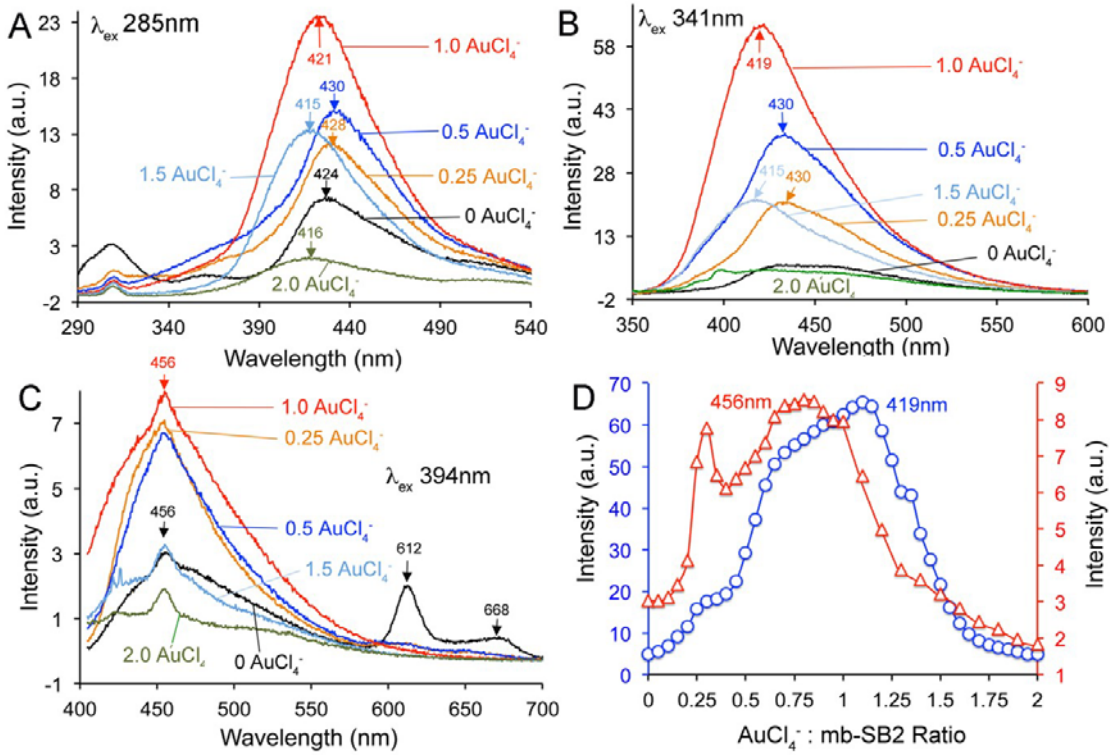

Figure S2. Emission spectra from SB2-MB following excitation at 285nm (**A**), 341nm (**B**) and 394nm (**C**) as isolated (—) and following the addition of 0.25 (**black**), 0.5 (**blue**), 1.0 (**red**), 1.5 (**light blue**) and 2.0 (**green**) $HAuCl_4$ per MB-SB2. **D**, Emission at 419nm (○) and at 456nm (△) following excitation at 341 and 394 nm, respectively, and following 0.05 molar additions of $HAuCl_4$.

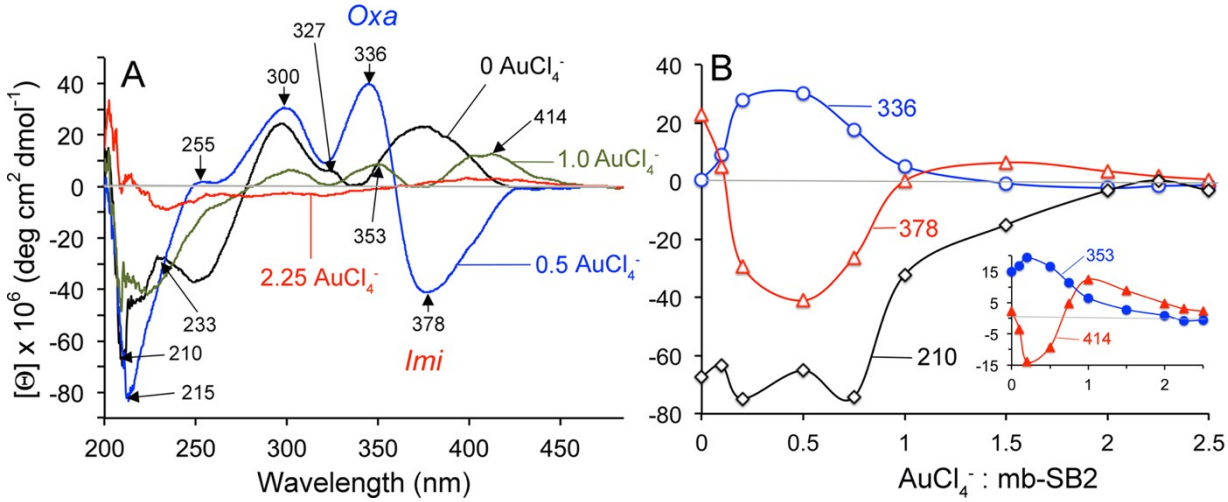

Figure S3. **A.** UV-visible CD spectra of MB-SB2 as isolated (**black**) and following the addition of 0.5 (**blue**), 1.0 (**green**) and 2.25 (**red**) $HAuCl_4$ per MB-SB2. **B.** Molar ellipticity changes at 210 (◇), 336 (○) and at 378 (△) nm following additions of $HAuCl_4$. **Insert.** Molar ellipticity changes at 353 (●) and at 414 (▲) nm following additions of $HAuCl_4$.

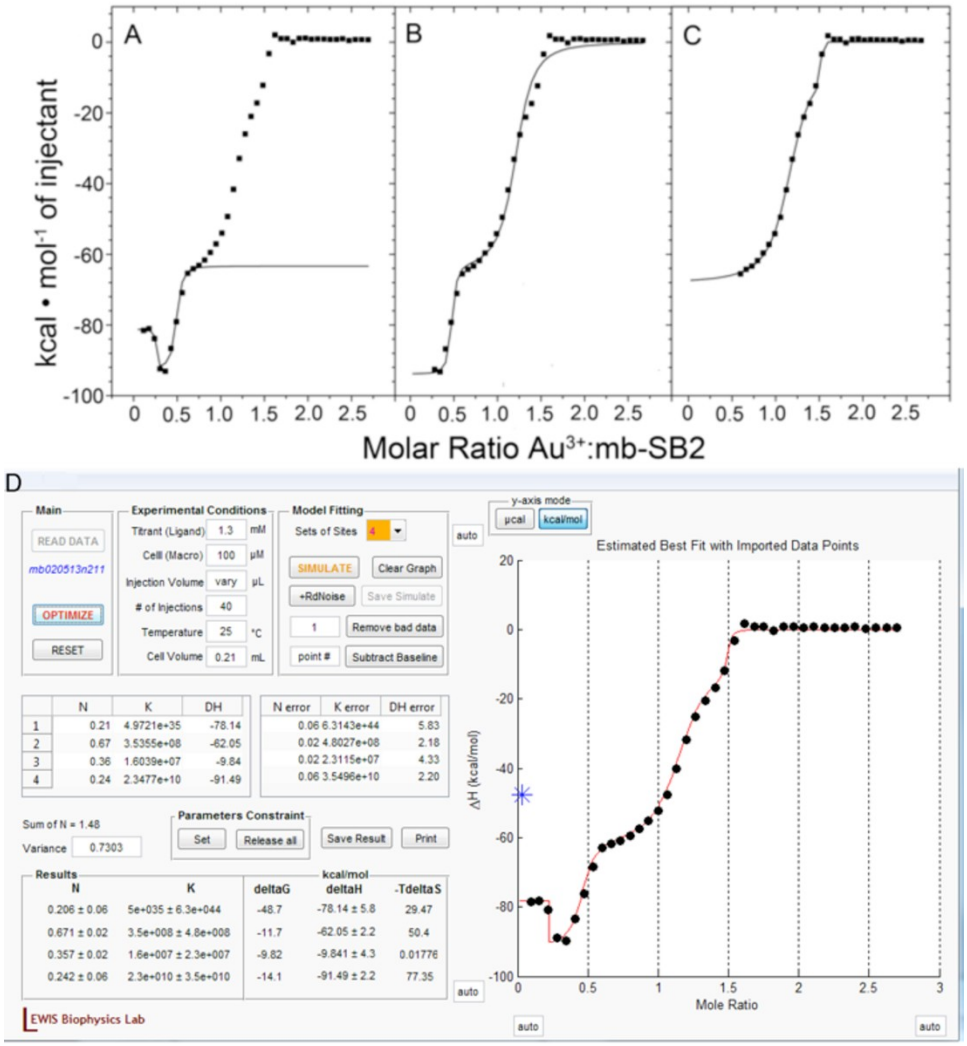

Figure S4. **A-C**. Binding isotherms from Origin software of $HAuCl_4$ titrations to MB-SB2 and following subtraction of the heat of dilution of $HAuCl_4$ into H_2O. Due to the complexity of the titration and limitations of the Origin software the data was divided to allow fitting. **D**. Screen capture of the MATLAB user interface of CHASM software showing a four-binding-site fit of the ITC data shown in panels A - C.

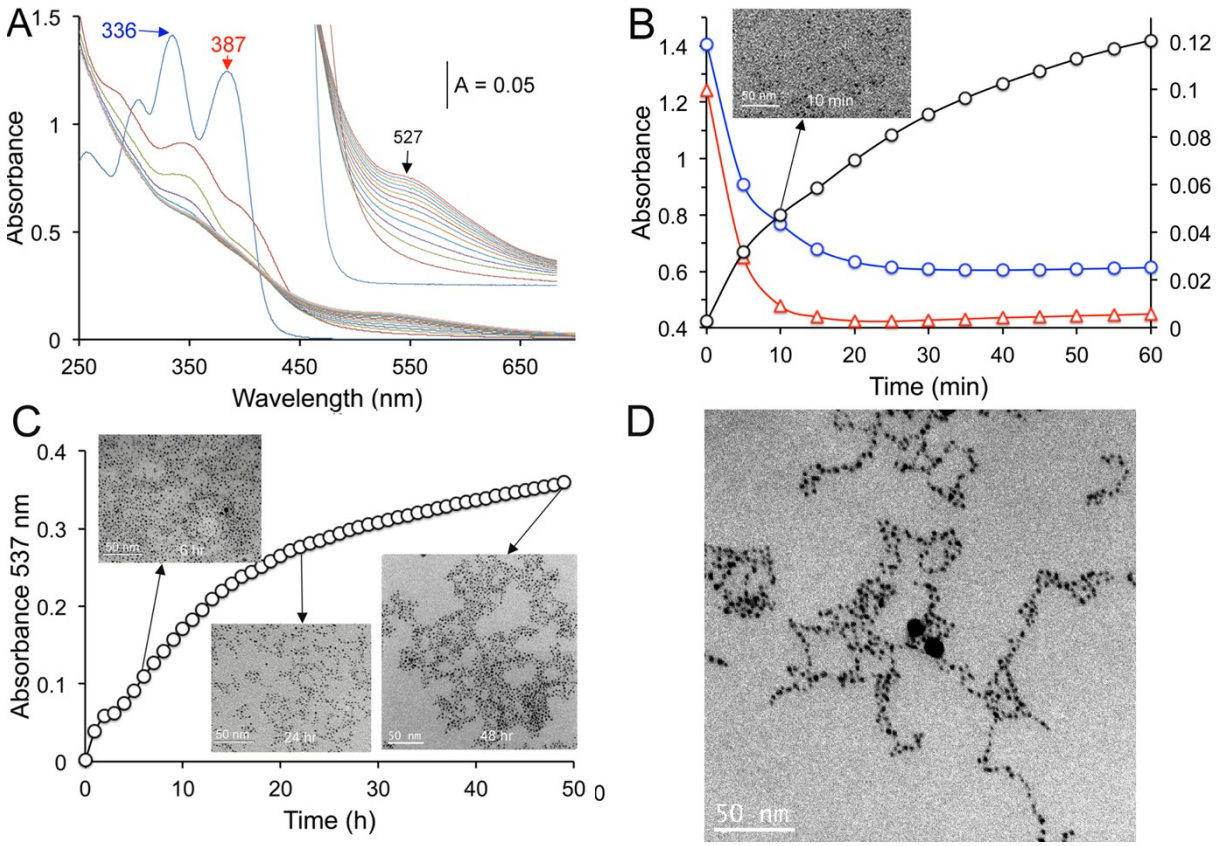

Figure S5. Spectral changes and nanoparticle formation overtime by MB-SB2 following the addition of 2.25 $HAuCl_4$ per MB-SB2. (**A**) UV-visible spectra of taken every 5 min following the addition of $HAuCl_4$ to MB-SB2. (**B**) Absorption changes at 336 (○), 387 (△) and 537 (○) nm, insert TEM of nanoparticles formed by MB-SB2 10 min after the addition of $HAuCl_4$. (**C**) Absorption changes at 537 nm, insert TEM of nanoparticles formed by MB-SB2 6, 24 and 59 hours after the addition of 2.25 $HAuCl_4$. (D) TEM of nanoparticles formed after 36 days in a solution containing 2.25 $HAuCl_4$ per MB-SB2.

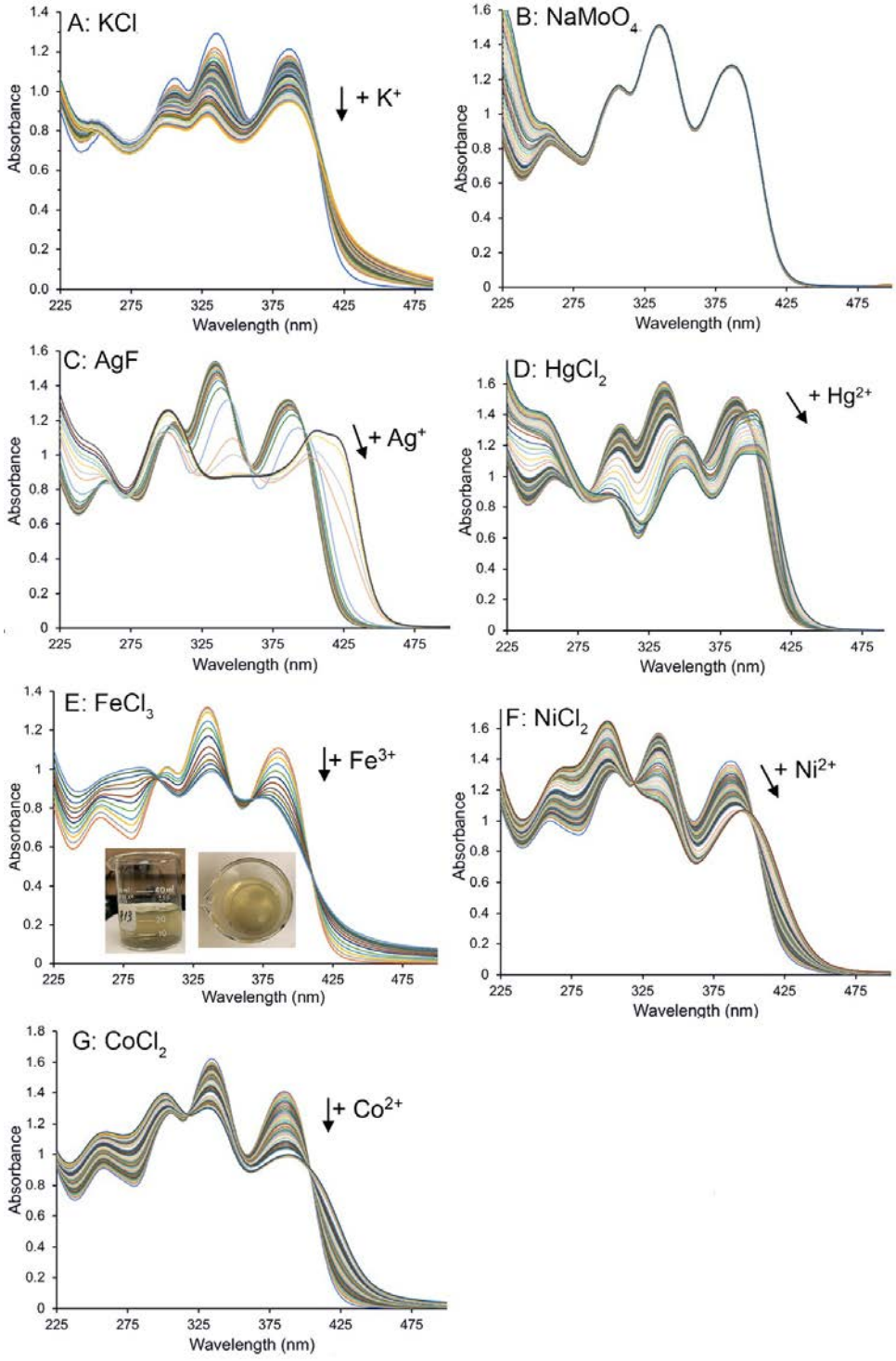

Figure S6. (**A)** UV-visible absorption spectra of 40µM SB2-MB as isolated and following molar additions of KCl (A), $NaMoO_4$ (B) AgF (C), $HgCl_2$ (D), $FeCl_3$ (E), $NiCl_2$ (F), or $CoCl_2$ (G). Panel D insert, equimolar $FeCl_3$ MB-SB2 solution.

CHAPTER 3. *MBNC* IS NOT REQUIRED FOR THE FOMATION OF THE N-TERMINAL OXAZOLONE IN THE METHANOBACTIN FROM *METHYLOSINUS TRICHOSPORIUM* OB3B

Philip Dershwitz[1,Ψ], Wenyu Gu[2Ψ‡], Julien Roche[1], Christina S. Kang-Yun[2†],Jeremy D. Semrau[2], Thomas A. Bobik[1], Hans Zischka[3], and Alan A. DiSpirito[1]*

[1]Roy J. Carver Department of Biochemistry, Biophysics and Molecular Biology. Iowa State University, Ames, IA 50011-3260, USA

[2]Department of Civil and Environmental Engineering, University of Michigan, Ann Arbor, MI, 48109-2125, USA

[3]Institute of Molecular Toxicology and Pharmacology, Helmholtz Center Münich, German Research Center and Environmental Health, Ingolsteadter Landstrasse, Germany and Technical University Münich, School of Medicine, Institute of Toxicology and Environmental Hygiene, Biedersteiner Strasse 29, D-80802 Munich, Germany.

[Ψ]Co-first authors

[‡]Current address: Department of Civil & Environmental Engineering, Stanford University, Stanford, CA, 94305, USA

[†]Current address: Biosciences and Biotechnology Division, Lawrence Livermore National Laboratory, Livermore, CA, 94550-9698, USA

Modified from the paper published in *Applied and Environmental Microbiology*

Abstract

Methanobactins (MBs) are ribosomally synthesized and posttranslationally modified peptides (RiPPs) produced by methanotrophs for copper uptake. The posttranslational modification that defines MBs is the formation of two heterocyclic groups with associated thioamines from X-Cys dipeptide sequences. Both heterocyclic groups in the MB from *Methylosinus trichosporium* OB3b (MB-OB3b) are oxazolone groups. The precursor gene for MB-OB3b is *mbnA,* which is part of a gene cluster that contains both annotated and unannotated genes. One of those unannotated genes, *mbnC*, is found in all MB operons and, in conjunction with *mbnB*, is reported to be involved in the formation of both heterocyclic groups in all MBs. To determine the function of *mbnC*, a deletion mutation was constructed in *M. trichosporium* OB3b, and the MB produced from the Δ*mbnC* mutant was purified and structurally characterized by UV-visible absorption spectroscopy, mass spectrometry, and solution nuclear magnetic resonance (NMR) spectroscopy. MB-OB3b from the Δ*mbnC* mutant was missing the C-terminal Met and was also found to contain a Pro and a Cys in place of the pyrrolidinyl-oxazolone-thioamide group. These results demonstrate *mbnC* is required for the formation of the C-terminal pyrrolidinyl-oxazolone-thioamide group from the Pro-Cys dipeptide, but not for the formation of the N-terminal 3-methylbutanol-oxazolone-thioamide group from the N-terminal dipeptide Leu-Cys.

Introduction

Methanobactins (MBs) are low-molecular-mass (,1,300 Da), posttranslationally modified copper-binding peptides excreted by some methanotrophs as the extracellular component of a copper acquisition system (DiSpirito *et al.,* 2016; El Ghazouani *et al.,* 2011; El Ghazouani *et al.,*

2012; Kim *et al.,* 2004; Krentz *et al.,* 2010; Semrau *et al.,* 2020; Semrau *et al.,* 2018). Structurally MBs are characterized by the presence of a C-terminal oxazolone group with a C2-associated thioamide and by the presence of an N-terminal oxazolone, imidazolone or pyrazinedione group with an associated thioamide. Some MBs also contain a sulfate group in-place of the hydroxyl group on a Tyr adjacent to the C-terminal oxazolone group. The best-characterized MB is from *Methylosinus trichosporium* OB3b (MB-OB3b), and the posttranslational modifications for this MB involve (i) deamination of the N-terminal Leu, (ii) conversion of the N-terminal Leu-Cys dipeptide to 1-(N-(mercapto-(5-oxo-2-(3-methylbutanoyl)oxazol-(Z)-4-ylidene)methyl), (iii) conversion of the C-terminal Pro-Cys dipeptide into pyrrolidin-2-yl-(mercapto-(5-oxo-oxazol-(Z)-4-ylidene)methyl), and (iv) cleavage of the leader sequence (El Ghazouani *et al.,* 2011; Kim *et al.,* 2004; Krentz *et al.,* 2010; Behling *et al.,* 2008; Gu *et al.,* 2017; Semrau *et al.,* 2020; Kenney *et al.,* 2018).

The gene encoding the MB precursor peptide, *mbnA* (Krentz *et al.,* 2010; Semrau *et al.,* 2020), is found in a gene cluster that contains both genes of known function, such as *mbnB* (Krentz *et al.,* 2010; Kenney *et al.,* 2018), *mbnN* (Gu *et al.,* 2017), and *mbnT* (Gu *et al.,* 2016), as well as unannotated genes, such as *mbnC* (Krentz *et al.,* 2010; Semrau *et al.,* 2020; Kenney *et al.,* 2018; Chou *et al.,* 2006). *mbnB* is a member of TIM barrel family as well as the DUF692 family of diiron enzymes (Kenney *et al.,* 2018; Chou *et al.,* 2006). In heterologous expression studies in *Escherichia coli*, *mbnBC* was shown to catalyze a dioxygen-dependent four-electron oxidation of Pro-Cys in *mbnA* (Kenney *et al.,* 2018; Chou *et al.,* 2006; Choi *et al.,* 2006). The roles of *mbnB* and *mbnC* could not be separately determined as attempts to separately purify these gene products in *E. coli* failed (Kenney *et al.,* 2018). From these data, it has been argued that *mbnBC* must act in concert and by doing so create both heterocyclic groups in MBs (Kenney

et al., 2018). Such conclusions, however, appear to be premature for several reasons. First, the reported spectra (Kenney *et al.,* 2018) only show the presence of the C-terminal oxazolone group, not the N-terminal oxazolone group, as the 394-nm absorption maximum is missing. Second, the absorption maximum at 302 nm, diagnostic for the presence of the N-terminal oxazolone group, was absent (Krentz *et al.,* 2010; Behling *et al.,* 2008; Eckert *et al.,* 2021). Third, no structural data were provided to support the presence of both oxazolone groups. To examine if *mbnB* and *mbnC* act in concert and are involved in the formation of both oxazolone groups in *M. trichosporium* OB3b, an *mbnC* deletion mutant (Δ*mbnC*) was constructed. The results show *mbnC* is required for the formation of the C-terminal oxazolone group, but not for the formation of the N-terminal oxazolone group.

Materials and Methods

Bacterial strains, growth media, and culture conditions

Plasmid construction was accomplished using *Escherichia coli* strain TOP10 (Invitrogen, Carlsbad, CA) as described previously (Gu *et al.,* 2017). Plasmids used and constructed during this study are shown in Table 1. The donor strain for conjugation of plasmids into *Methylosinus trichosporium* OB3b was *E. coli* S17-1 (Simon *et al.,* 1984). *E. coli* strains were cultivated at 37$^{\circ C}$ in Luria broth medium (Dot Scientific, Burton, MI). Methanotrophic strains (i.e., *M. trichosporium* OB3b wild type, *M. trichosporium* OB3b Δ*mbnAN*, *M. trichosporium* OB3b Δ*mbnC, Methylocystis* sp. strain SB2, and *Methylocystis parvus* OBBP) were cultivated at 30$^{\circ C}$ on nitrate mineral salts (NMS) medium (Whittenbury *et al.,* 1970), either in 250-ml flasks with side-arms at 200 rpm or in a 15-L New Brunswick Bioflow 310 fermenter (Eppendorf, Hauppauge, NY), using methane as the sole carbon and energy source. Where necessary, filter-

sterilized solutions of copper (as $CuCl_2$) and spectinomycin were added to culture media aseptically. A working concentration of 20 μg•ml^{-1} spectinomycin was used for maintaining pWG104 in the *M. trichosporium* OB3b Δ*mbnAN* deletion mutant (i.e., *M. trichosporium* OB3b Δ*mbnC*). Chemicals were purchased from Fisher Scientific(Waltham, MA) or Sigma-Aldrich (St. Louis, MO) of American Chemical Society reagent grade or better.

For ^{15}N NMR, $K^{14}NO3$ in NMS medium was replaced with $K^{15}NO3$ (Cambridge Isotope Laboratories, Cambridge, MA).

General DNA methods, transformation, and conjugation

DNA purification and plasmid extraction were performed using QIAquick and QIAprep kits from Qiagen following the manufacturer's instructions. DNA cloning, preparation of chemically competent cells, and plasmid transformation with E. coli were performed according to Sambrook *et al.*, 2001. Enzymes used for restriction digestion and ligation were purchased from New England Biolabs (Ipswich, MA). PCR of DNA for cloning purposes was accomplished using iProof high-fidelity polymerase (Bio-Rad, Hercules, CA). PCR for general purposes was accomplished using GoTaq DNA polymerase (Promega, Fitchburg, WI). PCR programs were set according to the manufacturer's suggestions. Plasmid pWG104 was conjugated into *M. trichosporium* OB3b Δ*mbnAN* with E. coli S17-1 as the donor strain as described by Martin *et al.*, 1995.

Construction of the *Methylosinus trichosporium* OB3b Δ*mbnC* strain

Previously, an *M. trichosporium* mutant was constructed in which *mbnA*BCMN was deleted using a counterselection technique (Gu *et al.*, 2017). To characterize the function of *mbnC*, a Δ*mbnC* mutant was constructed by introducing the pWG104 expression vector into the Δ*mbnAN* mutant. pWG104 was constructed by cloning two separate DNA fragments, one of

which was a 1.9-kb DNA fragment of *mbnA*B (created via use of primers mbnANf and mbn66) and the other of which was a 2.5-kb DNA fragment of *mbnMN* (created via use of primers mbn70 and mbnANr), leaving out *mbnC*. These two fragments were amplified with BamHI restriction sites as indicated in Fig. S2. These were then ligated together and cloned into the broad-host-range vector pTJS140 at the KpnI site.

Extraction of RNA and RT-PCR

To check the expression of genes restored to the *M. trichosporium* OB3b Δ*mbnC* mutant (e.g., *mbnA,-B, -M, and N*), genes associated with MB remaining in the chromosome (*mbnPH*), as well as the absence of *mbnC*, RNA from the Δ*mbnC* mutant was collected, purified, and reverse transcribed to cDNA to perform RT-PCR. Total RNA was isolated as described earlier (Gu *et al.,* 2017). Briefly, the Δ*mbnC* mutant was grown to the exponential phase, and RNA was extracted using a phenol-chloroform method modified from Griffiths *et al.,* 2000. Collected RNA was purified and removal of DNA confirmed by the absence of 16S rRNA PCR product from PCRs. The same amount of RNA (500 ng) was used for reverse transcription by SuperScript III reverse transcriptase (Invitrogen, Carlsbad, CA) for all reactions. RT-PCR analyses were performed to confirm the expression of *mbnABMNPH* as well as the absence of *mbnC* using primers listed in Table 1.

Isolation of MB from *Methylosinus trichosporium* OB3b, *Methylocystis* strain SB2, *Methylocystis parvus* OBBP, and the Δ*mbnC* mutant

MBs from all three methanotrophs were purified as previously described (Dershwitz *et al.,* 2021).

UV-visible absorption spectra

UV-visible absorption spectra of *mbnC*$^-$ high-performance liquid chromatography (HPLC) fractions from MB preparations from *M. trichosporium* OB3b and *Methylocystis* strain

SB2 and from the MB from *M. parvus* OBBP were determined as previously described (Bandow *et al.*, 2012; Choi *et al.*, 2006). Acid hydrolysis of the oxazolone groups in the MB from *M. parvus* OBBP was carried out in 85 μM acetic acid as previously described (Bandow *et al.*, 2012).

Structural characterization of the Δ*mbnC* mutant

UV-visible spectroscopy was recorded on a Cary 50 spectrometer (Agilent, Santa Clara, CA). Matrix-assisted laser desorption ionization-time of flight (MALDI-TOF) MS was performed on a Shimadzu AXIMA Confidence MALDI-TOF mass spectrometer (Shimadzu, Kyoto, Japan). Samples resuspended in 20 mM Tris-HCl buffer, pH 8.0 (10 to 20 $\mu g \bullet \mu l^{-1}$), were mixed in a 1:1 ratio with matrix Super dihydroxybenzoic acid (Super DHB), and 1 μl of this mixture was loaded on a DE1580TA plate (from Shimadzu) and allowed to dry at room temperature. Super DHB was prepared from 9 parts 2,5-dihydroxyben-zoic acid (DHB) and 1 part 2-hydroxy-5-methoxybenzoic acid (Sigma-Aldrich, St. Louis, MO), both prepared in 70% acetonitrile–29.9% H2O–0.1% trifluoroacetic acid. NMR experiments were performed on a Bruker Advance 700 (Bruker, Allentown, PA) with a Bruker 5-mm TCI 700 H/C/N cryoprobe or on a Bruker Advance 800 with a Bruker 5-mm TCI 800 H/C/N cryoprobe. NMR solutions were made using 15 to 40 mg uniformly labeled ^{15}N-MB-OB3b in a 90:10 H_2O-D_2O mixture at pH 6.5. Unless otherwise specified, all experiments were run at 265 K and 300,000,000 Pa. Samples were placed in 300,000,000-Pa-rated sapphire NMR tubes (Daedalus Innovations, LLC, Beaverdam, VA), and high pressure was generated by an Xtreme 60 (Daedalus Innovations). Analysis was per-formed in Mnova (Mestrelab Research, Escondido, CA).

Results

Generation of the Δ*mbnC* mutant

The previously constructed Δ*mbnAN* strain, whereby the *mbnABCMN* genes were deleted using a sucrose counterselection technique (Gu *et al.,* 2017), was back complemented with *mbnABMN* through selective amplification and ligation of *mbnAB* with *mbnMN*, deleting *mbnC*, and inserting this ligation product into pTJS140, creating pWG104 (Table 1). Successful removal of *mbnC* from this product was confirmed via sequencing (data not shown). The native σ^{70}-dependent promoter upstream of *mbnA* was also incorporated into pWG104, and expression of *mbnABMN* but not *mbnC* (from pWG104), as well as *mbnPH* (from the chromosome) was confirmed via reverse transcription-PCR (RT-PCR) (see Fig. S1 and S2 in the supplemental material).

UV-visible absorption and mass spectrometry of metal-free MB from *Methylosinus trichosporium* OB3b Δ*mbnC*

Comparison of the UV-visible absorption spectra of MB from *M. trichosporium* OB3b Δ*mbnC* to wild-type MB-OB3b suggested the of presence of the N-terminal oxazolone group, but the absence of C-terminal oxazolone (Fig. 1: see Fig. S3 in the supplemental material). The molecular mass of native, full-length MB-OB3b is 1,154 Da, and that of MB-OB3b lacking the C-terminal Met is 1,023 Da. It should be noted that both forms of MB-OB3b are present in most MB-OB3b preparations (El Ghazouani *et al.,* 2011; Krentz *et al.,* 2010; Bandow *et al.,* 2011). The molecular mass of Δ*mbnC* was 1,024 as determined by matrix-assisted laser desorption ionization-time of flight (MALDI-TOF) mass spectrometry (MS) (Fig. 2) (Gu *et al.,* 2017), which was within 1 Da of the predicted molecular mass of MB-OB3b, in which only one oxazolone group was formed. Taken together, the UV-visible absorption spectra and molecular mass data suggest the Δ*mbnC* mutant lacked the C-terminal Met as well as the N-terminal

oxazolone group with a 1-(N-[mercapto-(5-oxo-2-(3-methylbutanoyl)oxazol-(Z)-4-ylidene)methyl]-GSCYPCSC predicted structure (Fig. 3B). In contrast to wild-type MB-OB3b, the C-terminal Met was never observed in the Δ*mbnC* mutant.

Chemical structure of metal-free Δ*mbnC* mutant as determined by NMR spectroscopy

Metal-free MB has multiple conformations, making structural studies of MBs via solution nuclear magnetic resonance (NMR) or crystallography difficult (see Fig. S4 in the supplemental material). In prior structural studies of MB, the addition of Cu^{2+} (which is bound and reduced to Cu^{+} by native MB-OB3b) stabilizes MB-OB3b into one conformation, allowing for crystal formation and NMR characterization (Fig. S4) (El Ghazouani *et al.*, 2011; El Ghazouani *et al.*, 2012; Kim *et al.*, 2004; Krentz *et al.*, 2010; Behling *et al.*, 2008; Kenney *et al.*, 2016). Our initial efforts to investigate the structure of the MB intermediate produced by the Δ*mbnC* strain via NMR were unsuccessful.

In contrast to native MB, the MB intermediate from the Δ*mbnC* strain bound, but did not reduce Cu^{2+} to Cu^{+}, resulting in peak broadening from paramagnetic Cu^{2+}. This necessitated a different strategy. Substituting other metals with similar binding behavior for copper such as Au^{3+}, Zn^{2+}, Co^{2+}, and Ni^{2+} also failed to produce well-behaved complexes. Therefore, it was necessary to examine the metal-free Δ*mbnC* mutant.

At standard temperature and pressure, the Δ*mbnC* mutant undergoes exchange between multiple conformations on an intermediate time scale, leading to excessive line broadening (see Fig. S5 in the supplemental material). In order to slow down the rate of exchange and reduce line broadening, we sampled various temperature and hydrostatic pressure conditions. We found that two-dimensional (2D) 1H-15NNMR spectra of the Δ*mbnC* mutant recorded at high pressure (300,000,000 Pa) and low temperature (265 K) (Kenney *et al.*, 2016; Zischka *et al.*, 2017) show

significantly reduced line broadening and gave excellent spectra in the absence of copper (Fig. 4).

A series of NMR experiments were conducted on the Δ*mbnC* mutant, including homonuclear correlation spectroscopy (COSY), total correlation spectroscopy (TOCSY), rotating-frame nuclear Overhauser effect spectroscopy (ROESY), ^{1}H-^{15}N and ^{1}H-^{13}C heteronuclear single-quantum correlation spectroscopy (HSQC), and heteronuclear multiple-bond correlation spectroscopy (HMBC). These experiments enabled assigning all nonhydroxyl ^{1}H, nonconjugated ^{13}C, and all ^{15}N resonances (Table 2 and Fig. 4; see Fig. S6 in the supplemental material). The assigned chemical shifts show that the MB from the Δ*mbnC* mutant contains 8 amino acids—3 Cys, 2 Ser, 1 Gly, 1 Tyr and 1 Pro—and 1 oxazolone group (Fig. 4). The 1D ^{15}N experiment showed a peak at 109 ppm that was absent from the ^{1}H-^{15}N HSQC spectra and was assigned to proline. However, the glycine nitrogen peak was especially broad, and could only be assigned with the ^{1}H-^{15}N HSQC. Finally, while the 1D ^{15}N experiment had several resonances around 180 ppm—likely due to hydrolysis and deprotonation—only one of them had a correlation with ^{1}H in the ^{1}H-^{15}N HSQC, indicating a single oxazolone group. The NMR results are consistent with the UV-visible absorption spectra and the ESI MS results, as well as with the structure shown in Fig. 3B.

Discussion

Due to the variability in the core sequences of structurally characterized MBs, it is difficult to use the *mbnA* gene sequence to screen the potential ability of microbes to produce MB. Instead, *mbnB* and *mbnC* sequences are commonly used as they are found in all known mbn gene clusters (Krentz *et al.,* 2010; Kenney *et al.,* 2013). All known MBs contain two heterocyclic

rings, with the N-terminal ring found to be either an oxazolone, pyrazinedione, or imidazolone ring, while the C-terminal ring was always found to be an oxazolone. Given these data, it could be presumed that *mbnBC* is involved in the formation of the C-terminal oxazolone group along with an associated thioamide, while the N-terminal oxazolone group is formed via a different process, such as the involvement of an aminotransferase, as concluded earlier (Krentz *et al.,* 2010; Gu *et al.,* 2017; Semrau *et al.,* 2020; Kenney *et al.,* 2013).

Other researchers have attempted to elucidate the role of *mbnB* and *mbnC* in methanobactin maturation (Kenney *et al.,* 2018). These individuals were unable to separately heterologously express soluble protein from either *mbnB* or *mbnC*, but were able to coheterologously express *mbnBC* as a heterodimeric complex. In studies where the *mbnA* precursor polypeptide was incubated with this *mbnBC* complex, the authors conclude that *mbnBC* was involved in the formation of both oxazolone groups and the associated thioamides of MB-OB3b. It should be noted, however, that in this study, no structural evidence (i.e., solution NMR data) was provided to definitively show the presence of either ring: rather, such conclusions were largely based on mass spectral analyses of *mbnA* after incubation with the *mbnBC* complex. Further, the authors assumed that since their construct did not contain the N-terminal aminotransferase *mbnN*, the extended conjugation resulting from this reaction would result in both oxazolone groups having identical absorption maxima. The idea that the extended conjugation of the N-terminal oxazolone could be responsible for the bathochromic shift was first pro-posed as a possible reason for the 50-nm shift in the absorption maxima by Krentz *et al.,* 2010. Kenney *et al.,* 2018 used this theory to bolster their claim that both oxazolone groups were present in the product from their heterologous system, with both oxazolone groups showing identical absorption spectra . The evidence to support this claim came from their *M.*

trichosporium OB3b Δ*mbnN* strain. *mbnN* is responsible for the deamination of the N-terminal Leu in *M. trichosporium* OB3b, extending the conjugation one additional double bond. In this study, the authors claim they can stabilize the MB produced by the Δ*mbnN* strain by the addition of copper before purification. UV-visible absorption spectra of copper-containing Δ*mbnN* mutant suggest the possible presence of two oxazolone groups but no additional evidence was provided supporting this claim.

This observation was surprising as the MB produced by the Δ*mbnN* strain in our laboratory showed similar UV-visible absorption spectra throughout the growth cycle, suggesting the absence of the N-terminal oxazolone group (see Fig. S7 in the supple-mental material). In addition, the UV-visible absorption spectra, liquid chromatography (LC)-MS/MS, Fourier transform ion cyclotron resonance (FT-ICR) MS, amino acid analysis, number of thiol groups, copper-binding properties, and pattern of acid hydrolysis demonstrate the absence of the N-terminal oxazolone group in the Δ*mbnN* mutant (Gu *et al.*, 2017).

Additional evidence that the bathochromic shift in MBs with two oxazolone groups is unlikely to solely arise from the addition of one double bond following deamination of the N-terminal amine comes from examination of the group I MB from *Methylocystis parvus* OBBP. Acid hydrolysis of the MB from *M. parvus* OBBP shows a similar hydrolysis pattern to that observed with the MB from *M. trichosporium* OB3b, demonstrating the presence of two oxazolone groups, with absorption maxima at 340 and 390 nm (see Fig. S8 in the supplemental material). However, both MB operons from *M. parvus* OBBP lack *mbnN*, and without deamination of the N-terminal Phe, the conjugation around the N-terminal oxazolone group would not be extended. It is possible that another aminotransferase in the *M. parvus* OBBP genome may catalyze deamination of the N-terminal Phe. However, this appears unlikely as

deamination of the N-terminal amino acid has never been observed in structurally characterized MBs from operons lacking *mbnN* (El Ghazouani *et al.,* 2012; Krentz *et al.,* 2010). The results suggest deamination of the N-terminal amino acid is not solely responsible for the 40- to 50-nm absorption maximum difference between oxazolone groups in MBs. The absence of either the N-terminal or C-terminal oxazolone group in a small (0.5 to 2%) fraction of most MB-OB3b preparations (Fig. S3) also questions the suggestion that the absorption maximum difference between the N-terminal and C-terminal oxazolone groups is due solely to extending the conjugation of an additional double bond introduced following the deamination reaction.

The results presented here confirm *mbnC* is required for the formation of the C-terminal oxazolone group (Fig. 5). However, the results presented here also demonstrate *mbnC* is not required for the formation of the N-terminal oxazolone group in *M. trichosporium* OB3b, suggesting the formation of the two heterocyclic groups with associated thioamides from XC dipeptides does not utilize the same enzyme(s). Future studies will determine if *mbnB* is involved in the formation of the N-terminal oxazolone, pyrazinedione, or imidazolone groups. Resolution of the pathway and enzymes responsible for the posttranslational modifications required for the synthesis of MB in methanotrophic bacteria will aid in the production of MB derivatives with pharmacological properties specific for different metal-related diseases (Zischka *et al.,* 2017; Zischka *et al.,* 2011; Lichtmannegger *et al.,* 2016; Choi *et al.,* 2008; Summer *et al.,* 2011; Müller *et al.,* 2018) as well as for environmental applications (Semrau *et al.,* 2020; Lu *et al.,* 2017).

Acknowledgements

This research was supported by the U.S. Department of Energy Office of Science (grants DE-SC0018059 and DE-SC0020174 to J.D.S. and A.A.D.), the National Science Foundation

(grant 1912482 to J.D.S.), the Roy J. Carver Charitable Trust (Muscatine, IA, USA) (to J.R.), and an ISU Bailey Research and Career Development award (to T.A.B.). Use of the Bruker Advance 800 was made possible through a generous gift from the Roy J. Carver Charitable Trust.

We declare no conflict of interest.

References

1. DiSpirito AA, Semrau JD, Murrell JC, Gallagher WH, Dennison C, Vuilleumier S. 2016. Methanobactin and the link between copper and bacterial methane oxidation. Microbiol Mol Biol Rev 80:387–409. https://doi.org/10.1128/MMBR .00058-15.

2. El Ghazouani A, Basle A, Firbank SJ, Knapp CW, Gray J, Graham DW, Dennison C. 2011. Copper-binding properties and structures of methanobactins from *Methylosinus trichosporium* OB3b. Inorg Chem 50:1378–1391. https://doi.org/ 10.1021/ic101965j.

3. El Ghazouani A, Basle A, Gray J, Graham DW, Firbank SJ, Dennison C. 2012. Variations in methanobactin structure influences copper utilization by methane-oxidizing bacteria. Proc Natl Acad Sci U S A 109:8400–8404. https://doi.org/10.1073/pnas.1112921109.

4. Kim HJ, Graham DW, DiSpirito AA, Alterman MA, Galeva N, Larive CK, Asunskis D, Sherwood PM. 2004. Methanobactin, a copper-acquisition compound from methane-oxidizing bacteria. Science 305:1612–1615. https://doi.org/10.1126/science.1098322.

5. Krentz BD, Mulheron HJ, Semrau JD, DiSpirito AA, Bandow NL, Haft DH, Vuilleumier S, Murrell JC, McEllistrem MT, Hartsel SC, Gallagher WH. 2010. A comparison of methanobactins from *Methylosinus trichosporium* OB3b and *Methylocystis* strain SB2 predicts methanobactins are synthesized from diverse peptide precursors modified to create a common core for binding and reducing copper ions. Biochemistry 49:10117–10130. https://doi.org/10.1021/bi1014375.

6. Semau JD, DiSpirito AA, Obulisamy PK, Kang CS. 2020. Methanobactin from methanotrophs: genetics, structure, function and potential applications. FEMS Microbiol Lett 367:feaa045.

7. Semrau JD, DiSpirito AA, Gu W, Yoon S. 2018. Metals and methanotrophy. Appl Environ Micro biol 84:e02289-17. https://doi.org/10.1128/AEM.02289-17.

8. Behling LA, Hartsel SC, Lewis DE, DiSpirito AA, Choi DW, Masterson LR, Veglia G, Gallagher WH. 2008. NMR, mass spectrometry and chemical evidence reveal a different chemical structure for methanobactin that contains oxazolone rings. J Am Chem Soc 130:12604–12605. https://doi.org/ 10.1021/ja804747d.

9. Gu W, Baral BS, DiSpirito AA, Semrau JD. 2017. An aminotransferase is responsible for the deamination of the N-terminal leucine and required for formation of oxazolone ring A in methanobactin of *Methylosinus trichosporium* OB3b. Appl Environ Microbiol 83:e02619-16. https://doi.org/10 .1128/AEM.02619-16.

10. Semrau JD, DiSpirito AA, Obulisamy PK, Kang-Yun CS. 2020. Methanobactin from methanotrophs: genetics, structure, function and potential applications. FEMS Microbiol Lett 367:fnaa045. https://doi.org/10 .1093/femsle/fnaa045.

11. Kenney GE, Dassama LMK, Pandelia M-E, Gizzi AS, Martinie RJ, Gao P, DeHart CJ, Schachner LF, Skinner OS, Ro SY, Zhu X, Sadek M, Thomas PM, Almo SC, Bollinger MJ, Krebs C, Kelleher NL, Rosenzweig AC. 2018. The biosynthesis of methanobactin. Science 359:1411–1416. https://doi.org/ 10.1126/science.aap9437.

12. Gu W, Farhan Ul Haque M, Baral BS, Turpin EA, Bandow NL, Kremmer E, Flatley A, Zischka H, DiSpirito AA, Semrau JD. 2016. A TonB dependent transporter is responsible for methanobactin uptake by *Methylosinus trichosporium* OB3b. Appl Environ Microbiol 82:1917–1923. https://doi.org/ 10.1128/AEM.03884-15.

13. Kenney GE, Rosenzweig AC. 2013. Genome mining for methanobactins. BMC Biol 11:17. https://doi.org/10.1186/1741-7007-11-17.

14. Chou JC-C, Strafford VE, Kenney GE, Dassama LMK. 2021. The enzymology of oxazolone and thioamide synthesis in methanobactin. Methods Enzymol 656: 341–373. https://doi.org/10.1016/bs.mie.2021.04.008.

15. Choi DW, Do YS, Zea CJ, McEllistrem MT, Lee SW, Semrau JD, Pohl NL, Kisting CJ, Scardino LL, Hartsel SC, Boyd ES, Geesey GG, Riedel TP, Shafe PH, Kranski KA, Tritsch JR, Antholine WE, DiSpirito AA. 2006. Spectral and thermodynamic properties of Ag(I), Au(III), Cd(II), Co(II), Fe(III), Hg(II), Mn (II), Ni(II), Pb(II), U(IV), and Zn(II) binding by methanobactin from *Methylosinus trichosporium* OB3b. J Inorg Biochem 100:2150–2161. https://doi .org/10.1016/j.jinorgbio.2006.08.017.

16. Eckert P, Johs A, Semrau JD, DiSpirito AA, Richardson J, Sarangi R, Herndon E, Gu B, Pierce EM. 2021. Spectroscopic and computational investigations of organometallic complexation of group 12 transition metals by methanobactins from *Methylocystis* sp. SB2. J Inorg Biochem 223:111496. https://doi .org/10.1016/j.jinorgbio.2021.111496.

17. Bandow NL, Gallagher WH, Behling L, Choi DW, Semrau JD, Hartsel SC, Gilles VS, Dispirito AA. 2011. Isolation of methanobactin from the spent media of methane-oxidizing bacteria. Methods Enzymol 495:259–269. https://doi.org/10.1016/B978-0-12-386905-0.00017-6.

18. Kenney GE, Goering AW, Ross MO, DeHart CJ, Thomas PM, Hoffman BM, Kelleher NL, Rosenzweig AC. 2016. Characterization of methanobactin from *Methylosinus* sp. SW4. J Am Chem Soc 138:11124–11127. https://doi .org/10.1021/jacs.6b06821.

19. Zischka H, Lichtmannnegger J, DiSpirito AA, Semrau JD. 2017. Means and methods of treating copper-related diseases. World patent WO2017103094A2.

20. Zischka H, Lichtmannegger J, Schmitt S, Jagemann N, Schulz S, Wartini D, Jennen L, Rust C, Larochette N, Galluzzi L, Chajes V, Bandow N, Gilles VS, DiSpirito AA, Esposito I, Goettlicher M, Summer KH, Kroemer G. 2011. Liver mitochondrial membrane crosslinking and destruction in a rat model of Wilson disease. J Clin Invest 121:1508–1518. https://doi.org/10.1172/JCI45401.

21. Lichtmannegger J, Leitzinger C, Wimmer R, Schmitt S, Schulz S, Kabiri Y, Eberhagen C, Rieder T, Janik D, Neff F, Straub BK, Schirmacher P, DiSpirito AA, Bandow N, Baral BS, Flatley A, Kremmer E, Denk G, Reiter FP, Hohenester S, Eckardt-Schupp F, Dencher NA, Adamski J, Sauer V, Niemietz C, Schmidt HHJ, Merle U, Gotthardt DN, Kroemer G, Weiss KH, Zischka H. 2016. Methanobactin: a new effective treatment strategy against acute liver failure in a Wilson disease rat model. J Clin Invest 126:2721–2735. https://doi.org/10.1172/JCI85226.

22. Choi DW, Semrau JD, Antholine WE, Hartsel SC, Anderson RC, Carey JN, Dreis AM, Kenseth EM, Renstrom JM, Scardino LL, Van Gorden GS, Volkert AA, Wingad AD, Yanzer PJ, McEllistrem MT, de la Mora AM, DiSpirito AA. 2008. Oxidase, superoxide dismutase, and hydrogen peroxide reductase activities of methanobactin from types I and II methanotrophs. J Inorg Biochem 102:1571–1580. https://doi.org/10.1016/j .jinorgbio.2008.02.003.

23. Summer KH, Lichtmannegger J, Bandow N, Choi DW, DiSpirito AA, Michalke B. 2011. The biogenic methanobactin is an effective chelator for copper in a rat model for Wilson disease. J Trace Elem Med Biol 25:36–41. https://doi.org/10.1016/j.jtemb.2010.12.002.

24. Müller J-C, Lichtmannegger J, Zischka H, Sperling M, Karst U. 2018. High spatial resolution of LA-ICP-MS demonstrates massive liver copper depletion in Wilson disease rats upon methanobactin treatment. J Trace Elem Med Biol 49:119–127. https://doi.org/10.1016/j.jtemb.2018.05.009.

25. Lu X, Gu W, Zhao L, Fagan UHM, DiSpirito AA, Semrau JD, Gu B. 2017. Methylmercury uptake and degradation by methanotrophs. Science Adv 3:e1700041. https://doi.org/10.1126/sciadv.1700041.

26. Simon R. 1984. High frequency mobilization of Gram-negative bacterial replicons by the in vitro constructed Tn5-Mob transposon. Mol Gen Genet 196:413–420. https://doi.org/10.1007/BF00436188.

27. Whittenbury R, Phillips KC, Wilkinson JF. 1970. Enrichment, isolation and some properties of methane-utilizing bacteria. J Gen Microbiol 61:205–218. https://doi.org/10.1099/00221287-61-2-205.

28. Sambrook J, Russell DW. 2001. Molecular cloning: a laboratory manual, 3rd ed. Cold Spring Harbor Laboratory Press, Cold Spring Harbor, NY.

29. Martin H, Murrell JC. 1995. Methane monooxygenase mutants of *Methylosinus trichosporium* constructed by marker-exchange mutagenesis. FEMS Lett 127: 243–248. https://doi.org/10.1111/j.1574-6968.1995.tb07480.x.

30. Griffiths RI, Whiteley AS, O'Donnell AG, Bailey MJ. 2000. Rapid method for coextraction of DNA and RNA from natural environments for analysis of ribosomal DNA- and rRNA-based microbial community composition. Appl Environ Microbiol 66:5488–5491. https://doi.org/10.1128/AEM.66.12 .5488-5491.2000.

31. Dershwitz P, Bandow NL, Yang J, Semrau JD, McEllistrem MT, Heinze RA, Fonseca M, Ledesma JC, Jennett JR, DiSpirito AM, Athwal NS, Hargrove MS, Bobik TA, Zischka H, DiSpirito AA. 2021. Oxygen generation via water splitting by a novel biogenic metal ion binding compound. Appl Environ Microbiol 87:e00286-21. https://doi.org/10.1128/AEM.00286-21.

32. Bandow N, Gilles VS, Freesmeier B, Semrau JD, Krentz B, Gallaghe W, McEllistrem MT, Hartse SC, Cho DW, Hargrove MS, Heard TM, Chesner LM, Braunreiter KM, Cao BV, Gavitt MM, Hoopes JZ, Johnson JM, Polster EM, Schoenick BD, Am U, DiSpirito AA. 2012. Spectral and copper binding properties of methanobactin from the facultative methanotroph *Methylocystis* strain SB2. J Inorg Biochem 110:72–82. https://doi.org/10 .1016/j.jinorgbio.2012.02.002.

33. Choi DW, Zea CJ, Do YS, Semrau JD, Antholine WE, Hargrove MS, Pohl NL, Boyd ES, Geesey GG, Hartsel SC, Shafe PH, McEllistrem MT, Kisting CJ, Campbell D, Rao V, de la Mora AM, Dispirito AA. 2006. Spectral, kinetic, and thermodynamic properties of Cu(I) and Cu(II) binding by methanobactin from *Methylosinus trichosporium* OB3b. Biochemistry 45:1442–1453. https://doi.org/10.1021/bi051815t.

34. Smith TJ, Slade SE, Burton NP, Murrell JC, Dalton H. 2002. Improved system for protein engineering of the hydroxylase component of soluble methane monooxygenase. Appl Environ Microbiol 68:5265–5273. https://doi.org/10.1128/AEM.68.11.5265-5273.2002.

35. Semrau JD, Jagadevan S, DiSpirito AA, Khalifa A, Scanlan J, Bergman BH, Freemeier BC, Baral BS, Bandow NL, Vorobev A, Haft DH, Vuilleumier S, Murrell JC. 2013. Methanobactin and MmoD work in concert to act as the “copper switch” in methanotrophs. Environ Microbiol 15:3077–3086. https://doi.org/10.1111/1462-2920.12150.

36. DiSpirito AA, Semaru JD, Murrell JC, Gallagher WH, Dennison C, Vuilleumier S. 2016. Methanobactin and the link between copper and bacterial methane oxidation. Microbiol Mol Biol Rev 80:387-409.

37. Semau JD, DiSpirito AA, Obulisamy PK, Kang CS. 2020. Methanobactin from methanotrophs: genetics, structure, function and potential applications. FEMS Microbiol Lett 367:feaa045.

Tables

Table 1. Strains, plasmids, and primers used in this study

Strain, plasmid, or primer	Description	Restrctn. site	Reference or source
Strains			
Escherichia coli			
TOP10	F^- mcrA Δ (mrr-hsdRMS-mcrBC) ϕ80lacZΔM15 ΔlacX74 recA1 araD139 Δ(ara leu)7697 galU galK rpsL (St^r) endA1 nupG		Invitrogen
S17-1 λpir	recA1 thi pro hsdR mutant RP4-2Tc::Mu Km::Tn7 λpir		26
Methylosinus trichosporium			
OB3b	Wild-type strain		
Δ*mbnAN* mutant	*mbnABCMN* deleted		9
Δ*mbnC* mutant	Δ*mbnAN* carrying pWG104		This study
Plasmids			
pTJS140	Broad-host-range cloning vector; Mob Ap^r Sp^r Sm^r lacZ		34
pWG104	pTJS140 carrying *mbnA*BMN with its native promoter		This study
Primers			
mbnANf	ATTTTTggtaccGACGTTCGGGTCTTCTTCGC	KpnI	9
mbnANr	ATTTTTggtaccCGCCTCTAGATCATTCCGAC	KpnI	9
mbn66	ATTTTTggatccCGAACAATGTGTGCCAGTAG	BamHI	This study
mbn70	ATTTTTggatccGTTCGGCTATTTCCTGACGC	BamHI	This study
qmbnA_FO	TGGAAACTCCCTTAGGAGGAA		35
qmbnA_RO	CTGCACGGATAGCACGAAC		35
qmbnB_F1	TGGTCCAGCAGATGATCAAAG		This study
qmbnB_R2	TTCCCGAGCTTCTCCAATTC		This study
dmbnC_F	GGGAGAACAACCTCGCTTT		This study
dmbnC_R	CTTCCCAGCACGATCTGAC		This study
dmbnM_F	GCTAGGCTGGCTCCTTTATC		This study
dmbnM_R	GATGTTGACCACAAACCGAAAG		This study
dmbnN_F	CGATTCCATCCTTTCCGATGT		This study
dmbnN_R	CACTTTCGAAGACAAGGAGAGA		This study
dmbnP_F	AAAGGGAAGCACACACCCAT		This study
dmbnP_R	GTCGTGTTCTTGGCCGGATT		This study
dmbnH_F	ACTTACCGAAATACATCCCGC		This study
dmbnH_R	CGGAGAGGCGCTTATCGTAG		This study

Table 2. ^{1}H, ^{13}C, and ^{15}N resonances for metal-free Δ*mbnC* mutant. The table is presented in a two-column format (i.e., the table's two "Residue" columns and corresponding data are independent from one another).

		Chemical Shift (ppm)					Chemical Shift (ppm)		
Residue	Atom	^{1}H	^{13}C	^{15}N	Residue	Atom	^{1}H	^{13}C	^{15}N
3-Methyl-butanoyl	C^{1}		174.6		Tyr^{4}	C^{4}			
	C^{2}		50.5			H^{N}	7.44		
	C^{3}		38.0			H^{α}	2.96		
	C^{4}		19.6			H^{β}	2.79		
	C^{5}		19.6			H^{β}	1.20		
	H^{2}	4.15				$H^{2,6}$	6.11		
	H^{3}	2.17				$H^{3,5}$	6.45		
	H^{3}	2.72							
	H^{4}	1.88			Pro^{5}	N^{1}			109.6
	H^{5}	1.80				C^{2}		67.3	
						C^{3}		21.1	
Oxazolone	N			180.1		C^{4}		39.5	
	H^{N}	7.61				C^{5}		55.2	
						H^{2}	3.67		
Gly^{1}	N			125.1		H^{3}	1.06		
	C					H^{3}	2.13		
	C^{α}		26.6			H^{4}	1.28		
	H^{N}	9.57				H^{4}	2.29		
	H^{α}	1.46				H^{5}	2.79		
Ser^{2}	N			114.3	Cys^{6}	N			
	C		181.6			C			
	C^{α}		72			C^{α}			
	C^{β}					C^{β}			
	H^{N}	8.19				H^{N}			
	H^{α}	4.14				H^{α}			
	H^{β}	3.98				H^{β}			
	H^{β}	1.41				H^{β}			
Cys^{3}	N			118.1	Ser^{7}	N			117.5
	C		173.0			C			
	C^{α}		71.2			C^{α}		51.6	
	C^{β}		35.6			C^{β}		45.0	
	H^{N}	7.93				H^{N}	8.90		
	H^{α}	3.96				H^{α}	4.19		
	H^{β}	3.23				H^{β}	3.25		
	H^{β}	1.37				H^{β}	1.48		
Tyr^{4}	N			121.5	Cys^{8}	N			112.4
	C					C		172.6	
	C^{α}		48.9			C^{α}		42.3	

Table 2 Continued

		Chemical Shift (ppm)					Chemical Shift (ppm)		
Residue	Atom	^{1}H	^{13}C	^{15}N	Residue	Atom	^{1}H	^{13}C	^{15}N
Tyr^{4}					Cys^{8}				
	C^{β}		35.6			C^{β}		21.1	
	C^{1}					H^{N}	8.47		
	$C^{2,6}$					H^{α}	3.69		
	$C^{3,5}$		135.4			H^{β}	3.55		
						H^{β}	0.97		

Figures

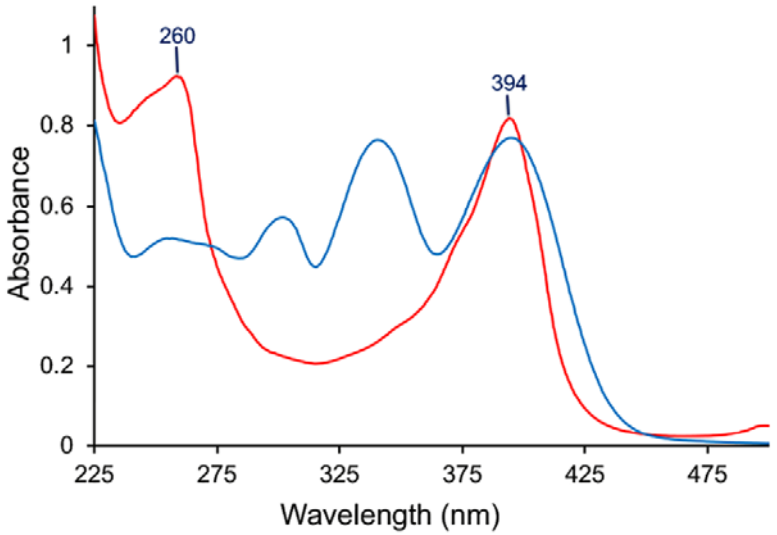

Figure 1. UV-visible absorption spectra of MB-OB3b (**blue**) and the Δ*mbnC* mutant (**red**). Abbreviations: OxaA, oxazolone A or the N-terminal oxazolone group; OxaB, oxazolone B or the C-terminal oxazolone group.

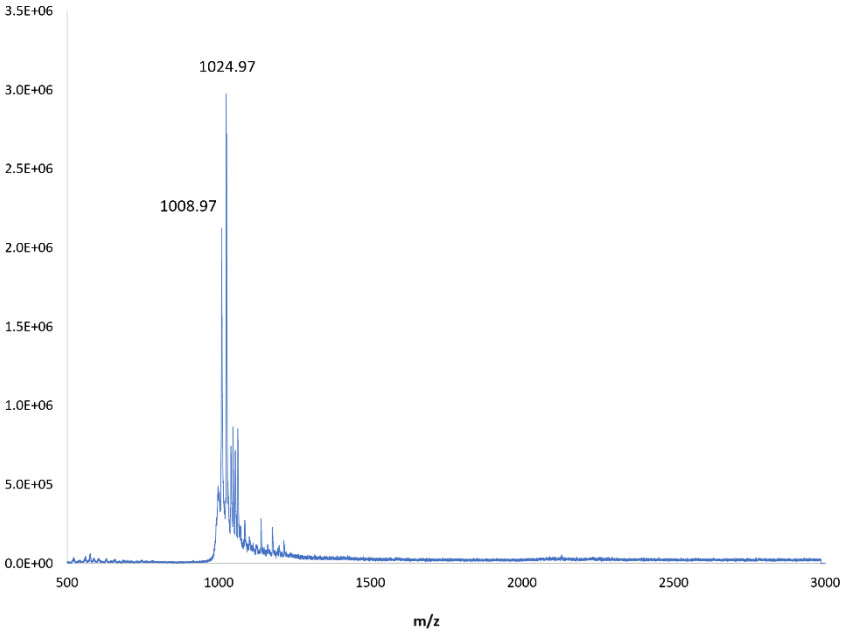

Figure 2. MALDI-TOF MS of methanobactin from Δ*mbnC*

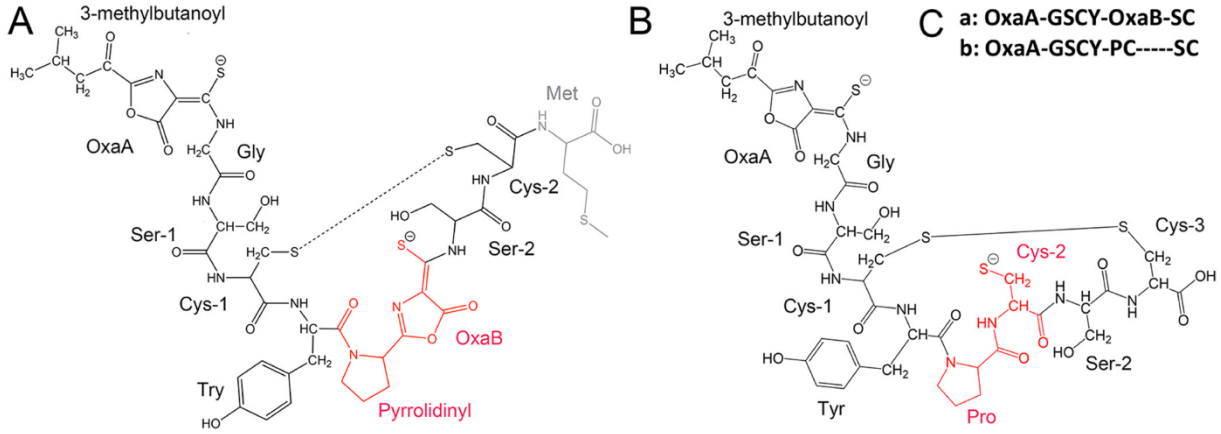

Figure 3. (A) Structure of wild-type MB-OB3b, with the labile terminal methionine in gray. (B) Proposed structure of the Δ*mbnC* mutant based on UV-visible absorption spectra, LC-MS, and NMR analysis. The differences between MB-OB3b-Met and the Δ*mbnC* mutant are highlighted in red. (C) Amino acid sequence of (a) wild-type MB-OB3b minus the C-terminal Met and (b) the Δ*mbnC* mutant.

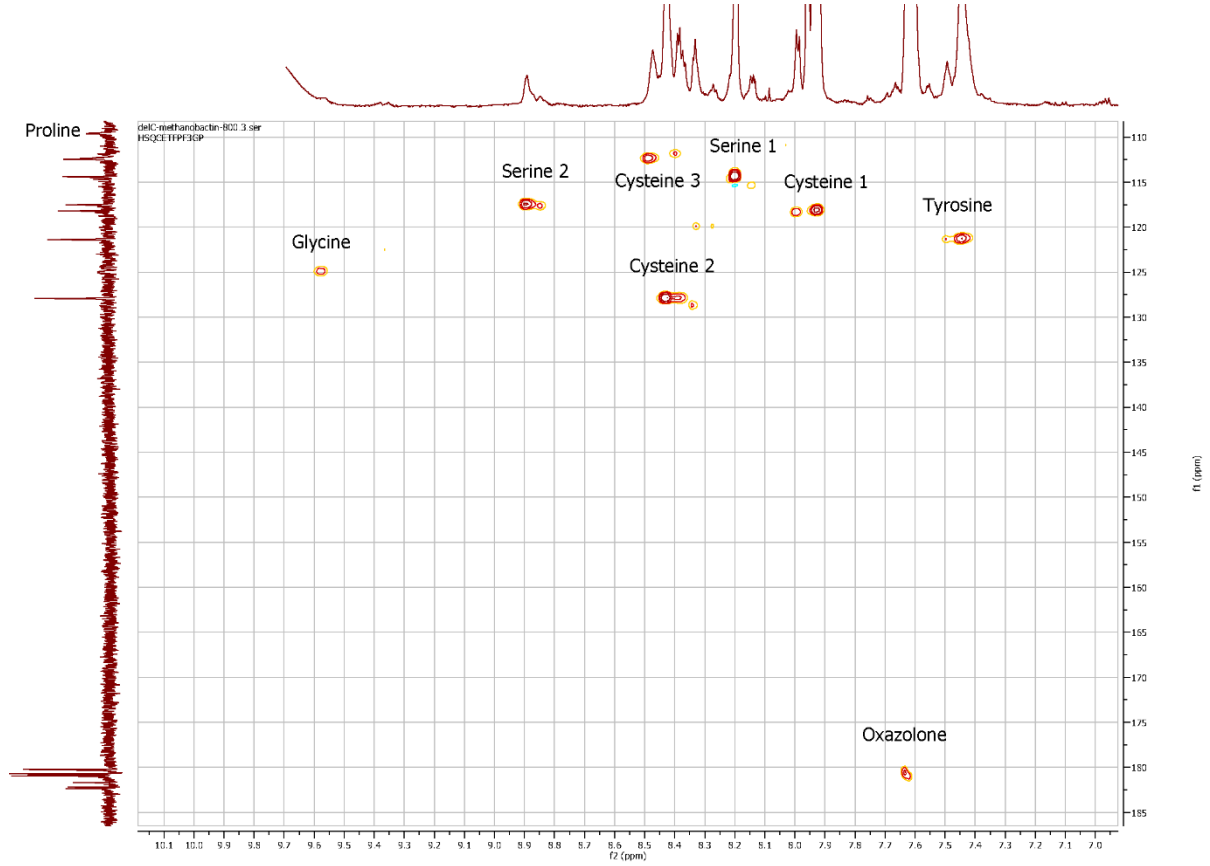

Figure 4. The 800-MHz ^{1}H-^{15}N-HSQC spectrum of uniformly ^{15}N-labeled Δ*mbnC* mutant in 90% 9 mM phosphate buffer (pH 6.5) and 10% D_2O at 265 K and 300,000,000 Pa. The horizontal and vertical 1D spectra are ^{1}H and N spectra, respectively.

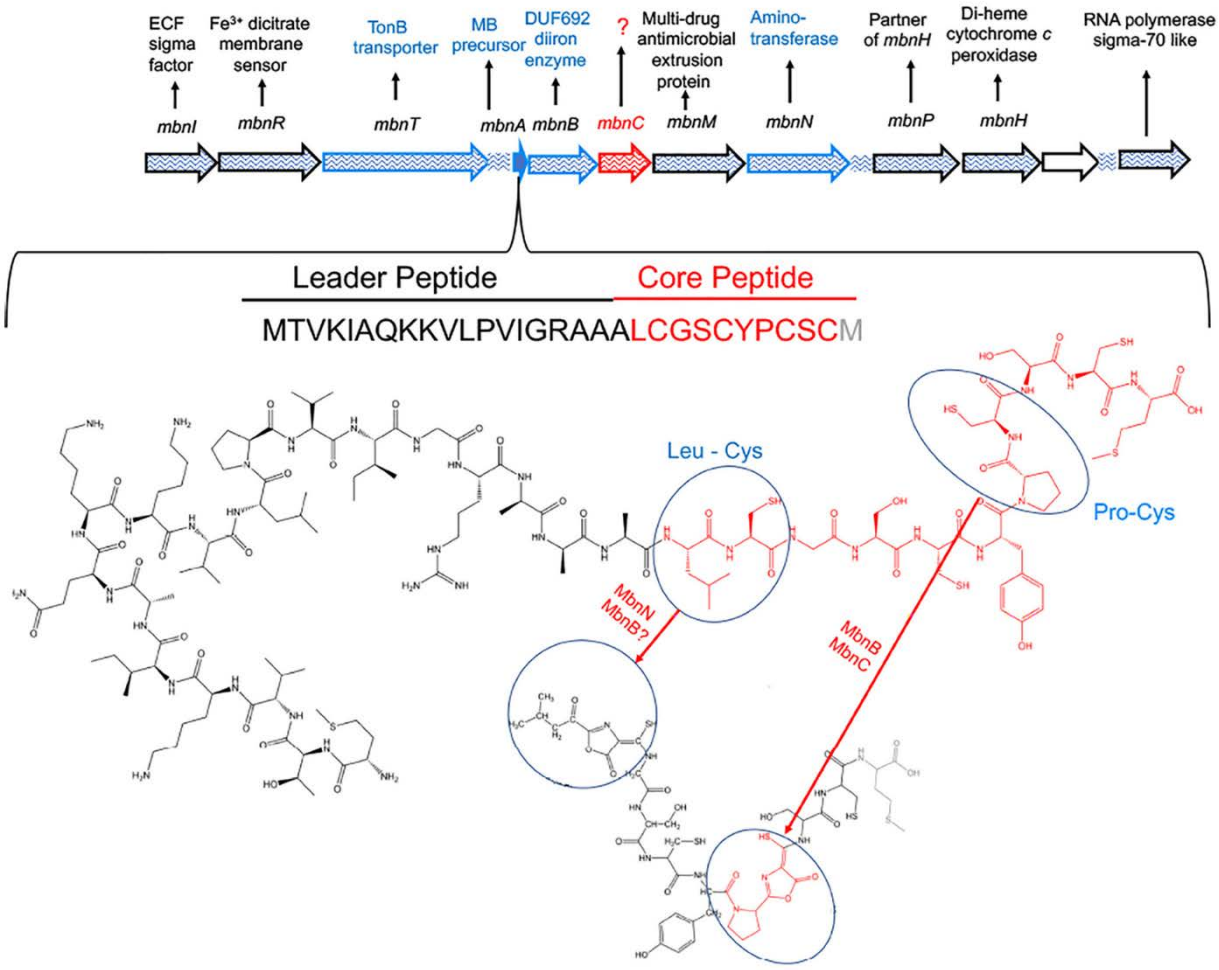

Figure 5. (Top) MB-OB3b gene cluster. Genes with known involvement in MB-OB3b synthesis and transport are shown in blue. (Bottom) Proposed genes involved in the biosynthesis of the oxazolone rings with associated thioamides from *mbnA*. Additional, yet to be identified genes may also be involved in the formation of oxazolone groups.

Supplemental Information

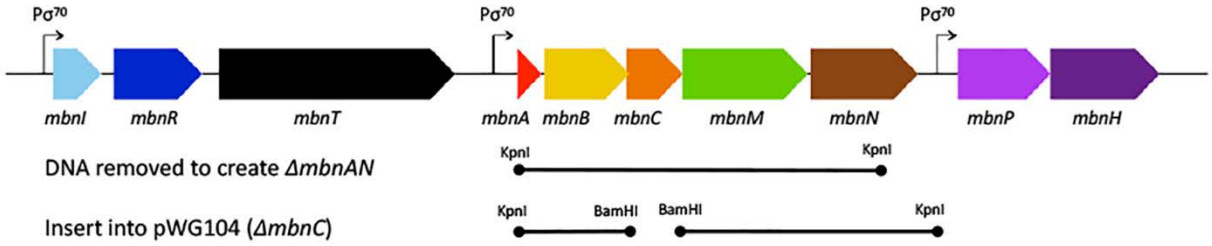

Figure S1. Methanobactin gene cluster of *M. trichosporium* OB3b. DNA removed/added to construct Δ*mbnAN* and Δ*mbnC* mutants indicated below the gene cluster.

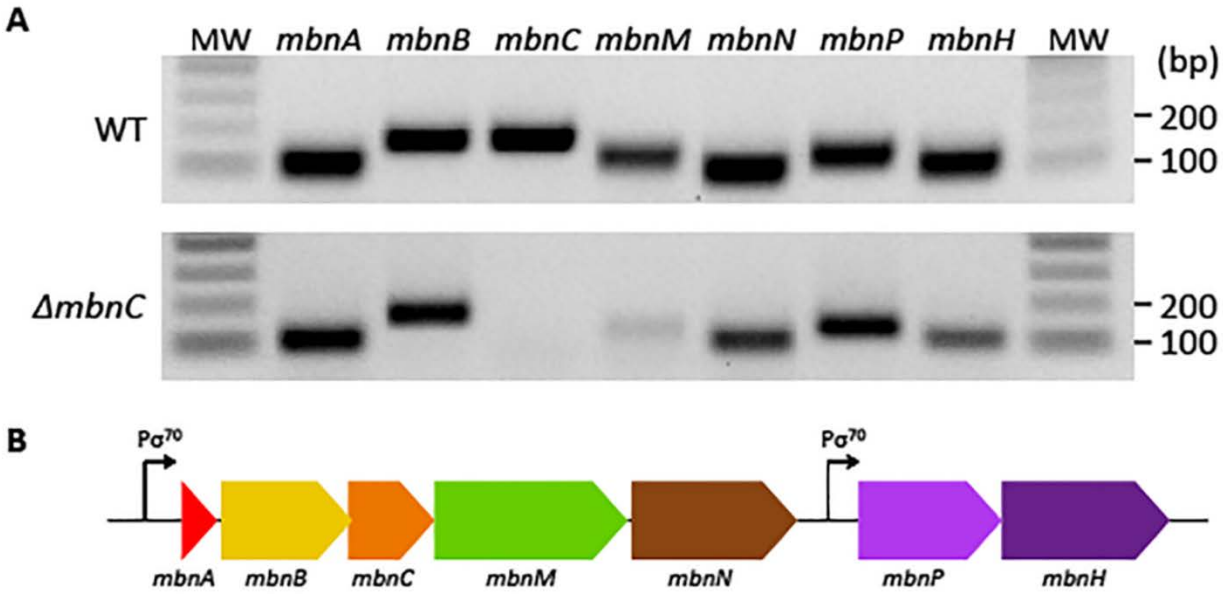

Figure S2. Expression of *mbn*ABCMNPH in *M. trichosporium* OB3b wildtype (WT) and Δ*mbnC* grown with 0.2 μM Cu as confirmed via RT-PCR. (A). mbn biosynthesis genes in *M. trichosporium* OB3b are shown in (B). MW – molecular weight marker.

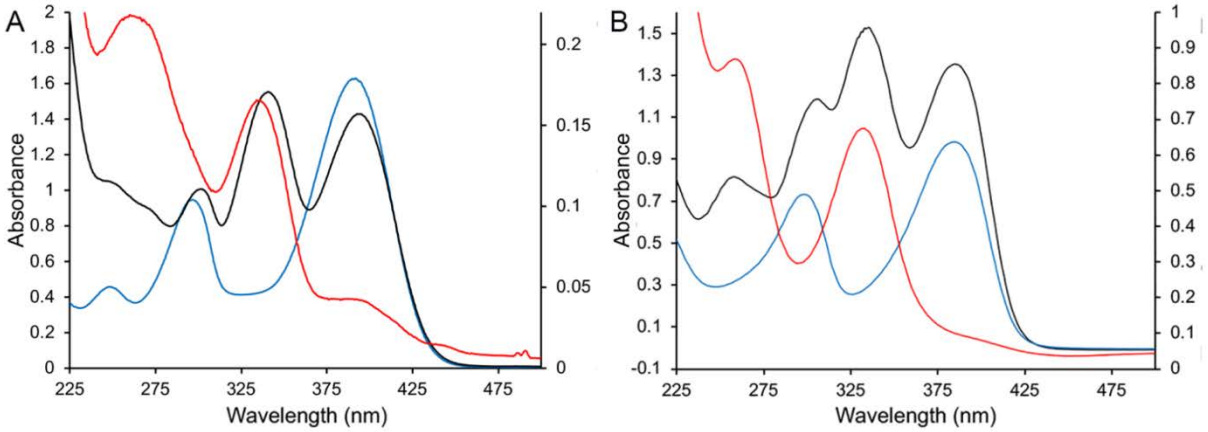

Figure S3. HPLC fractions of from freeze dried Dianion HP-20 samples from the spent media of *M. trichosporium* OB3b (A) and the Dianion HP-20 samples from the spent media of *Methylocystis* strain SB2 (B). (A) Holo-MB-OB3b fraction (**black**), MB-OB3b minus the C-terminal oxazolone group fraction (**blue**) and MB-OB3b minus the N-terminal oxazolone group (**red**). (B) Holo-MB-SB2 fraction (**black**), MB-SB2 minus imidazolone/pyrazinedione fraction (**red**), and MB-SB2 minus oxazolone fraction (**red**).

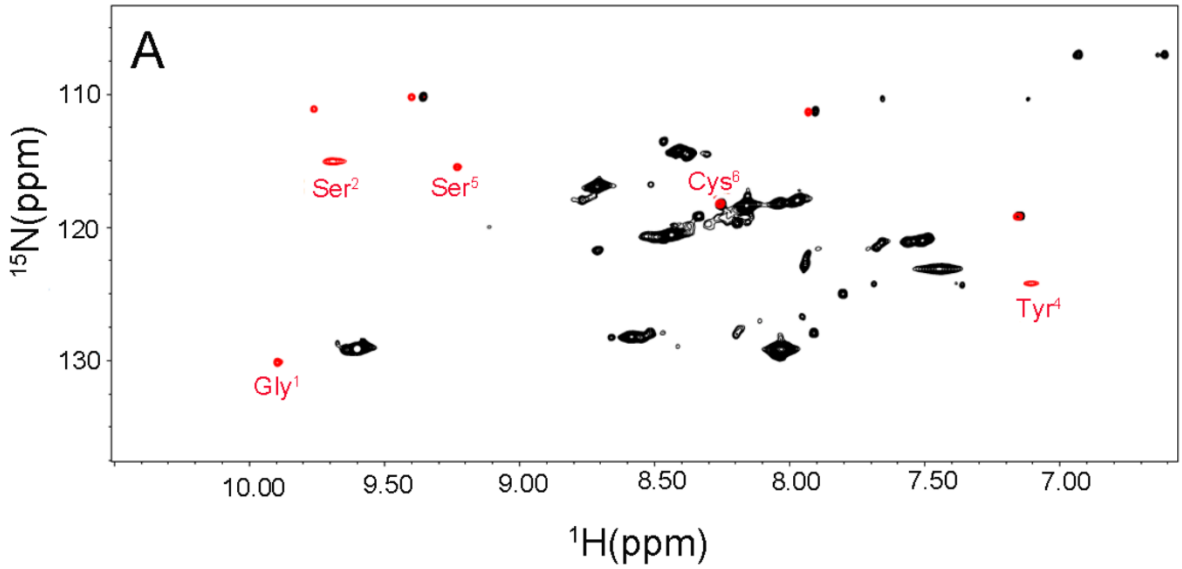

Figure S4. (A) 700 MHz ^{1}H,^{15}N-HSQC spectrum of uniformly ^{15}N-labeled MB from wild type MB-OB3b (**black**) and following the addition of equimolar Cu^{2+} (**red**)- in 90% 9 mM phosphate buffer, pH 6.5, and 10% D_2O at 298K and 1 bar.

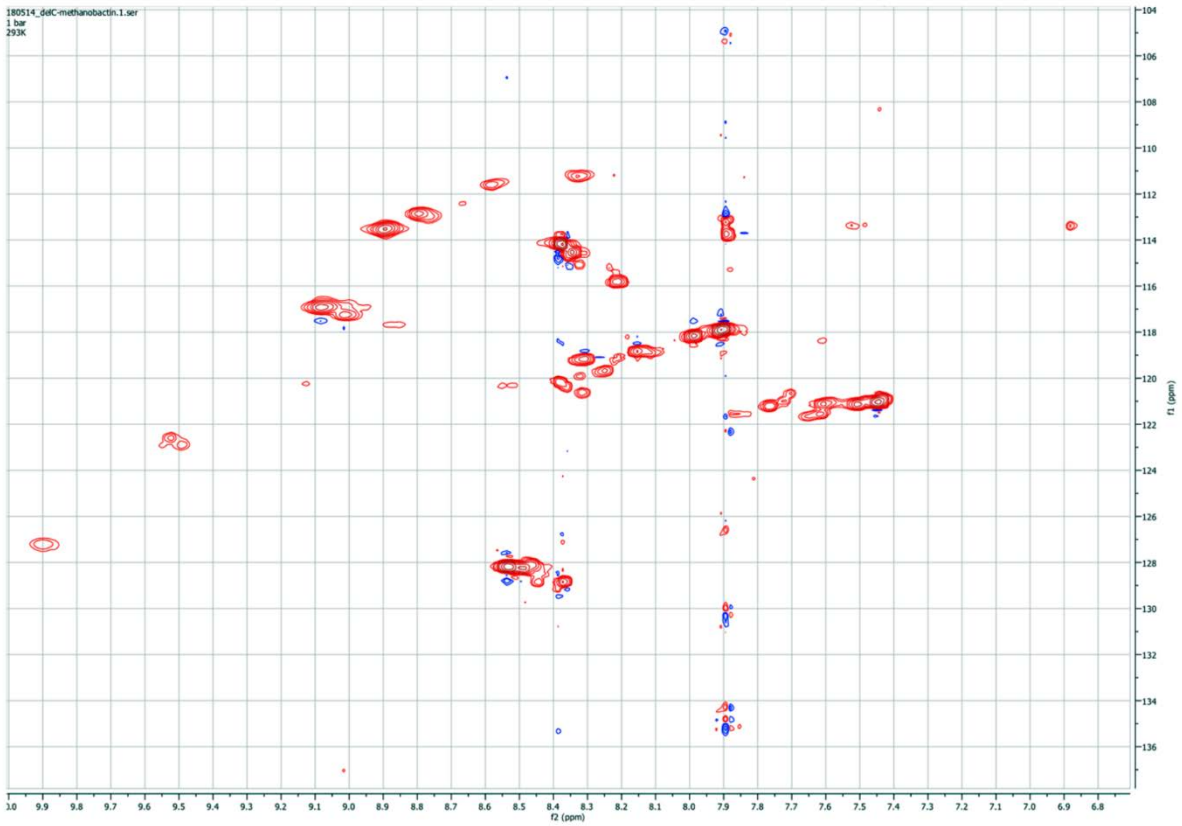

Figure S5. 800 MHz $^{1}H,^{15}N$-HSQC spectrum of uniformly ^{15}N-labeled Δ*mbnC* in 90% 9 mM phosphate buffer, pH 6.5, and 10% D_2O at 293K and 1 atm. Positive component is in red, negative component is in blue.

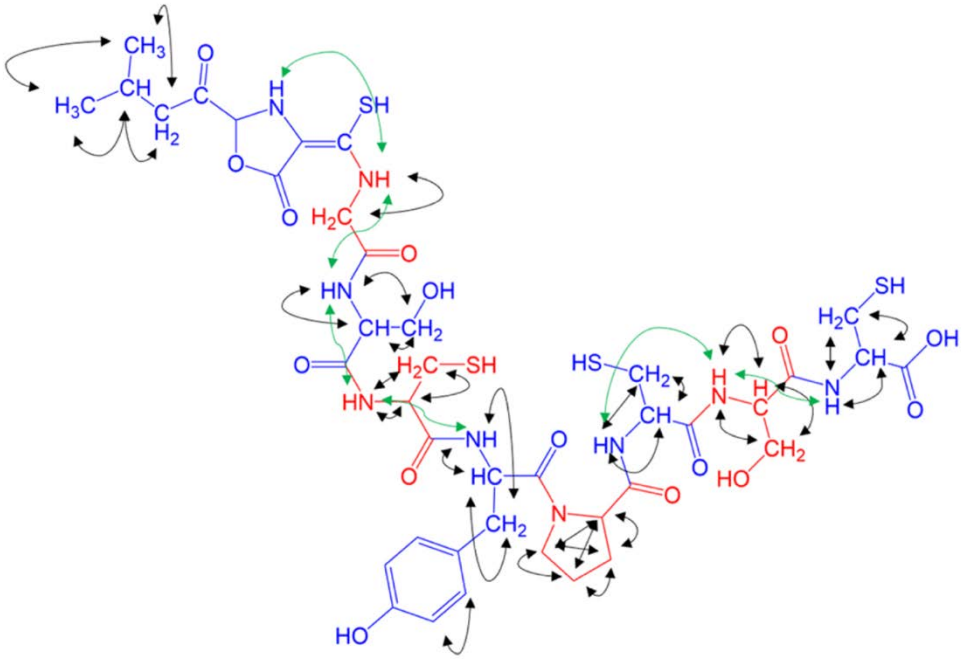

Figure S6. TOCSY (**black**) and ROESY (green) correlations observed in 2D NMR for Δ*mbnC*.

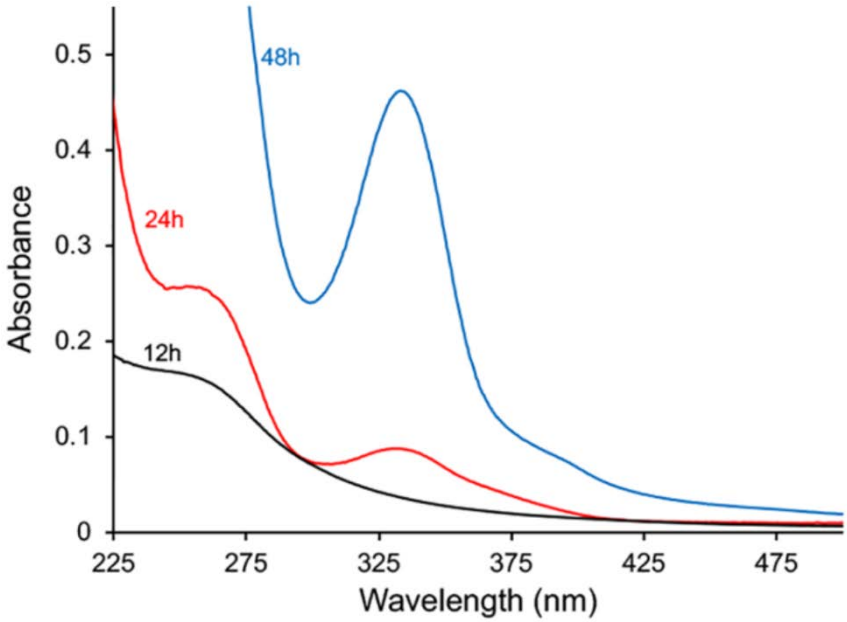

Figure S7. Spent media from Δ*mbnN* strain of *M. trichosporium* OB3b. Samples were taken 12h (**black**), 24h (**red**) and 48h (**blue**) following inoculation. Culture samples were centrifuged at 12,000 x g for 20 min, filtered through 0.2µm Millipore filter and assayed by UV-visible absorption spectra.

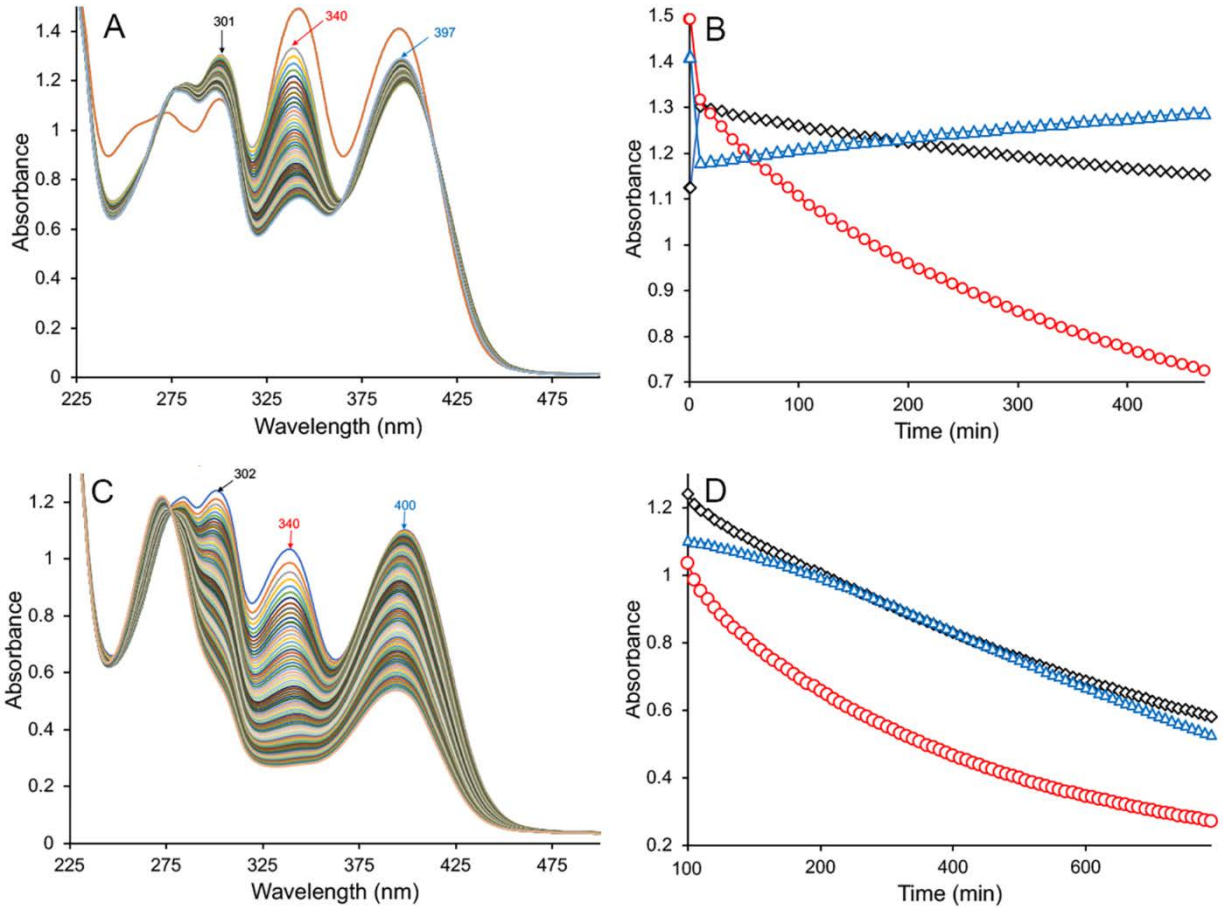

Figure S8. Acid hydrolysis of the group I methanobactin *M. parvus* OBBP (1). (A and C) Spectral changes in the absorbance spectra of the MB from *M. parvus* OBBP in 85µM acetic acid. (B and D) Absorbance changes at 302nm (◇), at 340 nm (○), and at 400nm (△) over time.

CHAPTER 4. CRYSTAL STRUCTURE OF *MBNF*: A NADPH-DEPENDENT FLAVIN MONOOXYGENASE FROM *METHYLOCYSTIS* STRAIN SB2

Andrew Stewart[1], Philip Dershwitz[1], Charles Stewart[1], Michael R. Sawaya[2], Todd O. Yeates, Jeremy D. Semrau[3], Hans Zischka[4], Alan A. DiSpirito[1] and Thomas A. Bobik[1*]

[1]Roy J. Carver Department of Biochemistry, Biophysics and Molecular Biology. Iowa State University, Ames, IA 50011-3260, USA

[2]UCLA-DOE Institute for Genomics and Proteomics, University of California, Los Angeles, CA, 90095-1570, USA.

[3]Department of Civil and Environmental Engineering, University of Michigan, Ann Arbor, MI, 48109-2125, USA

[4] Institute of Molecular Toxicology and Pharmacology, Helmholtz Center Munich, German Research Center for Environmental Health, Ingolstaedter Landstrasse 1, D-85764 Neuherberg, Germany and Technical University Munich, School of Medicine, Institute of Toxicology and Environmental Hygiene, Biedersteiner Strasse 29, D-80802 Munich, Germany.

Modified from a manuscript to be submitted to *Acta Physica*

Abstract

Methanobactins (MBs) are ribosomally-produced and post-translationally modified peptides (RiPPs) used by methanotrophs for copper acquisition. The signature post-translational modification of MBs is the formation of two heterocyclic groups, either an oxazolone, pyrazinedione, or imidazolone with an associated thioamide from an X-Cys dipeptide. The precursor peptide (*mbnA*) for MB formation is found in a gene cluster of MB associated genes. The exact biosynthetic pathway of MB formation is not yet fully understood, and there are still uncharacterized proteins in some MB gene clusters, particularly those that produce

pyrazinedione or imidazolone rings. One such protein is *mbnF*, a proposed flavin monooxygenase (FMO) based on homology. To help elucidate its possible function, *mbnF* from *Methylocystis* sp. strain SB2 was recombinantly produced in *Escherichia coli*, and the X-ray crystal structure was resolved to 2.6 Å. Based on structural features, *mbnF* appears to be a type A FMO. Preliminary functional characterization shows that *mbnF* will preferentially oxidize NADPH over NADH, supporting NAD(P)H mediated flavin reduction. *mbnF* binds the precursor peptide for MB, with the subsequent loss of the leader peptide sequence as well as last three C-terminal amino acids. Simulations revealed a channel in *mbnF* capable of accommodating the core *mbnA* fragment minus the three C-terminal amino acids.

Introduction

Recently it has been shown that, akin to siderophores used for iron uptake (Neilands, 1995), some microbes produce chalkophores or copper-binding compounds (DiSpirito *et al.*, 2016; Semrau *et al.*, 2020) for copper uptake. The best characterized chalkophore is methanobactin (MB) from methane-oxidizing bacteria (methanotrophs). MBs are small (less than 1300 Da) post-translationally modified peptides with two heterocyclic groups, either an imidazole, oxazolone or pyrazinedione, each associated with a thioamide and formed from an XC dipeptide. These heterocyclic groups, with an associated thioamide group, are responsible for copper binding (El Ghazouani *et al.*, 2011; El Ghazouani *et al.*, 2012; Kim *et al.*, 2004).

There is a great deal of interest in determining how mature MBs are formed from a polypeptide precursor as MBs have significant medical and environmental applications (Baral *et al.*, 2014; Johnson, 2006, Lu *et al.*, 2017; Semau *et al.*, 2020; Vorobev *et al.*, 2013; Chang *et al.*, 2018; Chang *et al.*, 2022; Einer *et al.*, 2019; Kang-Yun *et al.*, 2022; Lichmannegger *et al.*, 2016;

Zischka *et al.,* 2011). The proteins involved in the formation of the C-terminal oxazolone group with associated thioamide have been identified and characterized via selective knock-outs of genes in the Mb gene cluster (Gu *et al.,* 2017; Dershwitz *et al.,* 2022) as well as heterologous expression (Gu *et al.,* 2016; Gu *et al.,* 2017; Kenney *et al.,* 2018). Little is known, however, how the tautomeric imidazole/pyrazinedione N-terminal group is formed or how the leader sequence is removed to form mature MB. Interestingly, *mbnF* is present in all methanobactin biosynthesis operons known to produce MB with an N-terminal imidazolone/pyrazinedione group, but is absent in the three operons known to produce MB with an N-terminal oxazolone group (Semrau *et al.,* 2020), suggesting that *mbnF* is involved in the formation of the pyrazinedione/imidazolone group. To gain insight into the potential role of *mbnF* in MB biosynthesis, the crystal structure of *mbnF* was determined.

Materials and Methods

Protein Expression and Purification

E. coli codon optimized *mbnF* from *Methylocystis* sp. strain SB2 was ordered from GenScript in a pET-41 vector utilizing a C-terminal His_6 tag (*mbnF*-His). *mbnF*-His was expressed in BL21(DE3) cells. Cultures was grown at 37° C until 0.5 OD_{600} and induced with 0.5 mM isopropyl β-D-1-thiogalactopyranoside and grown for an additional 16 hours at 17° C. Cells were lysed with B-PER II plus (Thermo Fisher, Waltham, MA, USA) DNase and lysozyme. Cleared lysate was loaded onto a HisTrap column (Millipore-Sigma, Burlington, MA, USA) equilibrated with buffer A (50 mM Hepes pH 7.4 and 50 mM NaCl) and eluted with a gradient of 0 – 500 mM imidazole. The sample was washed with 3 column volumes 0 mM imidazole prior to a 5 column volume gradient, which was followed by 3 column volumes 500

mM imidazole wash. Eluate was collected in 2 ml fractions. *mbnF* containing fractions appeared yellow due to the presence of the associated flavin. Yellow fractions were dialyzed into 50 mM Hepes pH 7.4 and run on a MonoQ 10/100 GL anion exchange column, eluting with a gradient of 0 – 1 M NaCl. The sample was washed with 3 column volumes 0 mM NaCl prior to a 5 column volume gradient, which was followed by 3 column volumes 1 M NaCl wash. Yellow fractions were concentrated to 20 mg•ml^{-1} using an Amicon Ultra-15 centrifugal filter (MilliporeSigma, Burlington, MA, USA) and flash frozen with 10% glycerol in liquid nitrogen. All columns were run on an ÄKTA pure system.

Crystallization

Concentrated *mbnF* (20 mg•ml^{-1}) was subjected to high-throughput crystallization screening, using a Mosquito LCP robot (SPT Labtech) with the commercially available screens from JCSG-plus Eco, Ligand-Friendly Screen Eco, Morpheus and PACT premier Eco (Molecular Dimensions Inc., USA) and the XP Screen (MiTeGen, USA). Crystals were observed in well F2 of PACT premier Eco (**Table 1**). The crystals from the PACT screen were cryoprotected with 15% glycerol and flash-cooled in liquid nitrogen.

Data collection and processing

The crystals were sent to the GM/CA 23-ID-B beamline at the Advanced Photon Source (APS) for screening and data collection. Native data sets, wavelength 0.97931 Å, were collected from crystals; all datasets were indexed in space group *C 1 2 1*. The data were integrated and scaled with *XDS* (Kabsch, 2010) within the *xia*2 (Winter, 2010) data-processing pipeline (**Table 1**).

Structure solution and refinement

mbnF phases were determined by molecular replacement (MR) using *PHASER* (McCoy, 2007). *Autobuild* in the Phenix software suite was used for initial modeling building. *Coot* (Emsley *et al.,* 2010) and *phenix.refine* (Liebschner *et al.,* 2019) were subsequently used for visualization, manual rebuilding and structure refinement (**Table 1**). The *super* algorithm in *PyMOL* (version 2.4.1; Schrödinger) was used for r.m.s.d. calculations. Coordinates and structure factors were deposited in the worldwide Protein Data Bank (Berman *et al.,* 2003) as PDB entry 7SON.

Molecular dynamics

Molecular dynamics simulations were performed using gromacs (Abraham *et al.,* 2015) using the AMBER99SB force field (Hornak *et al.,* 2006) and SPC/E water model. The system was equilibrated with a 100 ps NVT simulation and a 100 ps NPT simulation, followed by a 10 ns production md run.

Enzyme Assays

Assays were conducted in a 500 µl reaction mixtures in 50 mM Hepes (VWR, Solon OH, USA) pH 7.4, 150 mM NaCl (Fisher, Ottawa ON, USA), containing 100 nmol NADPH or 75 nmol NADH (EMD Millipore, Burlington MA), and 3.9 nmol *mbnF* (NADPH) or 2.5 nmol *mbnF* (NADH), reactions were carried out in a quartz cuvette (FireflySci, Northport NY, USA). All reactions were monitored aerobically with a Cary 60 UV-visible absorption spectrophotometer (A_{340}, $\varepsilon = 6220$ M cm $^{-1}$). Reactions were carried out at 25°C and monitored for 50 minutes for the kinetics assay and overnight for the titration, using the Cary Kinetics application. For NADPH oxidation assays, solutions were prepared anaerobically in a Coy anaerobic chamber (Coy Laboratory Products, Grass Lake, MI, USA) and allowed to degas

overnight at 2°C. The reactions were initiated by addition of NADPH then bubbling in O_2. For NADH oxidation assays, solutions were prepared aerobically with NADH, and reactions were initiated by the addition of *mbnF*.

mbnA Peptide

mbnA peptide, sequence IRIAKRITLNVIGRASARCASTCAATNG, ~90% pure, was purchased from AnaSpec, (Fremont, CA, USA). *mbnA* experiments were performed on a mixture containing 1 mg•ml^{-1} *mbnA*, 500 μM *mbnF*, 250 mM NaCl and 50 mM HEPES at pH 7.4. ESI-MS experiments under acidic conditions were performed on a SYNAPT G2-Si High-Definition Mass Spectrometer (Waters, Milford MA, USA) with a Restek Ultra C4 5 μm 50x1mm column and a water+0.1% formic acid/ acetonitrile+0.1% formic acid gradient or under neutral pH conditions on an ACQUITY UPLC Protein BEH SEC column, 200A, 1.7 μm, 2.1x150mm under isocratic conditions using 50 mM ammonium acetate, pH 6.6, buffer. UV-vis experiments were again performed on a Cary 60 UV-visible spectrophotometer.

Results

Protein Expression and Purification

Codon optimized (for *E. coli*) C-terminally His tagged *mbnF* (*mbnF*-His) was expressed in *E. coli* using a pET41 vector and purified by Ni-NTA and MonoQ chromatography. *mbnF* eluted from the HisTrap column with a small upstream shoulder and a long downstream tail (**Figure S1**). The presence of *mbnF*-His in the tail was apparent by the yellow color of the fractions and supported by SDS-PAGE. *mbnF*-His eluted off the MonoQ column in a grouping of four peaks (**Figure S1**). This set of peaks ran as a single band on SDS-PAGE and ran as a single peak on gel filtration (**Figure S1**). The presence of *mbnF*-His as a grouping of peaks on

the MonoQ suggests that *mbnF*-His may form electronically distinct, but related, sub species. Molecular weight and oligomeric state were assessed by gel-filtration chromatography, where *mbnF*-His eluted with an estimated molecular mass of 50 kDa as compared to the computed molecular mass of 59.17 kDa suggesting that *mbnF*-His is a monomer in solution. Presence of FAD bound to *mbnF*-His throughout purification and crystallization was apparent by the yellow color of the solution and crystals; buffers were not supplemented with FAD.

Crystallization

Crystals of purified *mbnF* were obtained using a PACT premier Eco screen, which were greenish yellow in color (**Figure S2**). Diffraction data was collected at the Advanced Photon Source (APS). The structure of *mbnF* was solved by molecular replacement (**Figure 1**) and refined to a resolution of 2.61 Å (**Table 2**). The search model for molecular replacement was aklavinone hydroxylase (RdmE). RdmE is a flavin monooxygenase (FMO) that catalyzes the hydroxylation of aklavinone to ε-rhodomycinone using NADPH as a reductant (Lindqvist *et al.*, 2009), and is 39% identical over 96% of its length to *mbnF*. *mbnF* crystallized as a trimer, with all three subunits of the asymmetric unit bound to FAD in the same general conformation, all in the *in* conformation (**Figure 2)** (Ryan *et al.*, 2008). There are two *mbnF* structure predictions in the AlphaFold database (Jumper *et al.*, 2021; Varadi *et al.*, 2022), both from *Methylosinus* sp. sav-2 with 58 and 55% identity to the SB2 *mbnF* sequence used in this study. These two structures have an RMSD relative to the structure reported here of 7.0 and 3.6 Å respectively (**Figure S3**), but the overall topology is similar. However, the AlphaFold model does not include the FAD co-enzyme.

Oligomeric State

While *mbnF*-His crystallized as a trimer, it eluted as a monomer on size exclusion chromatography (**Figure S1)**, additionally, it appeared to run as a monomer on native-PAGE (data not shown). The trimer interface contains three distinct binding interfaces (**Figure S4**). Analysis of the crystallographic trimer using PISA Interface (PDBe) calculated that the interfaces represent 2.2 – 2.4% of the total solvent accessible surface area and predicts that they do not play a role in complex formation. One of the three interfaces interacts with like interfaces, while the other two interfaces form a binding pair. This latter interaction could potentially lead to oligomeric chain formation. It is possible, therefore, that the crystallographic state may represent an aggregation mode. This is supported by the abundance of charged residues in the binding interfaces (predominantly Glu, Asp, and Arg) and the observation that *mbnF* will visibly aggregate overtime (minutes to hours) when in low salt buffers, while the addition of salt reverses this aggregation. It is also of note that low salt did not influence the chromatogram on size exclusion chromatography. While it is not clear at this time what physiological significance this aggregation may have, it is likely that the crystallographic trimer may not be purely due to crystal contacts but represents an aggregated state accessible in solution.

Structural Features

mbnF has four major structural motifs (**Figures 3 and S6**), a 5-helix bundle that makes up the central core of *mbnF* and coordinates the isoalloxazine moiety of FAD, an N-terminal β-sandwich that coordinates the adenine moiety of FAD, a β-Hotdog motif that forms a channel adjacent to the flavin ring, and lastly a domain featuring β-α-β and β-β-α motifs connected to the 30 amino acid helix by a ~50 residue loop region. Additionally, adjacent to the helix bundle is a 30 amino acid helix at the protein surface. Interestingly, this helix has a proline 13 residue, a

residue not typically found in helices of soluble proteins (Cordes *et al.*, 2002). The presence of this residue introduces a kink of ~20°, which is fairly typical of proline induced helical kinks (Barlow & Thornton, 1988). This proline is not present in the RdmE search model. The two phosphate moieties of FAD are positioned at the N-terminal end of helix 2, implying that the dipole of the helix may contribute to the coordination of FAD. In all three monomers of the asymmetric unit, a bromide ion is observed coordinated between the isoalloxazine ring of the FAD and the N-terminal end of the helix 2. The presence of these anions may indicate coordination of negatively charged groups in the substrate. It is also of note that adjacent to the isoalloxazine ring is a channel that appears large enough to accommodate a peptide. This is of interest as *mbnA* is potentially the substrate of *mbnF*.

Molecular Dynamics

To test whether this channel could accommodate a peptide, *mbnA* was manually docked into the active site channel of *mbnF* 1-370 (removing the C-terminal domain and the loop region following helix 22, with FAD removed as well), with the C-terminal end of *mbnA* in the region adjacent to where the isoalloxazine ring of FAD would normally be. This *mbnF-mbnA* complex was run for 10 ns in a molecular dynamics (MD) simulation to test for any steric clashes and the plausibility of this channel accommodating a peptide (**Figure 4**). While there are no obvious interactions between *mbnA* and *mbnF*, 10 ns is likely too short of a simulation for these to develop (Bowman, 2016). It is interesting to note, however, that while most of the *mbnF* domains reached a relatively stable RMSD after 2 – 4 ns (**Figure 5**) the 30-residue helix containing a proline did not stabilize after 10 ns (**Figures S7**). It is possible that this helix was stabilized by the crystal environment as there is clear electron density for this helix, but it is not

clear what other structure it may adopt in solution. It is of note that this helix is connected directly to a ~50 residue loop region.

Functional Characterization

Putatively thought to be a flavin-dependent monooxygenase, the catalytic details of *mbnF* are unknown. In the presence of *mbnF*, NADH and NADPH were oxidized at a rate of 0.1 min^{-1} and 0.7 min^{-1} , respectively. This preference for NADPH over NADH has been observed in other FMOs (Chen *et al.*, 2011). *mbnA* bound to *mbnF* (Figure 6) and the *mbnF+mbnA* spectra showed a 786 Da shift versus the spectra of *mbnF* alone, corresponding to the mass of the core sequence in MB-SB2, i.e. RCASTCAA (Krentz et al., 2010). The result suggest *mbnF* may be responsible for the hydrolysis of the leader sequence as well as the C-terminal amino acids from the core peptide in *mbnA.* Alternatively, *mbnF* may be involved in one of the posttranslational modifications of the core *mbnA* peptide. However, no structural changes in *mbnA* were observed following incubation of *mbnA* with *mbnF* and NAD(P)H suggesting if *mbnF* does modify *mbnA* the reaction comes later in the biosynthetic pathway of MB following other post translational modification(s).

Discussion

Here the X-ray crystal structure of *mbnF* from *Methylocystis* sp. Strain SB2 at a resolution of 2.6 Å is presented, solved by molecular replacement using the aklavinone hydroxylase RdmE (PDB 3IHG, 39% identical) as a search model. *mbnF* crystalizes as a trimer but was observed to be monomeric by SEC and Native PAGE, although it is subject to aggregation, particularly at low salt concentrations. This aggregation behavior can be rationalized by the positioning of the interfaces and the presence of numerous charged residues

in these interfaces. It is unclear, however, whether this behavior has any physiological relevance. *mbnF* contains multiple structural features consistent with a type A FMO including multiple FAD binding motifs. Each monomer in the asymmetric unit crystallized with 2 – 6 bromide ions in 8 unique sites, 2 of which are conserved. It is interesting to note that there is a large channel through *mbnF* with the isoalloxazine ring of the FAD at one end and one of the two conserved bromide ions at the other end. The other conserved ion is directly adjacent to the isoalloxazine ring of the FAD (3.3 Å from N1). The presence of these ions indicates the possibility of negative charges being utilized in the coordination of substrate.

mbnF is present in all mbn operons known or proposed to contain an N-terminal imidazolone/pyrazinedione group and may be responsible for modifying an N-terminal intermediate oxazolone group to a pyrazinedione/imidazolone group, possibly via the addition of a hydroxyl group as observed with aklavinone—11-hydrolase (Lindqvist *et al.,* 2009). It is possible that the partial charge of the ketone in the oxazolone is used to coordinate the substrate in the active site, although this remains speculative. Further, manual docking of *mbnA* into the channel adjacent to the isoalloxazine of the FAD followed by a 10 ns MD simulation shows that this proposed active site channel is large enough to accommodate this peptide. More extensive simulations need to be done which include the FAD to assess any coordinated interactions between the peptide and *mbnF*. It is still unclear what exact reaction is catalyzed by *mbnF*.

Alternatively, the results presented here suggest *mbnF* may be involved in the hydrolysis of both the leader peptide as well as C-terminal amino acid(s). One to three C-terminal amino acid(s) of the precursor polypeptide are not observed in the final MB from mbn operons containing *mbnF* (Krentz *et al.,* 2010; El Ghazouani *et al.,* 2012; DiSpirito *et al.,* 2016). Here we show the loss of both the leader peptide as well as the three C-terminal amino acids following

incubation of *mbnA* and *mbnF*. The last two amino acids in *mbnA* from *Methylocystis* strain SB2 have never been observed in purified MB-SB2 samples and the third amino acid from the C-terminal end is only observed in a fraction of the final product (Krentz *et al.*,2010 and DiSpirito *et al.*, 2016). In structurally characterized MBs from mbn operons not containing *mbnF*, only one amino acid is occasionally missing from a fraction of the final product (El Ghazouani *et al.*, 2011 and Bandow *et al.*, 2011).

Here, we presented a high-resolution structure of *mbnF* from *Methylocystis* sp. strain SB2, and evidence supporting the plausibility of *mbnF* playing a catalytic role in methanobactin maturation, namely that *mbnF* is able to oxidize NAD(P)H consistent with its role as an FMO, and that the putative active site channel is able to accommodate a peptide such as *mbnA*. Further investigation is required to substantiate the role of *mbnF* in the maturation process of methanobactin of *Methylocystis* sp. strain SB2, and its catalytic mechanism.

Acknowledgements

This research was supported by the U.S. Department of Energy Office of Science (Grants #DE-SC0018059; JDS and ADS), the National Science Foundation (Grant #1912482; JDS) and the ISU Bailey Research and Career Development (TAB). Bruker Advance 800 use of was made possible through a generous gift from the Roy J. Carver Charitable Trust (Muscatine, Iowa).

Authors declare they have no competing interests.

References

1. Abraham, M. J., Murtola, T., Schulz, R., Páll, S., Smith, J. C., Hess, B. & E., L. Lindahl (2015). *SoftwareX* **Volumes 1–2**, Pages 19-25.

2. Bandow, N.L., Galleger, W.H., Behling, L., Choi, D.W., Semrau, J.D., Hartsel, S.C., Gilles, V.S., & DiSpirito A.A. (2011) Meth. Enzymol. 495, 260-269.

3. Baral, B. S., Bandow, N. L., Vorobev, A., Freemeier, B. C., Bergman, B. H., Herdendorf, T., Fuentes, N., Ellias, L., Turpin, E., Semrau, J. D. & DiSpirito, A. A. (2014). *J. Inorgan. Biochem.* **141**, 161 - 169.

4. Barlow, D. J. & Thornton, J. M. (1988). *J Mol Biol* **201**, 601-619.

5. Bowman, G. R. (2016). *J Comput Chem* **37**, 558-566.

6. Chang, J., Gu, W., Park, D., Semrau, J. D., DiSpirito, A. A. & Yoon, S. (2018). *ISME J.* **12**, 2086-2089.

7. Chang, J., Peng, P., D'iSpiirito, A. A. & Semrau, J. D. (2022). *Appl Environl Microbiol* **88**.

8. Chen, Y., Patel, N. A., Crombie, A., Scrivens, J. H., & Murrell, J. C. (2011). Bacterial flavin-containing monooxygenase is trimethylamine monooxygenase. *Proc. Nat. Acad. Sc USA, 108*(43), 17791–17796. https://doi.org/10.1073/pnas.111292810.

9. Cordes, F. S., Bright, J. N. & Sansom, M. S. (2002). *J Mol Biol* **323**, 951-960.

10. Dershwitz, P., Gu, W., Roche, J., Kang-Yun, C. S., Semaru, J. D., Bobik, T. A., Zischka, H. & DiSpirito, A. A. (2022). *Appl Environl Microbiol* **doi 10.1128/AEM.01841-21**.
11. DiSpirito, A. A., Semaru, J. D., Murrell, J. C., Gallagher, W. H., Dennison, C. & Vuilleumier, S. (2016). *Microbiol. Mol. Biol. Rev.* **80**, 387-409.

12. Einer, C., Leitzinger, C., Lichtmannegger, J., Eberhagen, C., Rieder, T., Borchard, S., Wimmer, R., Denk, G., Popper, B., Neff, F., Polishchuk, E. V., Polishchuk, R. S., Hauck, S. M., von Toerne, C., Karst, U., Mullert, J.-C., Baral, B. S., DiSpirito, A. A., Kremer, A. E., Semrau, J. D., Weiss, K. H., Hohenester, S. & Zischka, H. (2019). *J. Hepat.* **7**, 571-596.

13. El Ghazouani, A., Basle, A., Firbank, S. J., Knapp, C. W., Gray, J., Graham, D. W. & Dennison, C. (2011). *Inorg Chem* **50**, 1378-1391.

14. El Ghazouani, A., Basle, A., Gray, J., Graham, D. W., Firbank, S. J. & Dennison, C. (2012). *Proc. Nat. Acad. Sc USA***109**, 8400-8404.

15. Gu, W., Ul Haque, M. F., Baral, B. S., Turpin, E. A., Bandow, N. L., DiSpirito, A.A., Lichtmannegger, J., Kremmer, E., Zischka, H. & Semrau, J. D. (2016). *Appl Environl Microbiol*, 82(6), 1917–1923. https://doi.org/10.1128/AEM.03884-15

16. Gu, W., Baral, B. S., DiSpirito, A. A. & Semrau, J. D. (2017). *Appl Environl Microbiol* **82**, e01619-01616.

17. Hornak, V., Abel, R., Okur, A., Strockbine, B., Roitberg, A. & Simmerling, C. (2006). *Proteins* **65**, 712-725.

18. Johnson, C. L. (2006). thesis, Iowa State University.

19. Jumper, J., Evans, R., Pritzel, A., Green, T., Figurnov, M., Ronneberger, O., Tunyasuvunakool, K., Bates, R., Zidek, A., Potapenko, A., Bridgland, A., Meyer, C., Kohl, S. A. A., Ballard, A. J., Cowie, A., Romera-Paredes, B., Nikolov, S., Jain, R., Adler, J., Back, T., Petersen, S., Reiman, D., Clancy, E., Zielinski, M., Steinegger, M., Pacholska, M., Berghammer, T., Bodenstein, S., Silver, D., Vinyals, O., Senior, A. W., Kavukcuoglu, K., Kohli, P. & Hassabis, D. (2021). *Nature* **596**, 583-589.

20. Kang-Yun, C. S., Liang, X., Dershwitz, P., Gu, W., Schepers, A., Flatley, A., Lichmannegger, J., Zischka, H., Zhang, L., Lu, X., Gu, B., Ledesma, J. C., Pelger, D. J., DiSpirito, A. A. & Semrau, J. D. (2022). *ISME J* **16**, 211-220.

21. Kenney, G. E., Dassama, L. M. K., Pandelia, M.-E., Gizzi, A. S., Martinie, R. J., Gao, P., DeHart, C. J., Schachner, L. F., Skinner, O. S., Ro, S. Y., Zhu, X., Sadek, M., Thomas, P. M., Almo, S. C., Bollinger, M. J., Krebs, C., Kelleher, N. L. & Rosenzweig, A. C. (2018). *Science* **359**, 1411-1616.

22. Kim, H. J., Graham, D. W., DiSpirito, A. A., Alterman, M. A., Galeva, N., Larive, C. K., Asunskis, D. & Sherwood, P. M. (2004). *Science* **305**, 1612-1615.

23. Krentz, B.D., H.J. Mulherron, J.D. Semrau, A.A. DiSpirito, N.L. Bandow, D.H. Haft, S. Vuilleumier, J.C. Murrell, M.T. Mc. Ellistrem, S.C. Hartsel, and W.H. Gallagher W.H. (2019).Biochemistry 49: 10117-10130.

24. Lichmannegger, J., Leitinger, C., Winner, R., Schmitt, S., Schulz, S., Kabiri, Y., Eberhagen, C., Rieder, T., Janik, D., Neff, F., Aichler, M., DiSpirito, A. A., Bandow, N. L., Baral, B. S., Flatler, A., Kremmer, E., Denk, G., Hohenester, S., Eckardt-Schupp, F., Dencher, N., Adamski, J., Merle, U., Gotthardt, D. N., Kroemer, G., Weiss, K. H. & Zischka, H. (2016). *J. Clin Inves.* **126**, 2721-2735.

25. Lindqvist, Y., Koskiniemi, H., Jansson, A., Sandalova, T., Schnell, R., Liu, Z. L., Mantsala, P., Niemi, J. & Schneider, G. (2009). *J Mol Biol* **393**, 966-977.

26. Lu, X., Gu, W., Zhao, L., Fagan, U. H. M., DiSpirito, A. A., Semrau, J. D. & Gu, B. (2017). *Science Adv.* **3**, e1700041.

27. McCoy, A. J. (2007). *Acta Cryst* **D63**, 32-41.

28. Neilands, J.B.(1995) J. Biol. Chem. 270, 26723-26726

29. Ryan, K.S., Chakraborty, S., Howard-Jones, A.R., Walsh, C.T., Ballou, D.P., & Drennan, C.C. (2008) Biochemistry **47,** 13506-13513.

30. Semau, J. D., DiSpirito, A. A., Obulisamy, P. K. & Kang, C. S. (2020). *FEMS Microbiol. Lett.* **367**, feaa045.

31. Semrau, J. D., DiSpirito, A. A., Obulisamy, P. K. & Kang-Yun, C. S. (2020). *FEMS Microbiol. Lett.* **367**, fnaa045.

32. Varadi, M., Anyango, S., Deshpande, M., Nair, S., Natassia, C., Yordanova, G., Yuan, D., Stroe, O., Wood, G., Laydon, A., Zidek, A., Green, T., Tunyasuvunakool, K., Petersen, S., Jumper, J., Clancy, E., Green, R., Vora, A., Lutfi, M., Figurnov, M., Cowie, A., Hobbs, N., Kohli, P., Kleywegt, G., Birney, E., Hassabis, D. & Velankar, S. (2022). *Nucl. Acids Res* **50**, D439-D444.

33. Vorobev, A., Jagadevan, S., Baral, B. S., Dispirito, A. A., Freemeier, B. C., Bergman, B. H., Bandow, N. L. & Semrau, J. D. (2013). *Appl Environl Microbiol* **79**, 5918-5926.

34. Zischka, H., Lichtmannegger, J., Schmitt, S., Jagemann, N., Schulz, S., Wartini, D., Jennen, L., Rust, C., Larochette, N., Galluzzi, L., Chajes, V., Bandow, N., Gilles, V. S., DiSpirito, A. A., Esposito, I., Goettlicher, M., Summer, K. H. & Kroemer, G. (2011). *J. Clin. Invest.* **121**, 1508-1518.

Tables

Table 1. Crystallization information

Method	Vapor diffusion, sitting drop
Plate Type	96-3 Low volume reservoir INTELLI-PLATE® (Art Robbins Instruments, LLC)
Temperature (K)	291
Protein concentration (mg•ml^{-1})	20
Buffer composition of protein solution	50 mM HEPES pH 7.4, 50 mM NaCl
Composition of reservoir solution	100 mM Bis-Tris propane pH 6.5, 200 mM sodium bromide, 20% (*w*/*v*), PEG 3350
Volume and ratio of drop (nl)	105:105
Volume of reservoir (µl)	50

Table 2. Data collection and processing statistics

Property	**Value**
Space group	C121
Unit cell parameters: a, b, c	148.35 Å, 96.77 Å, 135.21 Å
α, β, γ	90.00°, 116.41°, 90.00°
Resolution (Å)	59.95 - 2.61
% Data completeness	99.6 (59.95 - 2.61)
$< I/\sigma(I) >$	1.19 (at 2.61 Å)
R, R_{free}	0.204, 0.254 0.205, 0.252
R_{free} test set	1999 reflections (3.82%)
Wilson B-factor (Å^2)	66.7
Anisotropy	0.429
Bulk solvent k_{sol}(e/Å^3), B_{sol}(Å^2)	0.40, 63.7
L-test for twinning	$<\|L\|> = 0.51$, $< L^2> = 0.34$
Estimated twinning fraction	No twinning to report
F_0, F_c correlation	0.96
Total number of atoms	12534
Average B, all atoms (Å^2)	71.0

Figures

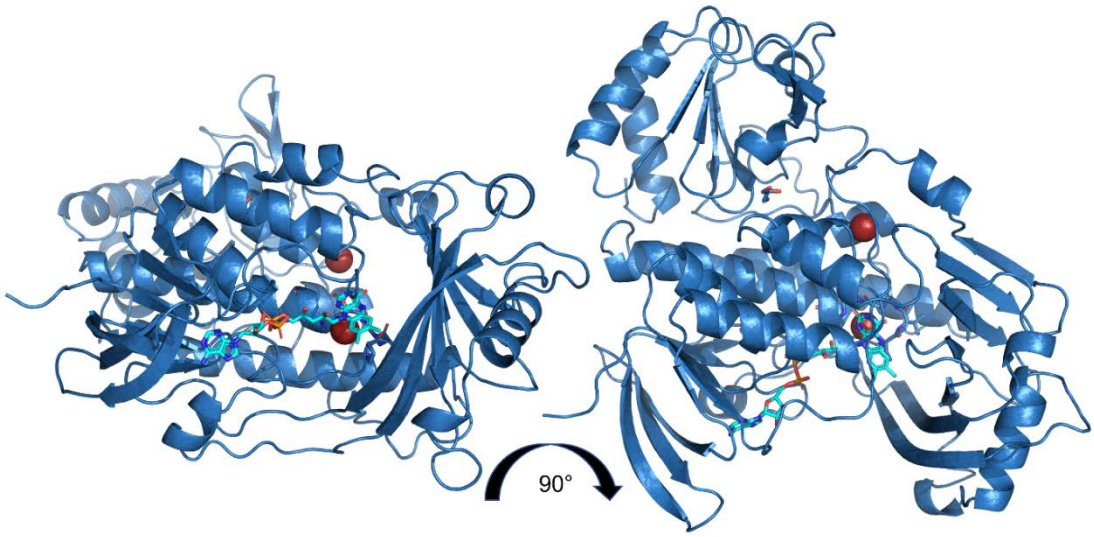

Figure 1. Structure of *mbnF* monomer rotated 90°. FAD is shown in cyan for contrast, as well as the two conserved bromide ions which co-crystalized with *mbnF* shown in red. A channel through the protein adjacent to the isoalloxazine ring of FAD is clearly visible on the left side presentation.

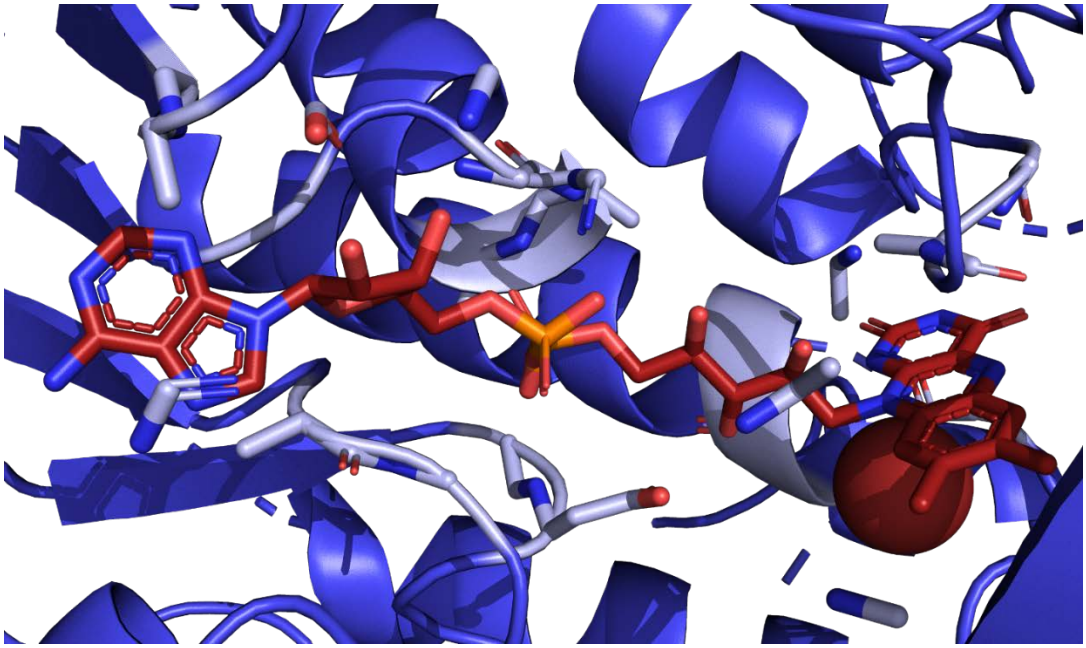

Figure 2. Closeup of FAD binding pocket. FAD is shown in red, *mbnF* is shown in blue, and atoms with 5 Å of FAD are shown in light blue (for contrast). Also shown is the two co-crystalized bromide ion which is coordinated by the FAD and the N-terminal end of the adjacent α-helix.

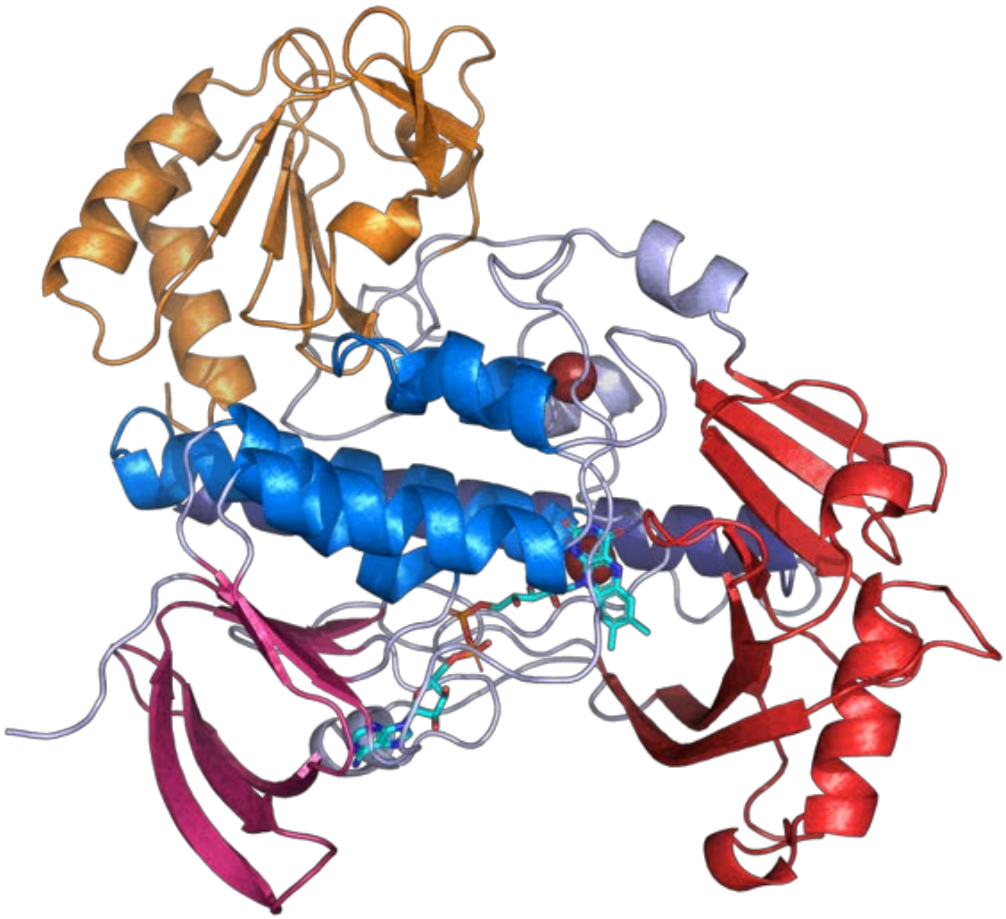

Figure 3. Structure of the *mbnF* monomer color-coded by structural domain and the FAD shown in cyan for contrast: 5-helix bundle (blue), β-sandwich coordinating the adenine moiety of FAD (pink), β-hotdog forming the putative active site (red), C-terminal domain featuring β-α-β and β-β-α motifs (orange), and a 30 aa helix containing a central proline (purple).

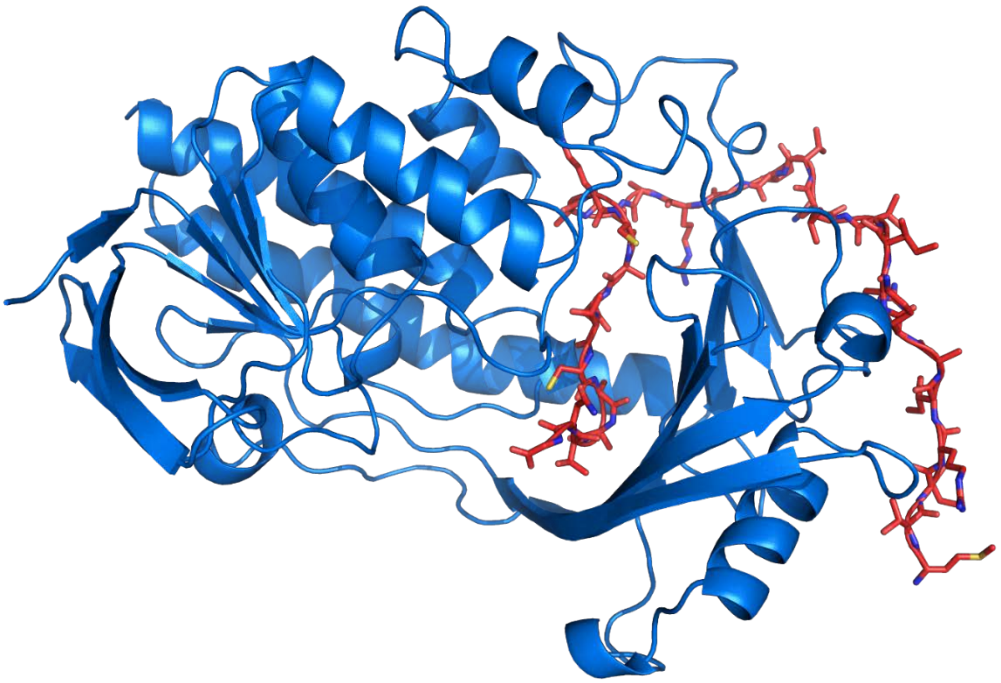

Figure 4. Molecular dynamic simulation of the *mbnF* crystal structure and docked *mbnA* in red, in active-site channel, showing this channel is large enough to accommodate a peptide without clashes. However, further analysis of any contacts between *mbnF* and *mbnA* are likely to be artefactual due to the short length of the simulation. The MD simulation was run in GROMACS using the AMBER99SB force field and SPC/E water model. The structure was equilibrated with a 100 ps NVT and NPT calculations followed by a 10 ns production run. The average RMSD was relatively flat by 4 ns.

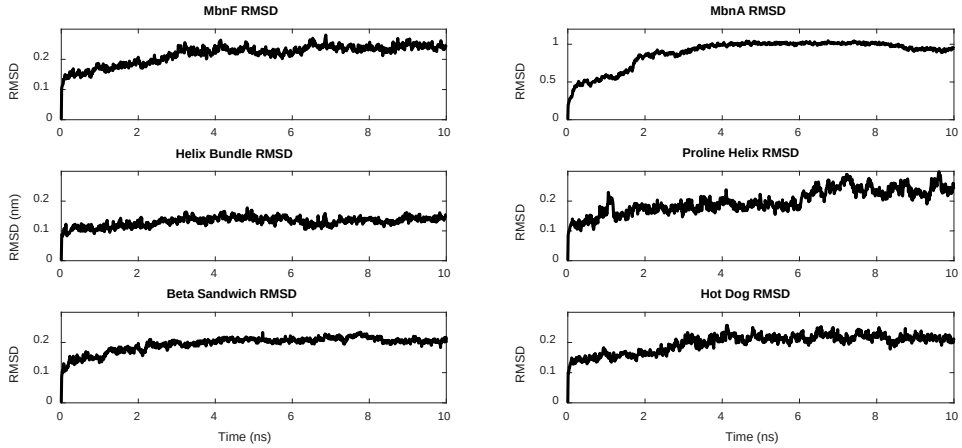

Figure 5. Backbone RMSD of *mbnF* with *mbnA*1 ns MD simulation, all graphs are plotted as RMSD (nm) against simulation time (ns), all graphs are scaled from 0 – 0.3 nm, except *mbnA* which is scaled 0 – 1.2 nm. From top to bottom and left to right is the RMSD for: Full *mbnF*, *mbnA* (the region not docked into the *mbnF* channel underwent large conformational changes), helix bundle domain (not included in the helix bundle), β-sandwich motif adjacent to the adenine moiety of FAD, and the β-hot dog motif adjacent to the alloxazine ring of FAD.

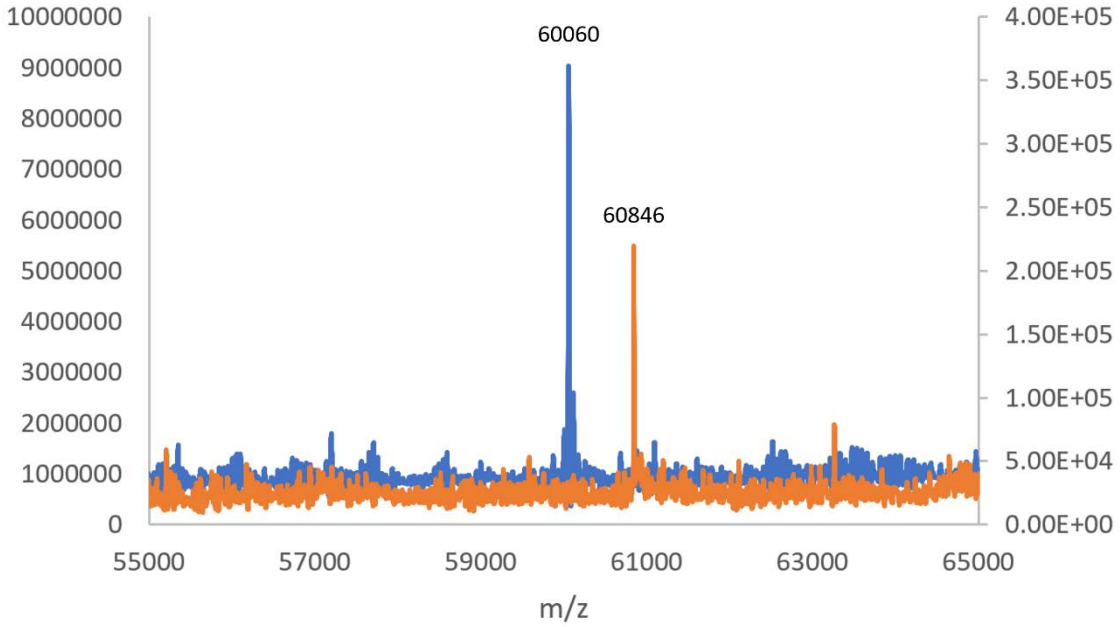

Figure 6. MS spectra of *mbnA*+*mbnF* on a C4 column (blue) and a SEC column (orange). Under acidic conditions *mbnA* separated from *mbnF* on a C4 column and only the *mbnF* is observed. Under neutral pH condition of the SEC column, *mbnA* remained bound to *mbnF* when chromatographed on a SEC column

Supplemental Information

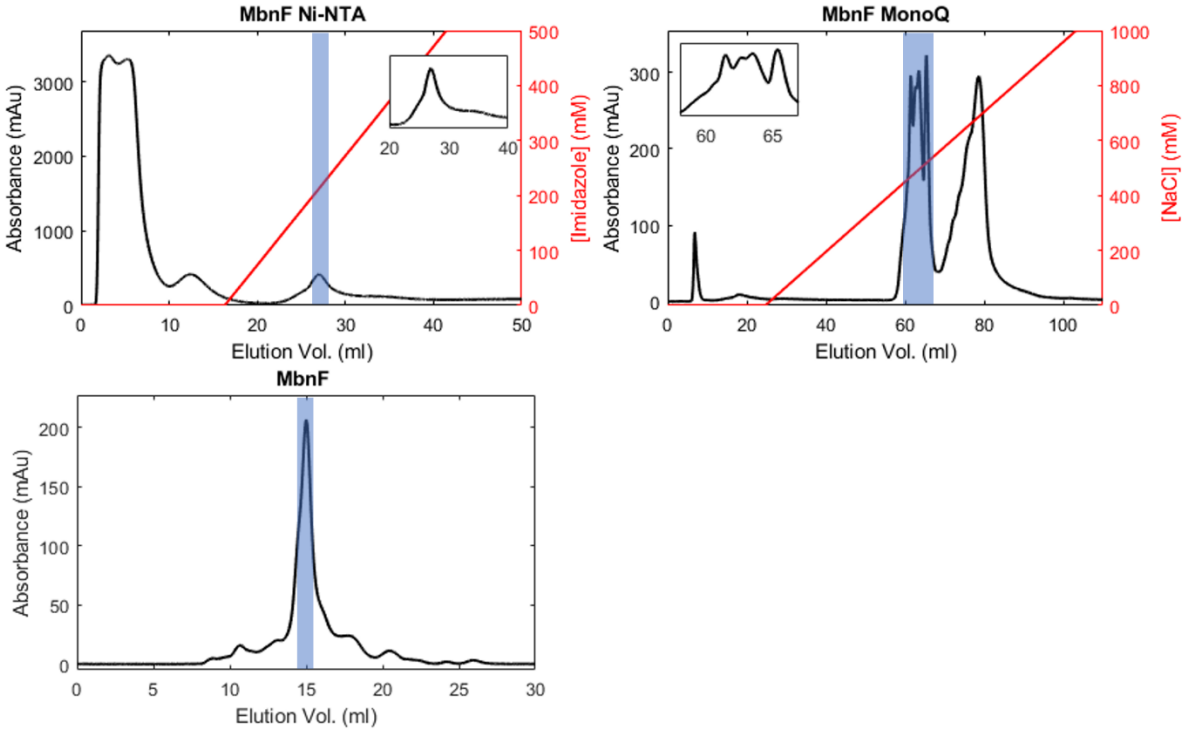

Figure S1. Chromatography chromatograms of *mbnF* purification with collected *mbnF* fractions highlighted in blue. All columns were run on an ÄKTA Pure system. (Top left) Elution profile of *mbnF* cleared lysate on HisTrap column. HisTrap column was equilibrated and run with 50 mM Hepes pH 7.4 and 50 mM NaCl, using an imidazole gradient from 0 – 500 mM. *mbnF* eluted at 27 ml (~200mM imidazole). Inset shows *mbnF* peak. Absorbance shown in black, and buffer B concentration shown in red. (Top right) Elution profile of *mbnF* eluted from a HisTrap on a MonoQ 10/100 GL column. The column was equilibrated and run with 50 mM Hepes pH 7.4, using an NaCl gradient from 0 – 1 M. *mbnF* eluted at 60 ml (~450 mM NaCl). Inset shows *mbnF* peak. Absorbance shown in black, and buffer B concentration shown in red. (Bottom left) Chromatogram of *mbnF* on Superdex 200 increase 10/300 GL. The column was equilibrated and run with 50 mM Hepes pH 7.4, 150 mM NaCl. *mbnF* eluted at 14.3 mL as the primary peak.

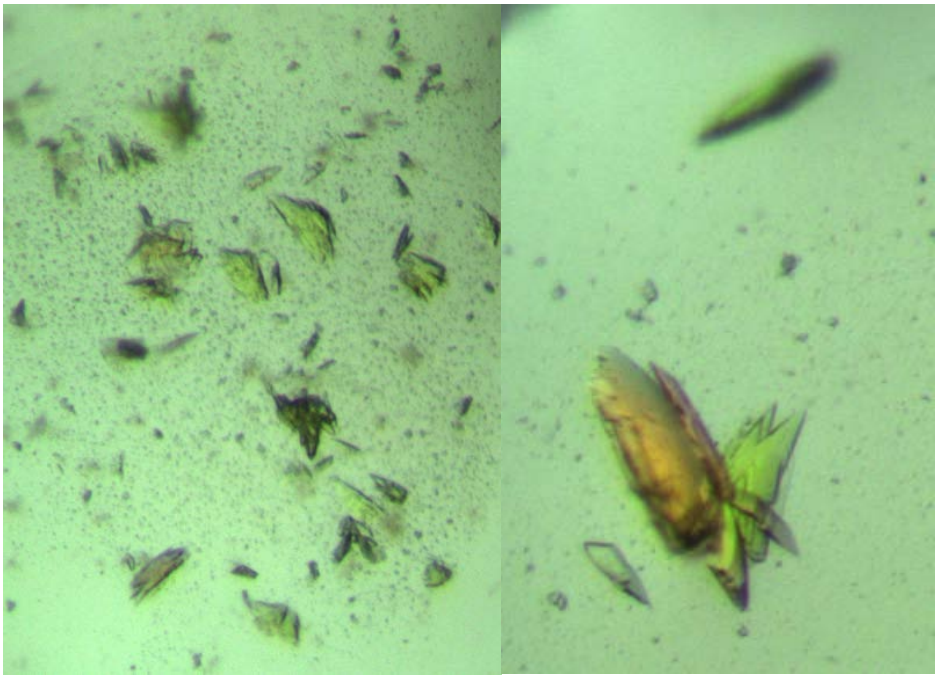

Figure S2. *mbnF* Crystals used for X-ray diffraction. Crystals were grown in 20% PEG 3350, 0.1 M Bis-Tris propane pH 6.5, 0.2 M sodium bromide (PACT premier Eco crystal screen well F2), and grown at 18 C.

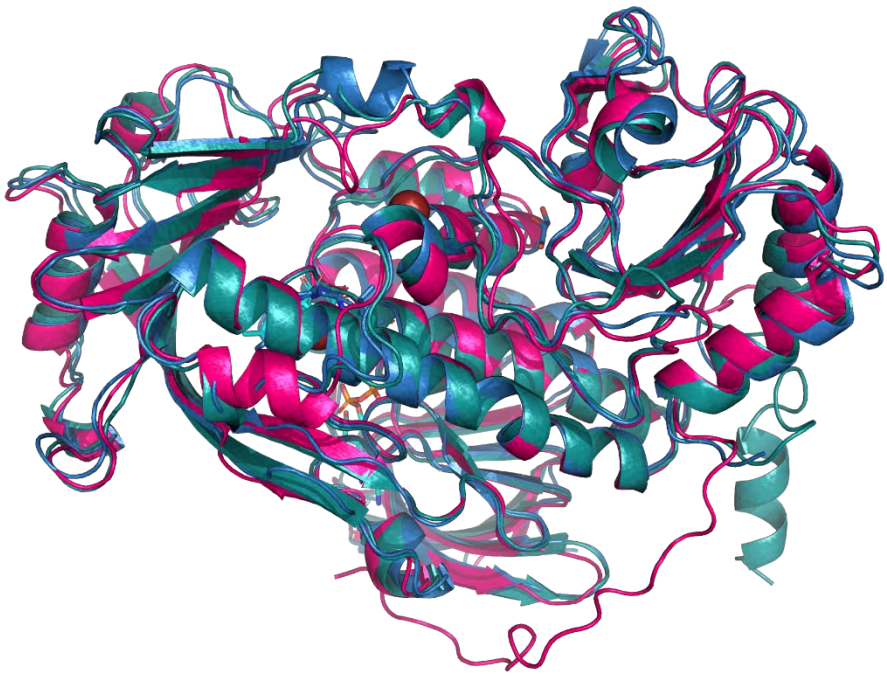

Figure S3. Crystal structure of *mbnF* (blue) aligned with the AlphaFold predictions for two *mbnF* proteins from Methylosinus sp. sav-2. The two proteins are 58 and 55% identical to the *mbnF* sequence from Methylocystis sp. Strain SB2 used in this study, with a relative RMSD of 7.0 and 3.6 Å respectively.

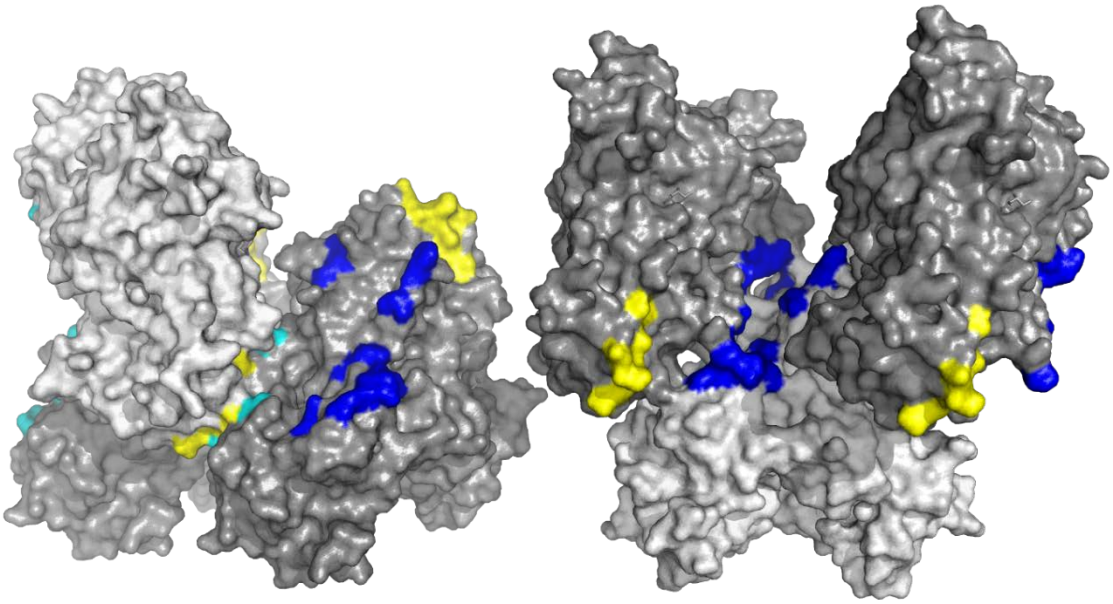

Figure S4. Crystallographic trimer of *mbnF* (rotated). Interfacial residues within 5 Å of binding partner were colored blue, yellow, or cyan representing three distinct binding interfaces and two distinct binding modes (blue/blue, and yellow/cyan). The relative position of the yellow and cyan interfaces illustrates the possibility of forming run-on oligomers.

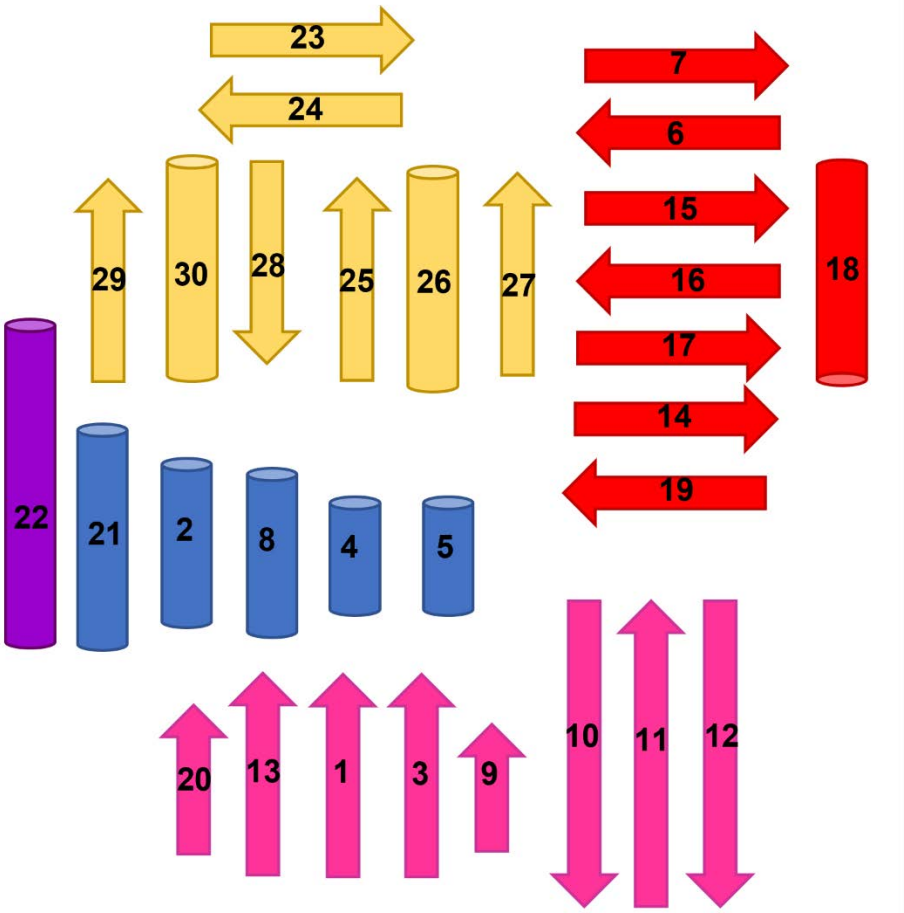

Figure S5. Topology of *mbnF* structural domains color-coded by domain. Numbering from 1 to 30 shows the relative position in the primary sequence from N to C terminals. It is of note that only the yellow domain is fully isolated from the other domains with ~50 residues between element 22 and 23. The other three domains all have inter-connected elements tying these domains together.

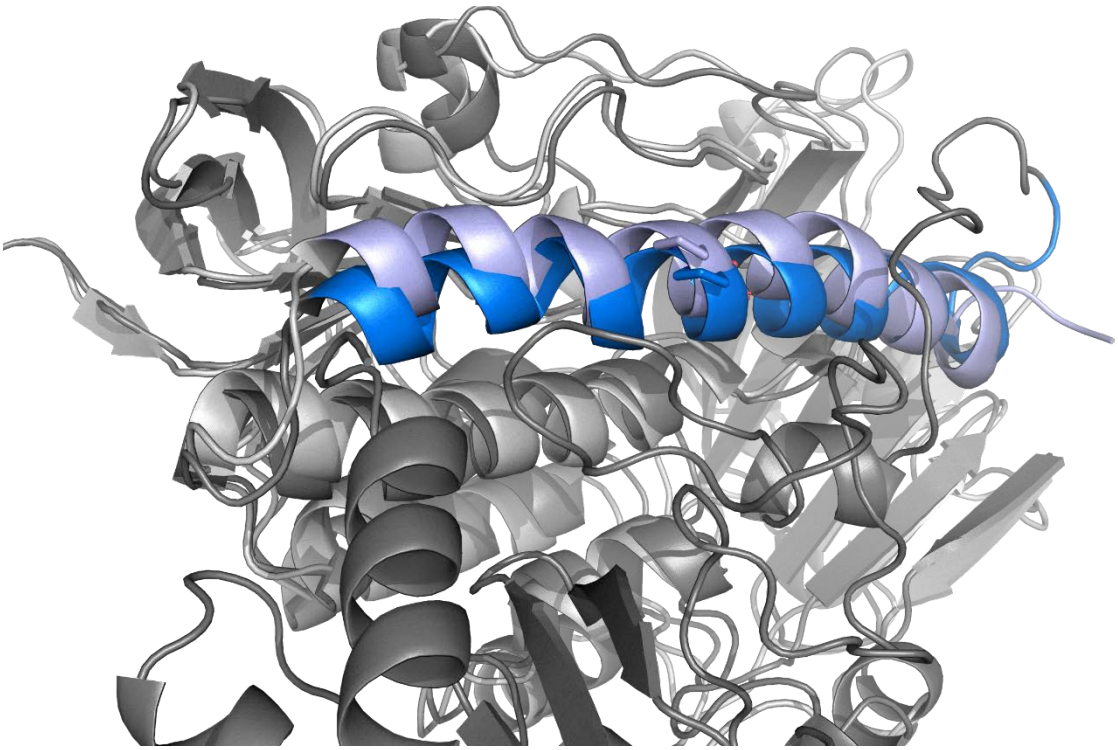

Figure S6. Close up of helix 22 which contains a central proline (shown as sticks for clarity). The helix from the crystal structure is shown blue, and the helix after a 10 ns MD simulation is shown in silver. While there is an apparent deviation from the crystal structure, it is of note that even after the 10 ns simulation, this helix had not yet come to equilibrium. A longer simulation would be required to assess the equilibrium state of this helix. It should be noted that the C-terminal domain and ~50 residue loop region connected to helix 22 was removed for the MD simulation.

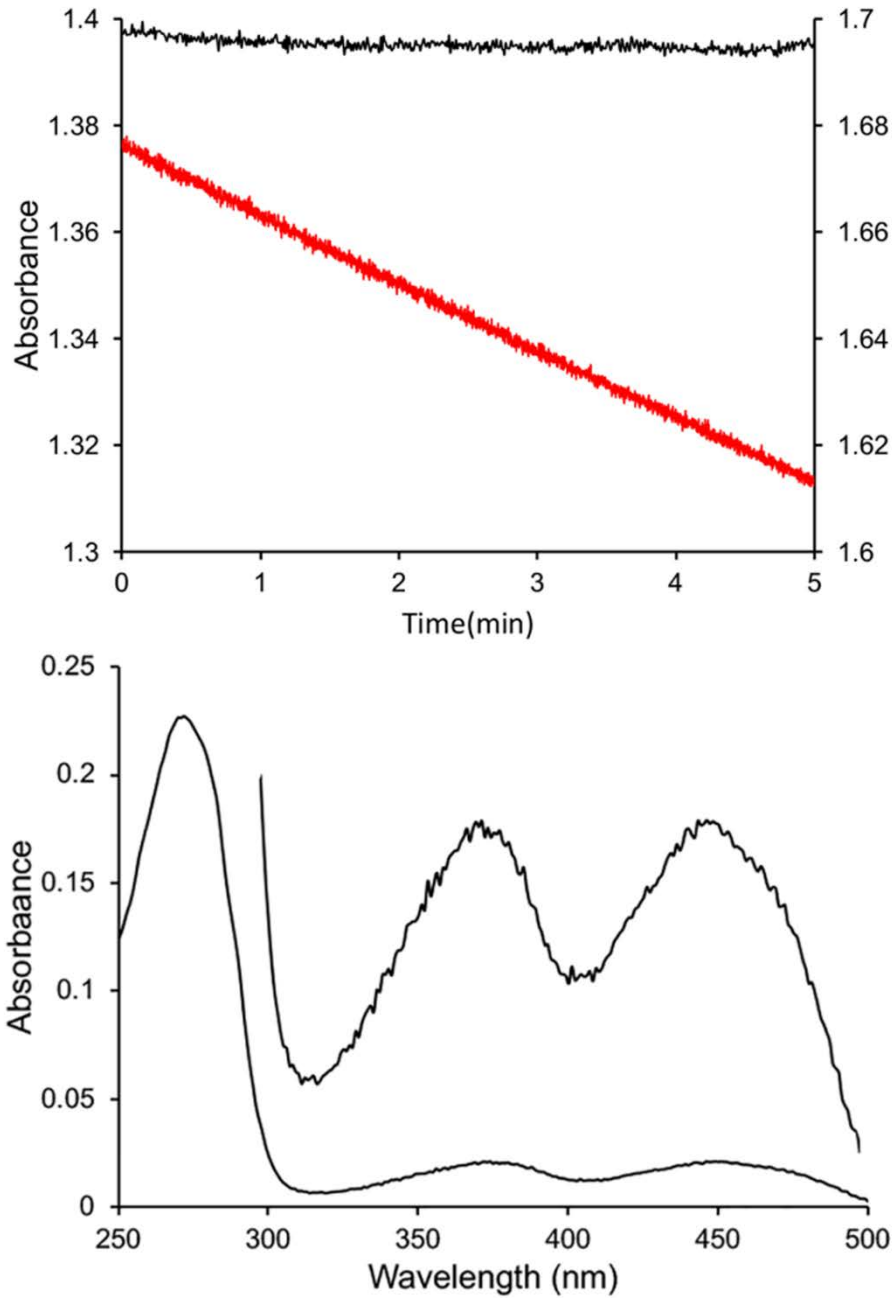

Figure S7. (Top) Kinetics assay showing the change in A340 for NADPH in the presence (**red**) and absence (**black**) of *mbnF*. (Bottom) UV-vis spectra of *mbnF*, with the flavin region zoomed in (inner trace).

CHAPTER 5. GENERAL CONCLUSIONS

Methanobactin (MB) is a member of the growing class of ribosomally synthesized and posttranslationally modified peptides (RiPPs) (DiSpirito *et al.,* 2016). It is produced by methanotrophs, especially during times of copper scarcity, and both functions as a chalkophore for acquiring physiological copper (Kenney *et al.,* 2013; DiSpirito *et al.,* 2016), and, as I have shown in this dissertation, possibly as an oxygen-generator to provide oxygen for methane monooxygenase (MMO) under anoxic conditions (Dershwitz *et al.,* 2021). This additional functionality could have significant ecological and societal implications, as it would convey a huge competitive advantage to methanotrophs that produce MBs, enabling them to metabolize methane, a potent greenhouse gas, in environments in which they otherwise would be unable to do so. This study showed that MB will catalyze O_2 generation from H_2O *in vitro,* and other indirect evidence points towards the presence of MMOs in anoxic environments in which methane oxidation occurs (Ettwig *et al.,* 2010; Bar-Or *et al.,* 2017; Liang *et al.,* 2019), but further study will be necessary to determine if this reaction occurs *in vivo* and in an ecologically-relevant manner.

Additionally, we further elucidated the biosynthesis of MB in two separate projects. First, we produced MB from a Δ*mbnC* mutant, then solved the structure using UV-visible absorption spectroscopy, mass spectrometry, and solution nuclear magnetic resonance (NMR) spectroscopy. We compared this structure to the structure of wild-type MB, and saw that not only was the C-terminal oxazolone absent, it never formed in the first place (Dershwitz *et al.,* 2022). From this we concluded that *mbnC* is required for the formation of the C-terminal oxazolone but not the N-terminal oxazolone in the MB from *Methylosinus trichosporium* OB3b.

Second, we crystallized the protein encoded by the *mbnF* gene in *Methylocystis* strain SB2, solved the crystal structure and performed enzymology and binding studies on the protein. From this we concluded that *mbnF* encodes an NADPH-dependent flavin monooxygenase, and that the protein will bind to the proto-MB encoded by the *mbnA* gene.

Given the interest in medical applications for MB, and the fact that different MBs appear to have different *in vivo* efficacies (Lichtmannegger *et al.*, 2016; Einer *et al*, in review), there is tremendous opportunity in fully elucidating the biosynthesis of MB and genetically modifying it. Future work would involve making Δ*mbnB*, ΔmbnG and ΔmbnH knockout mutants and determining the structure of the resulting MBs in the same manner as with *mbnC*. Additionally, the use of Δ*mbnAN* mutants with the entire MB biosynthetic operon removed have great potential as platforms for novel MB production. For example, if one clone the MB operon from *Methylocystis* strain SB2 into a Δ*mbnAN* mutant of *M. trichosporium* OB3b, they could conceivably produce the more clinically efficacious MB-SB2 (Einer *et al*, in review) in bacteria that have lost their slime layer and are significantly easier to grow at scale. With full mastery over the MB biosynthetic machinery, it will become possible to create a variety of novel MBs, and tailor them to specific applications, like targeting iron instead of copper so as to treat additional diseases of metal metabolism.

Related Work

1. Abraham, M. J., Murtola, T., Schulz, R., Páll, S., Smith, J. C., Hess, B., & Lindahl, E. (2015). GROMACS: High performance molecular simulations through multi-level parallelism from laptops to supercomputers. *SoftwareX*, *1–2*, 19–25. https://doi.org/https://doi.org/10.1016/j.softx.2015.06.001

2. Vorobev, A., S. Jagadevan, B.S. Baral, A.A. DiSpirito, B.C. Freemeier, B.H. Bergman, N.L. Bandow and J.D. Semrau (2013). Detoxification of Mercury by Methanobactin from *Methylosinus trichosporium* OB3b. *Applied and Environmental Microbiology*, *79*(19), 5918–5926. https://doi.org/10.1128/AEM.01673-13

3. Amaral, J. A., & Knowles, R. (1995). Growth of methanotrophs in methane and oxygen counter gradients. *FEMS Microbiology Letters*, *126*(3), 215–220. https://doi.org/10.1111/j.1574-6968.1995.tb07421.x

4. Anthony, C. (1992). The structure of bacterial quinoprotein dehydrogenases. *International Journal of Biochemistry*, *24*(1), 29–39. https://doi.org/https://doi.org/10.1016/0020-711X(92)90226-Q

5. Anthony, C. (1982). *The biochemistry of methylotrophs*. Academic Press Ltd., London

6. Apel, K., & Hirt, H. (2004). REACTIVE OXYGEN SPECIES: Metabolism, Oxidative Stress, and Signal Transduction. *Annual Review of Plant Biology*, *55*(1), 373–399. https://doi.org/10.1146/annurev.arplant.55.031903.141701

7. Bab-Dinitz, E., Shmuely, H., Maupin-Furlow, J., Eichler, J., & Shaanan, B. (2006). Haloferax volcanii PitA: an example of functional interaction between the Pfam chlorite dismutase and antibiotic biosynthesis monooxygenase families? *Bioinformatics*, *22*(6), 671–675. https://doi.org/10.1093/bioinformatics/btk043

8. Bandow, N.L. W.H. Gallager, L. Behling, D.W. Choi, J.D. Semrau, S.C. Hartsel, V.S. Gilles, and A.A. DiSpirito. (2011). Isolation of Methanobactin from the spent media of methane-oxidizing bacteria. *Methods in Enzymology*, *495*, 259–269. https://doi.org/10.1016/B978-0-12-386905-0.00017-6

9. Bandow, N. L. (2014). *Isolation and binding properties of methanobactin from the facultative methanotroph Methylocystis strain SB2*. Iowa State University.

10. Bandow, N., Gilles, V. S., Freesmeier, B., Semrau, J. D., Krentz, B., Gallagher, W., McEllistrem, M. T., Hartsel, S. C., Choi, D. W., Hargrove, M. S., Heard, T. M., Chesner, L. N., Braunreiter, K. M., Cao, B. V., Gavitt, M. M., Hoopes, J. Z., Johnson, J. M., Polster, E. M., Schoenick, B. D., Umlauf, A. M., DiSpirito, A. A. (2012). Spectral and copper binding properties of methanobactin from the facultative methanotroph *Methylocystis* strain SB2. *Journal of Inorganic Biochemistry*, *110*, 72–82. https://doi.org/https://doi.org/10.1016/j.jinorgbio.2012.02.002
11. Baral, B. S., Bandow, N. L., Vorobev, A., Freemeier, B. C., Bergman, B. H., Herdendorf, T. J., Fuentes, N., Ellias, L., Turpin, E., Semrau, J. D., DiSpirito, A. A. (2014). Mercury binding by methanobactin from Methylocystis strain SB2. *Journal of Inorganic Biochemistry*, *141*, 161–169. https://doi.org/https://doi.org/10.1016/j.jinorgbio.2014.09.004

12. Baral, B. S. (2017). *Methanobactin: Metal binding proterties, physiological functions and biosynthesis*. Iowa State University.

13. Barlow, D. J., & Thornton, J. M. (1988). Helix geometry in proteins. *Journal of Molecular Biology*, *201*(3), 601–619. https://doi.org/https://doi.org/10.1016/0022-2836(88)90641-9

14. Bar-Or, I., Elvert, M., Eckert, W., Kushmaro, A., Vigderovich, H., Zhu, Q., Ben-Dov, E., Sivan, O. (2017). Iron-Coupled Anaerobic Oxidation of Methane Performed by a Mixed Bacterial-Archaeal Community Based on Poorly Reactive Minerals. *Environmental Science & Technology*, *51*(21), 12293–12301. https://doi.org/10.1021/acs.est.7b03126

15. Baslé, A., El Ghazouani, A., Lee, J., & Dennison, C. (2018). Insight into Metal Removal from Peptides that Sequester Copper for Methane Oxidation. *Chemistry - A European Journal*, *24*(18), 4515–4518. https://doi.org/10.1002/chem.201706035

16. Basu, P., Katterle, B., Andersson, K. K., & Dalton, H. (2003). The membrane-associated form of methane mono-oxygenase from *Methylococcus capsulatus* (Bath) is a copper/iron protein. *Biochemical Journal*, *369*(2), 417–427. https://doi.org/10.1042/bj20020823

17. Behling, L.E., S.C. Hartsel, D.E. Lewis, A.A. DiSpirito, L.R. Masterson, G. Veglia, W.H. Gallagher. (2008). NMR, Mass Spectrometry and Chemical Evidence Reveal a Different Chemical Structure for Methanobactin That Contains Oxazolone Rings. *Journal of the American Chemical Society*, *130*(38), 12604–12605. https://doi.org/10.1021/ja804747d

18. Berova, N., Bari, L. Di, & Pescitelli, G. (2007). Application of electronic circular dichroism in configurational and conformational analysis of organic compounds. *Chemical Society Reviews*, *36*(6), 914–931. https://doi.org/10.1039/B515476F

19. Berson, O., & Lidstrom, M. E. (1997). Cloning and characterization of corA, a gene encoding a copper-repressible polypeptide in the type I methanotroph, *Methylomicrobium albus* BG8. *FEMS Microbiology Letters*, *148*(2), 169–174. https://doi.org/10.1111/j.1574-6968.1997.tb10284.x

20. Gilbert, B., McDonald, I. R., Finch, R., Stafford, G. P., Nielsen, A. K., & Murrell, J. C. (2000). Molecular Analysis of the pmo (Particulate Methane Monooxygenase) Operons from Two Type II Methanotrophs. *Applied and Environmental Microbiology*, *66*(3), 966–975. https://doi.org/10.1128/AEM.66.3.966-975.2000

21. Kalidass, B, M.F. Ul-Haque, B.S. Baral, A.A. DiSpirito, and J.D. Semrau (2015). Competition between Metals for Binding to Methanobactin Enables Expression of Soluble Methane Monooxygenase in the Presence of Copper. *Applied and Environmental Microbiology*, *81*(3), 1024–1031. https://doi.org/10.1128/AEM.03151-14

22. Bowman, G. R. (2016). Accurately modeling nanosecond protein dynamics requires at least microseconds of simulation. *Journal of Computational Chemistry*, *37*(6), 558–566. https://doi.org/https://doi.org/10.1002/jcc.23973

23. Cao, L., Caldararu, O., Rosenzweig, A. C., & Ryde, U. (2018). Quantum Refinement Does Not Support Dinuclear Copper Sites in Crystal Structures of Particulate Methane Monooxygenase. *Angewandte Chemie - International Edition*, *57*(1), 162–166. https://doi.org/10.1002/anie.201708977

24. Carter, P. (1971). Spectrophotometric determination of serum iron at the submicrogram level with a new reagent (ferrozine). *Analytical Biochemistry*, *40*(2), 450–458. https://doi.org/https://doi.org/10.1016/0003-2697(71)90405-2

25. Chan, S. I., Chen, K. H., Yu, S. S., Chen, C. L., & Kuo, S. S. (2004). Toward Delineating the Structure and Function of the Particulate Methane Monooxygenase from Methanotrophic Bacteria. *Biochemistry*, *43*(15), 4421–4430. https://doi.org/10.1021/bi0497603

26. Chandlee, G. C. (1940). *Reference Book of Inorganic Chemistry. Revised edition (Latimer, WM*; *Hildebrand, JH)*. ACS Publications.

27. Chang, J., Gu, W., Park, D., Semrau, J. D., DiSpirito, A. A., & Yoon, S. (2018). Methanobactin from *Methylosinus trichosporium* OB3b inhibits N2O reduction in denitrifiers. *ISME Journal*, *12*(8), 2086–2089. https://doi.org/10.1038/s41396-017-0022-8

28. Chatwood, L. L., Müller, J., Gross, J. D., Wagner, G., & Lippard, S. J. (2004). NMR Structure of the Flavin Domain from Soluble Methane Monooxygenase Reductase from *Methylococcus capsulatus* (Bath),. *Biochemistry*, *43*(38), 11983–11991. https://doi.org/10.1021/bi049066n

29. Chen, Y., Patel, N. A., Crombie, A., Scrivens, J. H., & Murrell, J. C. (2011). Bacterial flavin-containing monooxygenase is trimethylamine monooxygenase. *Proceedings of the National Academy of Sciences*, *108*(43), 17791–17796. https://doi.org/10.1073/pnas.1112928108

30. Chi Fru, E., Gray, N. D., McCann, C., Baptista, J. D. C., Christgen, B., Talbot, H. M., El Ghazouani, A., Dennison, C., Graham, D. W. (2011). Effects of copper mineralogy and methanobactin on cell growth and sMMO activity in *Methylosinus trichosporium* OB3b. *Biogeosciences*, *8*(10), 2887–2894. https://doi.org/10.5194/bg-8-2887-2011

31. Choi, D. W., Kunz, R. C., Boyd, E. S., Semrau, J. D., Antholine, W. E., Han, J. I., Zahn, J. A., Boyd, J. M., de la Mora, A. M., & DiSpirito, A. A. (2003). The Membrane-Associated Methane Monooxygenase (pMMO) and pMMO-NADH:Quinone Oxidoreductase Complex from *Methylococcus capsulatus* Bath. *Journal of Bacteriology*, *185*(19), 5755–5764. https://doi.org/10.1128/JB.185.19.5755-5764.2003

32. Choi, D. W., Do, Y. S., Zea, C. J., McEllistrem, M. T., Lee, S. W., Semrau, J. D., Pohl, N. L., Kisting, C. J., Scardino, L. L., Hartsel, S. C., Boyd, E. S., Geesey, G. G., Riedel, T. P., Shafe, P. H., Kranski, K. A., Tritsch, J. R., Antholine, W. E., & DiSpirito, A. A. (2006). Spectral and thermodynamic properties of Ag(I), Au(III), Cd(II), Co(II), Fe(III), Hg(II), Mn(II), Ni(II), Pb(II), U(IV), and Zn(II) binding by methanobactin from *Methylosinus trichosporium* OB3b. *Journal of Inorganic Biochemistry*, *100*(12), 2150–2161. https://doi.org/10.1016/j.jinorgbio.2006.08.017

33. Choi, D. W., Zea, C. J., Do, Y. S., Semrau, J. D., Antholine, W. E., Hargrove, M. S., Pohl, N. L., Boyd, E. S., Geesey, G. G., Hartsel, S. C., Shafe, P. H., McEllistrem, M. T., Kisting, C. J., Campbell, D., Rao, V., de la Mora, A. M., & Dispirito, A. A. (2006). Spectral, kinetic, and thermodynamic properties of Cu(I) and Cu(II) binding by methanobactin from *Methylosinus trichosporium* OB3b. *Biochemistry*, *45*(5), 1442–1453. https://doi.org/10.1021/bi051815t

34. Choi, D. W., Semrau, J. D., Antholine, W. E., Hartsel, S. C., Anderson, R. C., Carey, J. N., Dreis, A. M., Kenseth, E. M., Renstrom, J. M., Scardino, L. L., Van Gorden, G. S., Volkert, A. A., Wingad, A. D., Yanzer, P. J., McEllistrem, M. T., de la Mora, A. M., & DiSpirito, A. A. (2008). Oxidase, superoxide dismutase, and hydrogen peroxide reductase activities of methanobactin from types I and II methanotrophs. *Journal of Inorganic Biochemistry*, *102*(8), 1571–1580. https://doi.org/https://doi.org/10.1016/j.jinorgbio.2008.02.003

35. Choi, D. W., Bandow, N. L., McEllistrem, M. T., Semrau, J. D., Antholine, W. E., Hartsel, S. C., Gallagher, W., Zea, C. J., Pohl, N. L., Zahn, J. A., & DiSpirito, A. A. (2010). Spectral and thermodynamic properties of methanobactin from γ-proteobacterial methane oxidizing bacteria: A case for copper competition on a molecular level. *Journal of Inorganic Biochemistry*, *104*(12), 1240–1247. https://doi.org/https://doi.org/10.1016/j.jinorgbio.2010.08.002

36. Chou, J. C.-C., Stafford, V. E., Kenney, G. E., & Dassama, L. M. K. (2021). The enzymology of oxazolone and thioamide synthesis in methanobactin. In E. J. B. T.-M. in E. Petersson (Ed.), *Synthetic and Enzymatic Modifications of the Peptide Backbone* (Vol. 656, pp. 341–373). https://doi.org/https://doi.org/10.1016/bs.mie.2021.04.008

37. Colby, J., & Dalton, H. (1978). Resolution of the methane mono-oxygenase of Methylococcus capsulatus (Bath) into three components. Purification and properties of component C, a flavoprotein. *Biochemical Journal*, *171*(2), 461–468. https://doi.org/10.1042/bj1710461

38. Cooper, S. R., McArdle, J. V, & Raymond, K. N. (1978). Siderophore electrochemistry: relation to intracellular iron release mechanism. *Proceedings of the National Academy of Sciences*, *75*(8), 3551–3554. https://doi.org/10.1073/pnas.75.8.3551

39. Cordes, F. S., Bright, J. N., & Sansom, M. S. P. (2002). Proline-induced Distortions of Transmembrane Helices. *Journal of Molecular Biology*, *323*(5), 951–960. https://doi.org/https://doi.org/10.1016/S0022-2836(02)01006-9

40. Crawford, R. L., & Hanson, R. S. (1984). *Microbial growth on C 1 compounds: proceedings* (No. CONF-8309357--). American Society for Microbiology.

41. Csáki, R., Bodrossy, L., Klem, J., Murrell, J. C., & Kovács, K. L. (2003). Genes involved in the copper-dependent regulation of soluble methane monooxygenase of *Methylococcus capsulatus* (Bath): cloning, sequencing and mutational analysis. *Microbiology (Reading, England)*, *149*(Pt 7), 1785–1795. https://doi.org/10.1099/mic.0.26061-0

42. Dershwitz, P., Gu, W., Roche, J., Kang-Yun, C. S., Semrau, J. D., Bobik, T. A., Fulton, B., Zischka, H., DiSpirito, A. A. (2022). *mbnC* Is Not Required for the Formation of the N-Terminal Oxazolone in the Methanobactin from *Methylosinus trichosporium* OB3b. *Applied and Environmental Microbiology*, *88*(2), e01841-21. https://doi.org/10.1128/AEM.01841-21

43. Dershwitz, P., Bandow, N. L., Yang, J., Semrau, J. D., McEllistrem, M. T., Heinze, R. A., Fonseca, M., Ledesma, J. C., Jennett, J. R., DiSpirito, A. M., Athwal, N. S., Hargrove, M. S., Bobik, T. A., Zischka, H., & DiSpirito, A. A. (2022). *mbnC* Is Not Required for the Formation of the N-Terminal Oxazolone in the Methanobactin from *Methylosinus trichosporium* OB3b. *Applied and Environmental Microbiology*, *88*(2), e01841-21. https://doi.org/10.1128/AEM.01841-21

44. Dennison, C. (2019). The Coordination Chemistry of Copper Uptake and Storage for Methane Oxidation. *Chemistry - A European Journal*, *25*(1), 74–86. https://doi.org/10.1002/chem.201803444

45. DiSpirito, A. A., Lipscomb, J. D., & Lidstrom, M. E. (1990). Soluble cytochromes from the marine methanotroph *Methylomonas* sp. strain A4. *Journal of Bacteriology*, *172*(9), 5360–5367. https://doi.org/10.1128/jb.172.9.5360-5367.1990

46. DiSpirito, A. A., Kunz, R. C., Choi, D.-W., & Zahn, J. A. (2004). *Respiration in Methanotrophs* (D. Zannoni, Ed.). https://doi.org/10.1007/978-1-4020-3163-2_7

47. DiSpirito, A. A., Semrau, J. D., Murrell, J. C., Gallagher, W. H., Dennison, C., & Vuilleumier, S. (2016). Methanobactin and the Link between Copper and Bacterial Methane Oxidation. *Microbiology and Molecular Biology Reviews : MMBR*, *80*(2), 387–409. https://doi.org/10.1128/MMBR.00058-15

48. Dou, C., Long, Z., Li, S., Zhou, D., Jin, Y., Zhang, L., Zhang, X., Zheng, Y., Li, L., Zhu, X., Liu, Z., He, S., Yan, W., Yang, L., Xiong, J., Fu, X., Qi, S., Ren, H., Chen, S., Dai, L., Cheng, W. (2022). Crystal structure and catalytic mechanism of the *mbnBC* holoenzyme required for methanobactin biosynthesis. *Cell Research*, (November 2021). https://doi.org/10.1038/s41422-022-00620-2

49. Eckert, P., Johs, A., Semrau, J. D., DiSpirito, A. A., Richardson, J., Sarangi, R., Herndon, E., Gu, B., & Pierce, E. M. (2021). Spectroscopic and computational investigations of organometallic complexation of group 12 transition metals by methanobactins from *Methylocystis* sp. SB2. *Journal of Inorganic Biochemistry*, *223*, 111496. https://doi.org/https://doi.org/10.1016/j.jinorgbio.2021.111496

50. Einer, C., Leitzinger, C., Lichtmannegger, J., Eberhagen, C., Rieder, T., Borchard, S., Wimmer, R., Denk, G., Popper, B., Neff, F., Polishchuk, E. V., Polishchuk, R. S., Hauck, S. M., von Toerne, C., Müller, J. C., Karst, U., Baral, B. S., DiSpirito, A. A., Kremer, A. E., Semrau, J., Weiss, K. H., Hohenester, S., Zischka, H. (2019). A High-Calorie Diet Aggravates Mitochondrial Dysfunction and Triggers Severe Liver Damage in Wilson Disease Rats. *Cellular and Molecular Gastroenterology and Hepatology*, *7*(3), 571–596. https://doi.org/https://doi.org/10.1016/j.jcmgh.2018.12.005

51. El Ghazouani, A., Baslé, A., Firbank, S. J., Knapp, C. W., Gray, J., Graham, D. W., & Dennison, C. (2011). Copper-binding properties and structures of methanobactins from *Methylosinus trichosporium* OB3b. *Inorganic Chemistry*, *50*(4), 1378–1391. https://doi.org/10.1021/ic101965j

52. El Ghazouani, A., Baslé, A., Gray, J., Graham, D. W., Firbank, S. J., & Dennison, C. (2012). Variations in methanobactin structure influences copper utilization by methane-oxidizing bacteria. *Proceedings of the National Academy of Sciences*, *109*(22), 8400–8404. https://doi.org/10.1073/pnas.1112921109

53. Elango, N. A., Radhakrishnan, R., Froland, W. A., Wallar, B. J., Earhart, C. A., Lipscomb, J. D., & Ohlendorf, D. H. (1997). Crystal structure of the hydroxylase component of methane monooxygenase from *Methylosinus trichosporium* OB3b. *Protein Science*, *6*(3), 556–568. https://doi.org/https://doi.org/10.1002/pro.5560060305

54. Ettwig, K. F., Butler, M. K., Le Paslier, D., Pelletier, E., Mangenot, S., Kuypers, M. M., Schreiber, F., Dutilh, B. E., Zedelius, J., de Beer, D., Gloerich, J., Wessels, H. J., van Alen, T., Luesken, F., Wu, M. L., van de Pas-Schoonen, K. T., Op den Camp, H. J., Janssen-Megens, E. M., Francoijs, K. J., Stunnenberg, H., Weissenbach, J., Jetten, M. S. M., Strous, M. (2010). Nitrite-driven anaerobic methane oxidation by oxygenic bacteria. *Nature*, *464*(7288), 543–548. https://doi.org/10.1038/nature08883

55. Fjellbirkeland, A., Kleivdal, H., Joergensen, C., Thestrup, H., & Jensen, H. B. (1997). Outer membrane proteins of *Methylococcus capsulatus* (Bath). *Archives of Microbiology*, *168*(2), 128–135. https://doi.org/10.1007/s002030050478

56. Fjellbirkeland, A., Kruger, P. G., Bemanian, V., Høgh, B. T., Murrell, C. J., & Jensen, H. B. (2001). The C-terminal part of the surface-associated protein MopE of the methanotroph *Methylococcus capsulatus* (Bath) is secreted into the growth medium. *Archives of Microbiology*, *176*(3), 197–203. https://doi.org/10.1007/s002030100307

57. Fox, B. G., Froland, W. A., Dege, J. E., & Lipscomb, J. D. (1989). Methane monooxygenase from Methylosinus trichosporium OB3b: Purification and properties of a three-component system with high specific activity from a type II methanotroph. *Journal of Biological Chemistry*, *264*(17), 10023–10033. https://doi.org/https://doi.org/10.1016/S0021-9258(18)81762-8

58. Fox, B. G., Hendrich, M. P., Surerus, K. K., Andersson, K. K., Froland, W. A., Lipscomb, J. D., & Munck, E. (1993). Moessbauer, EPR, and ENDOR studies of the hydroxylase and reductase components of methane monooxygenase from *Methylosinus trichosporium* OB3b. *Journal of the American Chemical Society*, *115*(9), 3688–3701. https://doi.org/10.1021/ja00062a039

59. Gilman, A., Fu, Y., Hendershott, M., Chu, F., Puri, A. W., Smith, A. L., Pesesky, M., Lieberman, R., Beck, D., & Lidstrom, M. E. (2017). Oxygen-limited metabolism in the methanotroph *Methylomicrobium buryatense* 5GB1C. *PeerJ*, *5*, e3945. https://doi.org/10.7717/peerj.3945

60. Griffiths, R. I., Whiteley, A. S., O'Donnell, A. G., & Bailey, M. J. (2000). Rapid Method for Coextraction of DNA and RNA from Natural Environments for Analysis of Ribosomal DNA- and rRNA-Based Microbial Community Composition. *Applied and Environmental Microbiology*, *66*(12), 5488–5491. https://doi.org/10.1128/AEM.66.12.5488-5491.2000

61. Gu, W., Farhan Ul Haque, M., DiSpirito, A. A., & Semrau, J. D. (2016). Uptake and effect of rare earth elements on gene expression in *Methylosinus trichosporium* OB3b. *FEMS Microbiology Letters*, *363*(13), fnw129. https://doi.org/10.1093/femsle/fnw129

62. Gu, W., Farhan Ul Haque, M., Baral, B. S., Turpin, E. A., Bandow, N. L., Kremmer, E., Flatley, A., Zischka, H., DiSpirito, A. A., & Semrau, J. D. (2016). A TonB-Dependent Transporter Is Responsible for Methanobactin Uptake by *Methylosinus trichosporium* OB3b. *Applied and Environmental Microbiology*, *82*(6), 1917–1923. https://doi.org/10.1128/AEM.03884-15

63. Gu, W., Baral, B. S., DiSpirito, A. A., & Semrau, J. D. (2016). An Aminotransferase Is Responsible for the Deamination of the N-Terminal Leucine and Required for Formation of Oxazolone Ring A in Methanobactin of *Methylosinus trichosporium* OB3b. *Applied and Environmental Microbiology*, *83*(1), e02619-16. https://doi.org/10.1128/AEM.02619-16

64. Hanson, R. S., & Hanson, T. E. (1996). Methanotrophic bacteria. *Microbiological Reviews*, *60*(2), 439–471. Retrieved from http://www.ncbi.nlm.nih.gov/pubmed/8801441%0Ahttp://www.pubmedcentral.nih.gov/articlerender.fcgi?artid=PMC239451

65. Harada, N., Nakanishi, K., & Berova, N. (2012). Electronic CD Exciton Chirality Method: Principles and Applications. In *Comprehensive Chiroptical Spectroscopy* (pp. 115–166). https://doi.org/https://doi.org/10.1002/9781118120392.ch4

66. Harris, D. C. (2010). *Quantitative chemical analysis*. Macmillan.

67. Hayyan, M., Hashim, M. A., & Al Nashef, I. M. (2016). Superoxide Ion: Generation and Chemical Implications. *Chemical Reviews*, *116*(5), 3029–3085. https://doi.org/10.1021/acs.chemrev.5b00407

68. Helland, R., Fjellbirkeland, A., Karlsen, O. A., Ve, T., Lillehaug, J. R., & Jensen, H. B. (2008). An Oxidized Tryptophan Facilitates Copper Binding in *Methylococcus capsulatus*-secreted Protein MopE*. *Journal of Biological Chemistry*, *283*(20), 13897–13904. https://doi.org/10.1074/jbc.M800340200

69. Henckel, T., Roslev, P., & Conrad, R. (2000). Effects of O2 and CH4 on presence and activity of the indigenous methanotrophic community in rice field soil. *Environmental Microbiology*, *2*(6), 666–679. https://doi.org/https://doi.org/10.1046/j.1462-2920.2000.00149.x

70. Holmes, A. J., Costello, A., Lidstrom, M. E., & Murrell, J. C. (1995). Evidence that participate methane monooxygenase and ammonia monooxygenase may be evolutionarily related. *FEMS Microbiology Letters*, *132*(3), 203–208. https://doi.org/10.1016/0378-1097(95)00311-R

71. Hornak, V., Abel, R., Okur, A., Strockbine, B., Roitberg, A., & Simmerling, C. (2006). Comparison of multiple Amber force fields and development of improved protein backbone parameters. *Proteins: Structure, Function, and Bioinformatics*, *65*(3), 712–725. https://doi.org/https://doi.org/10.1002/prot.21123

72. Jiang, H., Chen, Y., Jiang, P., Zhang, C., Smith, T. J., Murrell, J. C., & Xing, X.-H. (2010). Methanotrophs: Multifunctional bacteria with promising applications in environmental bioengineering. *Biochemical Engineering Journal*, *49*(3), 277–288. https://doi.org/https://doi.org/10.1016/j.bej.2010.01.003

73. Johnson, C. L. (2006). *Methanobactin: a potential novel biopreservative for use against the foodborne pathogen Listeria monocytogenes*. Iowa State University.

74. Johnson, K. A., Ve, T., Larsen, Ø., Pedersen, R. B., Lillehaug, J. R., Jensen, H. B., … Karlsen, O. A. (2014). CorA Is a Copper Repressible Surface-Associated Copper(I)-Binding Protein Produced in *Methylomicrobium album* BG8. *PLOS ONE*, *9*(2), e87750. Retrieved from https://doi.org/10.1371/journal.pone.0087750

75. Jollie, D. R., & Lipscomb, J. D. (1991). Formate dehydrogenase from *Methylosinus trichosporium* OB3b: Purification and spectroscopic characterization of the cofactors. *Journal of Biological Chemistry*, *266*(32), 21853–21863. https://doi.org/10.1016/s0021-9258(18)54716-5

76. Jollie, D. R., & Lipscomb, J. D. B. T.-M. in E. (1990). Formate dehydrogenase from *Methylosinus trichosporium* OB3b. In *Hydrocarbons and Methylotrophy* (Vol. 188, pp. 331–334). https://doi.org/https://doi.org/10.1016/0076-6879(90)88051-B

77. Jumper, J., Evans, R., Pritzel, A., Green, T., Figurnov, M., Ronneberger, O., Tunyasuvunakool, K., Bates, R., Žídek, A., Potapenko, A., Bridgland, A., Meyer, C., Kohl, S., Ballard, A. J., Cowie, A., Romera-Paredes, B., Nikolov, S., Jain, R., Adler, J., Back, T., … Hassabis, D. (2021). Highly accurate protein structure prediction with AlphaFold. *Nature*, *596*(7873), 583–589. https://doi.org/10.1038/s41586-021-03819-2

78. Kaler, S. G. (2016). Microbial peptide de-coppers mitochondria: implications for Wilson disease. *The Journal of Clinical Investigation*, *126*(7), 2412–2414. https://doi.org/10.1172/JCI88617

79. Kalyuzhnaya, M. G., Puri, A. W., & Lidstrom, M. E. (2015). Metabolic engineering in methanotrophic bacteria. *Metabolic Engineering*, *29*, 142–152. https://doi.org/10.1016/j.ymben.2015.03.010

80. Kang, C. S., Dunfield, P. F., & Semrau, J. D. (2019). The origin of aerobic methanotrophy within the Proteobacteria. *FEMS Microbiology Letters*, *366*(9), 1–11. https://doi.org/10.1093/femsle/fnz096

81. Kang-Yun, C. S., Liang, X., Dershwitz, P., Gu, W., Schepers, A., Flatley, A., Lichtmannegger, J., Zischka, H., Zhang, L., Lu, X., Gu, B., Ledesma, J. C., Pelger, D. J., DiSpirito, A. A. & Semrau, J. D. (2022). Evidence for methanobactin “Theft” and novel chalkophore production in methanotrophs: impact on methanotrophic-mediated methylmercury degradation. *The ISME Journal*, *16*(1), 211–220. https://doi.org/10.1038/s41396-021-01062-1

82. Kenney, G. E., Dassama, L. M. K., Manesis, A. C., Ross, M. O., Chen, S., Hoffman, B. M., & Rosenzweig, A. C. (2019). mbnH is a diheme MauG-like protein associated with microbial copper homeostasis. *Journal of Biological Chemistry*. https://doi.org/10.1074/jbc.RA119.010202

83. Kenney, G. E., Dassama, L., Pandelia, M. E., Gizzi, A. S., Martinie, R. J., Gao, P., DeHart, C. J., Schachner, L. F., Skinner, O. S., Ro, S. Y., Zhu, X., Sadek, M., Thomas, P. M., Almo, S. C., Bollinger, J. M., Jr, Krebs, C., Kelleher, N. L., & Rosenzweig, A. C. (2018). The biosynthesis of methanobactin. *Science*, *359*(6382), 1411–1416. https://doi.org/10.1126/science.aap9437

84. Kenney, G. E., Goering, A. W., Ross, M. O., DeHart, C. J., Thomas, P. M., Hoffman, B. M., Kelleher, N. L., & Rosenzweig, A. C. (2016). Characterization of Methanobactin from *Methylosinus* sp. LW4. *Journal of the American Chemical Society*, *138*(35), 11124–11127. https://doi.org/10.1021/jacs.6b06821

85. Kenney, G. E., & Rosenzweig, A. C. (2012). Chemistry and Biology of the Copper Chelator Methanobactin. *ACS Chemical Biology*, *7*(2), 260–268. https://doi.org/10.1021/cb2003913

86. Kenney, G. E., & Rosenzweig, A. C. (2013). Genome mining for methanobactins. *BMC Biology*, *11*(1), 17. https://doi.org/10.1186/1741-7007-11-17

87. Kenney, G. E., Sadek, M., & Rosenzweig, A. C. (2016). Copper-responsive gene expression in the methanotroph *Methylosinus trichosporium* OB3b. *Metallomics*, *8*(9), 931–940. https://doi.org/10.1039/c5mt00289c

88. Kim, H. J., Graham, D. W., DiSpirito, A. A., Alterman, M. A., Galeva, N., Larive, C. K., Asunskis, D., & Sherwood, P. M. (2004). Methanobactin a Copper-Acquisition Compound from Methane-Oxidizing Bacteria. *Science*, *305*(274), 935–939. https://doi.org/10.1086/275028

89. Kits, K. D., Klotz, M. G., & Stein, L. Y. (2015). Methane oxidation coupled to nitrate reduction under hypoxia by the Gammaproteobacterium Methylomonas denitrificans, sp. nov. type strain FJG1. *Environmental Microbiology*, *17*(9), 3219–3232. https://doi.org/https://doi.org/10.1111/1462-2920.12772

90. Koo, C. W., Tucci, F. J., He, Y., & Rosenzweig, A. C. (2022). Recovery of particulate methane monooxygenase structure and activity in a lipid bilayer. *Science*, *375*(6586), 1287–1291. https://doi.org/10.1126/science.abm3282

91. Krentz, B. D., Mulheron, H. J., Semrau, J. D., Dispirito, A. A., Bandow, N. L., Haft, D. H., Vuilleumier, S., Murrell, J. C., McEllistrem, M. T., Hartsel, S. C., & Gallagher, W. H. (2010). A Comparison of Methanobactins from *Methylosinus trichosporium* OB3b and *Methylocystis* Strain SB2 Predicts Methanobactins Are Synthesized from Diverse Peptide Precursors Modified To Create a Common Core for Binding and Reducing Copper Ions. *Biochemistry*, *49*(47), 10117–10130. https://doi.org/10.1021/bi1014375

92. Le, V. H., Buscaglia, R., Chaires, J. B., & Lewis, E. A. (2013). Modeling complex equilibria in isothermal titration calorimetry experiments: Thermodynamic parameters estimation for a three-binding-site model. *Analytical Biochemistry*, *434*(2), 233–241. https://doi.org/https://doi.org/10.1016/j.ab.2012.11.030

93. Lee, H. J., Jeong, S. E., Kim, P. J., Madsen, E., & Jeon, C. O. (2015). High resolution depth distribution of Bacteria, Archaea, methanotrophs, and methanogens in the bulk and rhizosphere soils of a flooded rice paddy . *Frontiers in Microbiology* , Vol. 6. Retrieved from https://www.frontiersin.org/articles/10.3389/fmicb.2015.00639

94. Lee, S. J., McCormick, M. S., Lippard, S. J., & Cho, U.-S. (2013). Control of substrate access to the active site in methane monooxygenase. *Nature*, *494*(7437), 380–384. https://doi.org/10.1038/nature11880

95. Li, Y.-M., Milne, J. C., Madison, L. L., Kolter, R., & Walsh, C. T. (1996). From Peptide Precursors to Oxazole and Thiazole-Containing Peptide Antibiotics: Microcin B17 Synthase. *Science*, *274*(5290), 1188–1193. https://doi.org/10.1126/science.274.5290.1188

96. Liang, L., Wang, Y., Sivan, O., & Wang, F. (2019). Metal-dependent anaerobic methane oxidation in marine sediment: Insights from marine settings and other systems. *Science China Life Sciences*, *62*(10), 1287–1295. https://doi.org/10.1007/s11427-018-9554-5

97. Lichtmannegger, J., Leitzinger, C., Wimmer, R., Schmitt, S., Schulz, S., Kabiri, Y., Eberhagen, C., Rieder, T., Janik, D., Neff, F., Straub, B. K., Schirmacher, P., DiSpirito, A. A., Bandow, N., Baral, B. S., Flatley, A., Kremmer, E., Denk, G., Reiter, F. P., Hohenester, S., Eckardt-Schupp, F., Dencher, N. A., Adamski, J., Sauer, V., Niemietz, C., Schmidt, H. H. J., Merle, U., Gotthardt, D. N., Kroemer, G., Weiss, K. H., Zischka, H. (2016). Methanobactin reverses acute liver failure in a rat model of Wilson disease. *The Journal of Clinical Investigation*, *126*(7), 2721–2735. https://doi.org/10.1172/JCI85226

98. Lieberman, R. L., & Rosenzweig, A. C. (2005). Crystal structure of a membrane-bound metalloenzyme that catalyses the biological oxidation of methane. *Nature*, *434*(7030), 177–182. https://doi.org/10.1038/nature03311

99. Liew, E. F., Tong, D., Coleman, N. V, & Holmes, A. J. (2014). Mutagenesis of the hydrocarbon monooxygenase indicates a metal centre in subunit-C, and not subunit-B, is essential for copper-containing membrane monooxygenase activity. *Microbiology (Reading, England)*, *160*(Pt 6), 1267–1277. https://doi.org/10.1099/mic.0.078584-0

100. Lindqvist, Y., Koskiniemi, H., Jansson, A., Sandalova, T., Schnell, R., Liu, Z., Mäntsälä, P., Niemi, J., & Schneider, G. (2009). Structural Basis for Substrate Recognition and Specificity in Aklavinone-11-Hydroxylase from Rhodomycin Biosynthesis. *Journal of Molecular Biology*, *393*(4), 966–977. https://doi.org/https://doi.org/10.1016/j.jmb.2009.09.003

101. Lipscomb, J. D. (1994). Biochemistry of the Soluble Methane Monooxygenase. *Annual Review of Microbiology*, *48*(1), 371–399. https://doi.org/10.1146/annurev.mi.48.100194.002103

102. Liu, J., Wu, P., Yan, S., Li, Y., Cao, Z., & Wang, B. (2021). Spin-Regulated Inner-Sphere Electron Transfer Enables Efficient O—O Bond Activation in Nonheme Diiron Monooxygenase MIOX. *ACS Catalysis*, 6141–6152. https://doi.org/10.1021/acscatal.1c00898

103. Lu, X., Gu, W., Zhao, L., Farhan Ul Haque, M., DiSpirito, A. A., Semrau, J. D., & Gu, B. (2017). Methylmercury uptake and degradation by methanotrophs. *Science Advances*, *3*(5), e1700041. https://doi.org/10.1126/sciadv.1700041

104. Mandal, M., Kawashima, K., Saito, K., & Ishikita, H. (2020). Redox Potential of the Oxygen-Evolving Complex in the Electron Transfer Cascade of Photosystem II. *The Journal of Physical Chemistry Letters*, *11*(1), 249–255. https://doi.org/10.1021/acs.jpclett.9b02831

105. Martin, H., & Murrell, J. C. (1995). Methane monooxygenase mutants of *Methylosinus trichosporium* constructed by marker-exchange mutagenesis. *FEMS Microbiology Letters*, *127*(3), 243–248. https://doi.org/10.1111/j.1574-6968.1995.tb07480.x

106. Martinho, M., Choi, D. W., DiSpirito, A. A., Antholine, W. E., Semrau, J. D., & Münck, E. (2007). Mössbauer Studies of the Membrane-Associated Methane Monooxygenase from *Methylococcus capsulatus* Bath: Evidence for a Diiron Center. *Journal of the American Chemical Society*, *129*(51), 15783–15785. https://doi.org/10.1021/ja077682b

107. McCoy, A. J. (2007). Solving structures of protein complexes by molecular replacement with {\it Phaser}. *Acta Crystallographica Section D*, *63*(1), 32–41. https://doi.org/10.1107/S0907444906045975

108. Meruvu, H., Wu, H., Jiao, Z., Wang, L., & Fei, Q. (2020). From nature to nurture: Essence and methods to isolate robust methanotrophic bacteria. *Synthetic and Systems Biotechnology*, *5*(3), 173–178. https://doi.org/https://doi.org/10.1016/j.synbio.2020.06.007

109. Milucka, J., Kirf, M., Lu, L., Krupke, A., Lam, P., Littmann, S., Kuypers, M. M., & Schubert, C. J. (2015). Methane oxidation coupled to oxygenic photosynthesis in anoxic waters. *The ISME Journal*, *9*(9), 1991–2002. https://doi.org/10.1038/ismej.2015.12

110. Moody, M. D., & Dailey, H. A. (1983). Aerobic ferrisiderophore reductase assay and activity stain for native polyacrylamide gels. *Analytical Biochemistry*, *134*(1), 235–239. https://doi.org/https://doi.org/10.1016/0003-2697(83)90290-7

111. Müller, J. C., Lichtmannegger, J., Zischka, H., Sperling, M., & Karst, U. (2018). High spatial resolution LA-ICP-MS demonstrates massive liver copper depletion in Wilson disease rats upon Methanobactin treatment. *Journal of Trace Elements in Medicine and Biology*, *49*(May), 119–127. https://doi.org/10.1016/j.jtemb.2018.05.009

112. Murrell, J. C., McDonald, I. R., & Gilbert, B. (2000). Regulation of expression of methane monooxygenases by copper ions. *Trends in Microbiology*, *8*(5), 221–225. https://doi.org/10.1016/S0966-842X(00)01739-X

113. Neilands, J. B. (1995). Siderophores: Structure and Function of Microbial Iron Transport Compounds. *Journal of Biological Chemistry*, *270*(45), 26723–26726. https://doi.org/10.1074/jbc.270.45.26723

114. Nicholls, P., Fita, I., & Loewen, P. C. (2000). Enzymology and structure of catalases. *Advances in Inorganic Chemistry, 51*, 51-106. https://doi.org/10.1016/S0898-8838(00)51001-0

115. Nielsen, A. K., Gerdes, K., & Murrell, J. C. (1997). Copper-dependent reciprocal transcriptional regulation of methane monooxygenase genes in Methylococcus capsulatus and Methylosinus trichosporium. *Molecular Microbiology*, *25*(2), 399–409. https://doi.org/https://doi.org/10.1046/j.1365-2958.1997.4801846.x

116. Ogra, Y., Aoyama, M., & Suzuki, K. T. (2006). Protective role of metallothionein against copper depletion. *Archives of Biochemistry and Biophysics*, *451*(2), 112–118. https://doi.org/https://doi.org/10.1016/j.abb.2006.04.017

117. Oswald, K., Jegge, C., Tischer, J., Berg, J., Brand, A., Miracle, M. R., Soria, X., Vicente, E., Lehmann, M. F., Zopfi, J., & Schubert, C. J. (2016). Methanotrophy under Versatile Conditions in the Water Column of the Ferruginous Meromictic Lake La Cruz (Spain) . *Frontiers in Microbiology* , Vol. 7. Retrieved from https://www.frontiersin.org/articles/10.3389/fmicb.2016.01762

118. Oswald, K., Milucka, J., Brand, A., Littmann, S., Wehrli, B., Kuypers, M. M. M., & Schubert, C. J. (2015). Light-Dependent Aerobic Methane Oxidation Reduces Methane Emissions from Seasonally Stratified Lakes. *PLOS ONE*, *10*(7), e0132574. Retrieved from https://doi.org/10.1371/journal.pone.0132574

119. Park, Y. J., Jodts, R. J., Slater, J. W., Reyes, R. M., Winton, V. J., Montaser, R. A., Thomas, P. M., Dowdle, W. B., Ruiz, A., Kelleher, N. L., Bollinger Jr., J. M., Krebs, C., Hoffman, B. M., Thomas, P. M., Rosenzweig, A. C. (2022). A mixed-valent Fe(II)Fe(III) species converts cysteine to an oxazolone/thioamide pair in methanobactin biosynthesis. *Proceedings of the National Academy of Sciences of the United States of America*, *119*(13), e2123566119. https://doi.org/10.1073/pnas.2123566119

120. Peng, P., Gu, W., DiSpirito, A. A., & Semrau, J. D. (2022). Multiple Mechanisms for Copper Uptake by Methylosinus trichosporium OB3b in the Presence of Heterologous Methanobactin. *MBio*. https://doi.org/10.1128/mbio.02239-22

121. Peng, P., Kang-Yun, C. S., Chang, J., Gu, W., DiSpirito, A. A., & Semrau, J. D. (2022). Two TonB-Dependent Transporters in Methylosinus trichosporium OB3b Are Responsible for Uptake of Different Forms of Methanobactin and Are Involved in the Canonical "Copper Switch." *Applied and Environmental Microbiology*, *88*(1), e01793-21. https://doi.org/10.1128/AEM.01793-21

122. Pesch, M. L., Hoffmann, M., Christl, I., Kraemer, S. M., & Kretzschmar, R. (2013). Competitive ligand exchange between Cu–humic acid complexes and methanobactin. *Geobiology*, *11*(1), 44–54. https://doi.org/https://doi.org/10.1111/gbi.12010

123. Picone, N., & Op den Camp, H. J. M. (2019). Role of rare earth elements in methanol oxidation. *Current Opinion in Chemical Biology*, *49*, 39–44. https://doi.org/https://doi.org/10.1016/j.cbpa.2018.09.019

124. Read, J., Gill, R., Dales, S. L., Cooper, J. B., Wood, S. P., & Anthony, C. (1999). The molecular structure of an unusual cytochrome c2 determined at 2.0 å; the cytochrome ch from M*ethylobacterium extorquens*. *Protein Science*, *8*(6), 1232–1240. https://doi.org/https://doi.org/10.1110/ps.8.6.1232

125. Rhee, S.-K., Awala, S. I., & Nguyen, N.-L. (2019). Enrichment and Isolation of Aerobic and Anaerobic Methanotrophs. In E. Y. Lee (Ed.), *Methanotrophs: Microbiology Fundamentals and Biotechnological Applications* (pp. 39–69). https://doi.org/10.1007/978-3-030-23261-0_2

126. Ro, S. Y., & Rosenzweig, A. C. (2018). Recent Advances in the Genetic Manipulation of *Methylosinus trichosporium* OB3b. In *Methods in Enzymology* (1st ed., Vol. 605). https://doi.org/10.1016/bs.mie.2018.02.011

127. Robinson, N. J. (2008). A bacterial copper metallothionein. *Nature Chemical Biology*, *4*(10), 582–583. https://doi.org/10.1038/nchembio1008-582

128. Ross, M. O., MacMillan, F., Wang, J., Nisthal, A., Lawton, T. J., Olafson, B. D., Mayo, S. L., Rosenzweig, A. C., & Hoffman, B. M. (2019). Particulate methane monooxygenase contains only mononuclear copper centers. *Science*, *364*(6440), 566–570. https://doi.org/10.1126/science.aav2572

129. Ryan, K. S., Chakraborty, S., Howard-Jones, A. R., Walsh, C. T., Ballou, D. P., & Drennan, C. L. (2008). The FAD Cofactor of RebC Shifts to an IN Conformation upon Flavin Reduction,. *Biochemistry*, *47*(51), 13506–13513. https://doi.org/10.1021/bi801229w

130. Scanlan, J., Dumont, M. G., & Murrell, J. C. (2009). Involvement of MmoR and MmoG in the transcriptional activation of soluble methane monooxygenase genes in Methylosinus trichosporium OB3b. *FEMS Microbiology Letters*, *301*(2), 181–187. https://doi.org/10.1111/j.1574-6968.2009.01816.x

131. Schalk, I. J. (2008). Metal trafficking via siderophores in Gram-negative bacteria: Specificities and characteristics of the pyoverdine pathway. *Journal of Inorganic Biochemistry*, *102*(5), 1159–1169. https://doi.org/https://doi.org/10.1016/j.jinorgbio.2007.11.017

132. Semrau, J. D., DiSpirito, A. A., Gu, W., & Yoon, S. (2018). Metals and Methanotrophy. *Applied and Environmental Microbiology*, *84*(6), e02289--17. https://doi.org/10.1128/AEM.02289-17

133. Semrau, J. D., & DiSpirito, A. A. (2019). *Methanobactin: A Novel Copper-Binding Compound Produced by Methanotrophs BT - Methanotrophs: Microbiology Fundamentals and Biotechnological Applications* (E. Y. Lee, Ed.). https://doi.org/10.1007/978-3-030-23261-0_7

134. Semrau, J. D., Dispirito, A. A., Gu, W., Yoon, S. (2019). *Methanotrophs: Microbiology Fundamentals and Biotechnological Applications* (Vol. 84).

135. Semrau, J. D., Dispirito, A. A., Obulisamy, P. K., & Kang-Yun, C. S. (2020). Methanobactin from methanotrophs: Genetics, structure, function and potential applications. *FEMS Microbiology Letters*. https://doi.org/10.1093/femsle/fnaa045

136. Semrau, J. D., DiSpirito, A. A., & Yoon, S. (2010). Methanotrophs and copper. *FEMS Microbiology Reviews*, *34*(4), 496–531. https://doi.org/10.1111/j.1574-6976.2010.00212.x

137. Semrau, J. D., Jagadevan, S., DiSpirito, A. A., Khalifa, A., Scanlan, J., Bergman, B. H., Freemeier, B. C., Baral, B. S., Bandow, N. L., Vorobev, A., Haft, D. H., Vuilleumier, S., & Murrell, J. C. (2013). Methanobactin and MmoD work in concert to act as the 'copper-switch' in methanotrophs. *Environmental Microbiology*, *15*(11), 3077–3086. https://doi.org/https://doi.org/10.1111/1462-2920.12150

138. Simon, R. (1984). High frequency mobilization of gram-negative bacterial replicons by the in vitro constructed Tn5-Mob transposon. *Molecular and General Genetics MGG*, *196*(3), 413–420. https://doi.org/10.1007/BF00436188

139. Singh, B. K., Bardgett, R. D., Smith, P., & Reay, D. S. (2010). Microorganisms and climate change: terrestrial feedbacks and mitigation options. *Nature Reviews Microbiology*, *8*(11), 779–790. https://doi.org/10.1038/nrmicro2439

140. Smith, T. J., Slade, S. E., Burton, N. P., Murrell, J. C., & Dalton, H. (2002). Improved System for Protein Engineering of the Hydroxylase Component of Soluble Methane Monooxygenase. *Applied and Environmental Microbiology*, *68*(11), 5265–5273. https://doi.org/10.1128/AEM.68.11.5265-5273.2002

141. Söhngen, N. L. (1906). Über bakterien, welche methan als kohlenstoffnahrung und energiequelle gebrauchen. *Zentrabl Bakteriol Parasitenk Infektionskr*, *15*, 513–517.

142. Stafford, G. P., Scanlan, J., McDonald, I. R., & Murrell, J. C. (2003). rpoN, mmoR and mmoG, genes involved in regulating the expression of soluble methane monooxygenase in *Methylosinus trichosporium* OB3b. *Microbiology (Reading, England)*, *149*(Pt 7), 1771–1784. https://doi.org/10.1099/mic.0.26060-0

143. Stanley, S. H., Prior, S. D., Leak, D. J., & Dalton, H. (1983). Copper stress underlies the fundamental change in intracellular location of methane mono-oxygenase in methane-oxidizing organisms: Studies in batch and continuous cultures. *Biotechnology Letters*, *5*(7), 487–492. https://doi.org/10.1007/BF00132233

144. Storhoff, J. J., Lazarides, A. A., Mucic, R. C., Mirkin, C. A., Letsinger, R. L., & Schatz, G. C. (2000). What Controls the Optical Properties of DNA-Linked Gold Nanoparticle Assemblies? *Journal of the American Chemical Society*, *122*(19), 4640–4650. https://doi.org/10.1021/ja993825l

145. Summer, K. H., Lichtmannegger, J., Bandow, N., Choi, D. W., DiSpirito, A. A., & Michalke, B. (2011). The biogenic methanobactin is an effective chelator for copper in a rat model for Wilson disease. *Journal of Trace Elements in Medicine and Biology*, *25*(1), 36–41. https://doi.org/https://doi.org/10.1016/j.jtemb.2010.12.002

146. Sung-Woo, L., R., K. D., Dong-Hee, L., A., D. A., & D., S. J. (2006). Mixed Pollutant Degradation by *Methylosinus trichosporium* OB3b Expressing either Soluble or Particulate Methane Monooxygenase: Can the Tortoise Beat the Hare? *Applied and Environmental Microbiology*, *72*(12), 7503–7509. https://doi.org/10.1128/AEM.01604-06

147. Suzuki, K. T., Someya, A., Komada, Y., & Ogra, Y. (2002). Roles of metallothionein in copper homeostasis: responses to Cu-deficient diets in mice. *Journal of Inorganic Biochemistry*, *88*(2), 173–182. https://doi.org/https://doi.org/10.1016/S0162-0134(01)00376-2

148. Thi, D., Nguyen, N., Lee, O. K., Nguyen, T. T., & Lee, E. Y. (2021). Type II methanotrophs : A promising microbial cell-factory platform for bioconversion of methane to chemicals. *Biotechnology Advances*, *47*(February), 107700. https://doi.org/10.1016/j.biotechadv.2021.107700

149. Tinberg, C. E., & Lippard, S. J. (2011). Dioxygen Activation in Soluble Methane Monooxygenase. *Accounts of Chemical Research*, *44*(4), 280–288. https://doi.org/10.1021/ar1001473

150. van Grinsven, S., Sinninghe Damsté, J. S., Harrison, J., & Villanueva, L. (2020). Impact of Electron Acceptor Availability on Methane-Influenced Microorganisms in an Enrichment Culture Obtained From a Stratified Lake . *Frontiers in Microbiology* , Vol. 11. Retrieved from https://www.frontiersin.org/articles/10.3389/fmicb.2020.00715

151. Varadi, M., Anyango, S., Deshpande, M., Nair, S., Natassia, C., Yordanova, G., Yuan, D., Stroe, O., Wood, G., Laydon, A., Žídek, A., Green, T., Tunyasuvunakool, K., Petersen, S., Jumper, J., Clancy, E., Green, R., Vora, A., Lutfi, M., Figurnov, M., Cowie, A., Hobbs, N., Kohli, P., Kleywegt, G., Birney, E., Hassabis, D., Velankar, S. (2022). AlphaFold Protein Structure Database: massively expanding the structural coverage of protein-sequence space with high-accuracy models. *Nucleic Acids Research*, *50*(D1), D439–D444. https://doi.org/10.1093/nar/gkab1061

152. Vass, I., & Styring, S. (1991). pH-Dependent charge equilibria between tyrosine-D and the S states in photosystem II. Estimation of relative midpoint redox potentials. *Biochemistry*, *30*(3), 830–839. https://doi.org/10.1021/bi00217a037

153. Ve, T., Mathisen, K., Helland, R., Karlsen, O. A., Fjellbirkeland, A., Røhr, Å. K., Andersson, K. K., Pedersen, R. B., Lillehaug, J. R., & Jensen, H. B. (2012). The Methylococcus capsulatus (Bath) Secreted Protein, MopE*, Binds Both Reduced and Oxidized Copper. *PLOS ONE*, *7*(8), e43146. Retrieved from https://doi.org/10.1371/journal.pone.0043146

154. Vita, N., Landolfi, G., Baslé, A., Platsaki, S., Lee, J., Waldron, K. J., & Dennison, C. (2016). Bacterial cytosolic proteins with a high capacity for Cu(I) that protect against copper toxicity. *Scientific Reports*, *6*(1), 39065. https://doi.org/10.1038/srep39065

155. Vita, N., Platsaki, S., Baslé, A., Allen, S. J., Paterson, N. G., Crombie, A. T., Murrell, J. C., Waldron, K. J., & Dennison, C. (2015). A four-helix bundle stores copper for methane oxidation. *Nature*, *525*(7567), 140–143. https://doi.org/10.1038/nature14854

156. Vorholt, J. A. (2002). Cofactor-dependent pathways of formaldehyde oxidation in methylotrophic bacteria. *Archives of Microbiology*, *178*(4), 239–249. https://doi.org/10.1007/s00203-002-0450-2

157. Vorholt, J. A., Chistoserdova, L., Lidstrom, M. E., & Thauer, R. K. (1998). The NADP-Dependent Methylene Tetrahydromethanopterin Dehydrogenase in *Methylobacterium extorquens* AM1. *Journal of Bacteriology*, *180*(20), 5351–5356. https://doi.org/10.1128/JB.180.20.5351-5356.1998

158. Vorholt, J. A., Chistoserdova, L., Stolyar, S. M., Thauer, R. K., & Lidstrom, M. E. (1999). Distribution of Tetrahydromethanopterin-Dependent Enzymes in Methylotrophic Bacteria and Phylogeny of Methenyl Tetrahydromethanopterin Cyclohydrolases. *Journal of Bacteriology*, *181*(18), 5750–5757. https://doi.org/10.1128/JB.181.18.5750-5757.1999

159. Ward, N., Larsen, Ø., Sakwa, J., Bruseth, L., Khouri, H., Durkin, A. S., Dimitrov, G., Jiang, L., Scanlan, D., Kang, K. H., Lewis, M., Nelson, K. E., Methé, B., Wu, M., Heidelberg, J. F., Paulsen, I. T., Fouts, D., Ravel, J., Tettelin, H., Ren, Q., Read, T., DeBoy, R. T., Seshadri, R., Salzberg, S. L., Jensen, H. B., Birkeland, N. K., Nelson, W. C., Dodson, R. J., Grindhaug, S. H., Holt, I., Eidhammer, I., Jonasen, I., Vanaken, S., Utterback, T., Feldblyum, T. V., Fraser, C. M., Lillehaug, J. R., Eisen, J. A. (2004). Genomic Insights into Methanotrophy: The Complete Genome Sequence of Methylococcus capsulatus (Bath). *PLOS Biology*, *2*(10), null. https://doi.org/10.1371/journal.pbio.0020303

160. Whittenbury, R., Phillips, K. C., & Wilkinson, J. F. (1970). Enrichment, Isolation and Some Properties of Methane-utilizing Bacteria. *Journal of General Microbiology*, *61*(2), 205–218. https://doi.org/10.1099/00221287-61-2-205

161. Williams, P. A., Coates, L., Mohammed, F., Gill, R., Erskine, P. T., Coker, A., Wood, S. P., Anthony, C., & Cooper, J. B. (2005). The atomic resolution structure of methanol dehydrogenase from *Methylobacterium extorquens*. *Acta Crystallographica Section D*, *61*(1), 75–79. Retrieved from https://doi.org/10.1107/S0907444904026964

162. Yoch, D. C., Chen, Y. P., & Hardin, M. G. (1990). Formate dehydrogenase from the methane oxidizer *Methylosinus trichosporium* OB3b. *Journal of Bacteriology*, *172*(8), 4456–4463. https://doi.org/10.1128/jb.172.8.4456-4463.1990

163. Youngblut, M. D., Tsai, C. L., Clark, I. C., Carlson, H. K., Maglaqui, A. P., Gau-Pan, P. S., Redford, S. A., Wong, A., Tainer, J. A., & Coates, J. D. (2016). Perchlorate Reductase Is Distinguished by Active Site Aromatic Gate Residues. *Journal of Biological Chemistry*, *291*(17), 9190–9202. https://doi.org/10.1074/jbc.M116.714618

164. Zahn, J. A., & DiSpirito, A. A. (1996). Membrane-associated methane monooxygenase from *Methylococcus capsulatus* (Bath). *Journal of Bacteriology*, *178*(4), 1018–1029. https://doi.org/10.1128/jb.178.4.1018-1029.1996

165. Zahn, J. A., Bergmann, D. J., Boyd, J. M., Kunz, R. C., & DiSpirito, A. A. (2001). Membrane-Associated Quinoprotein Formaldehyde Dehydrogenase from *Methylococcus capsulatus* Bath. *Journal of Bacteriology*, *183*(23), 6832–6840. https://doi.org/10.1128/JB.183.23.6832-6840.2001

166. Zannoni, D. (2004). *Respiration in archaea and bacteria*. Springer.

167. Zhao, P., Li, N., & Astruc, D. (2013). State of the art in gold nanoparticle synthesis. *Coordination Chemistry Reviews*, *257*(3), 638–665. https://doi.org/https://doi.org/10.1016/j.ccr.2012.09.002

168. Zheng, Y., Wang, H., Liu, Y., Zhu, B., Li, J., Yang, Y., Qin, W., Chen, L., Wu, X., Chistoserdova, L., Zhao, F. (2020). Methane-Dependent Mineral Reduction by Aerobic Methanotrophs under Hypoxia. *Environmental Science & Technology Letters*, *7*(8), 606–612. https://doi.org/10.1021/acs.estlett.0c00436

169. Zischka, H., Lichtmannegger, J., DiSpirito, A. A., & Semrau, J. D. (2021, December 2). *Means and methods for treating copper-related diseases*. International Patent application WO 2017/103094 A2 (**2020**); US Patent **11,000,568 B2** (**2021**).

170. Zischka, H., Lichtmannegger, J., Schmitt, S., Jägemann, N., Schulz, S., Wartini, D., Jennen, L., Rust, C., Larochette, N., Galluzzi, L., Chajes, V., Bandow, N., Gilles, V. S., DiSpirito, A. A., Esposito, I., Goettlicher, M., Summer, K. H., & Kroemer, G. (2011). Liver mitochondrial membrane crosslinking and destruction in a rat model of Wilson disease. *The Journal of Clinical Investigation*, *121*(4), 1508–1518. https://doi.org/10.1172/JCI45401